

2007

Phenotypic properties and intrinsic currents of neurons involved in the neural generation of mammalian breathing

John A. Hayes

College of William & Mary - Arts & Sciences

Follow this and additional works at: <https://scholarworks.wm.edu/etd>



Part of the [Neurosciences Commons](#), and the [Physiology Commons](#)

Recommended Citation

Hayes, John A., "Phenotypic properties and intrinsic currents of neurons involved in the neural generation of mammalian breathing" (2007). *Dissertations, Theses, and Masters Projects*. Paper 1539623329.

<https://dx.doi.org/doi:10.21220/s2-avmw-2e56>

This Dissertation is brought to you for free and open access by the Theses, Dissertations, & Master Projects at W&M ScholarWorks. It has been accepted for inclusion in Dissertations, Theses, and Masters Projects by an authorized administrator of W&M ScholarWorks. For more information, please contact scholarworks@wm.edu.

**Phenotypic Properties and Intrinsic Currents of Neurons Involved in the
Neural Generation of Mammalian Breathing**

John Ashley Hayes

Williamsburg, VA

**Master of Science, the College of William and Mary, 2004
Bachelor of Science, Clemson University, 2001**

**A Dissertation presented to the Graduate Faculty
of the College of William and Mary in Candidacy for the Degree of
Doctor of Philosophy**

Department of Applied Science

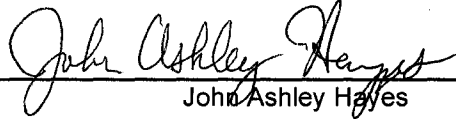
**The College of William and Mary
August, 2007**

© 2007, John Ashley Hayes

APPROVAL PAGE


This Dissertation is submitted in partial fulfillment of
the requirements for the degree of

Doctor of Philosophy

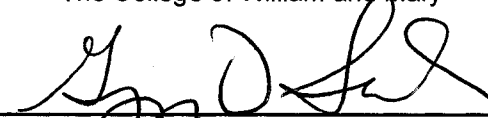


John Ashley Hayes

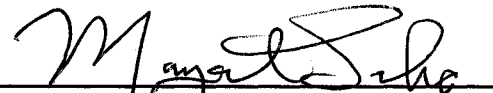
Approved by the Committee, June, 2007




Committee Chair
Assistant Professor Christopher Del Negro, Applied Science
The College of William and Mary



Associate Professor Gregory Smith, Applied Science
The College of William and Mary



Professor Margaret Saha, Biology
The College of William and Mary



Professor Patrice Guyenet, Pharmacology
University of Virginia

ABSTRACT PAGE

Breathing is essential for mammalian life. Although there is an emerging consensus that the inspiratory respiratory rhythm is generated in a lower brainstem region known as the preBötzinger Complex (preBötC), the mechanism of rhythmogenesis is still unclear. Additionally, the modulation of intrinsic currents within preBötC neurons has yet to be fully elucidated. This dissertation addresses both of these issues and relies on imaging, electrophysiological, and modeling techniques. The first chapter examines the size and composition of the preBötC. Previously, it has been shown that preBötC neurons expressing substance P (SP)-sensitive neurokinin receptors (NKR) are essential for normal breathing *in vivo*. Combined with an *in vitro* study that indicated that nearly all inspiratory neurons respond to SP, these data suggested that the critical rhythmogenic population of neurons are NKR⁺. We show that ~40% of the putatively rhythmogenic population of neurons could be identified as NKR⁺ *in vitro* whereas most of the neurons responded to SP. We also show how this disparity may be attributed to gap junctions between inspiratory neurons that transmit the response of SP to neighboring neurons. This may resolve much of the conflict between the previous *in vitro* and *in vivo* studies that reached widely disparate conclusions about the number of rhythmogenic neurons that express NKRs. Using additional data, we also offer a rough estimate of the size of the rhythmogenic population of neurons. The chapter also describes the means by which SP excites the vast majority of preBötC neurons by illustrating the characteristics of the SP-activated current (I_{SP}) in these neurons. In the subsequent chapter, we characterize a voltage-dependent potassium current that is involved in maintaining stable rhythms during normal fictive breathing. This study shows that the majority of putatively rhythmogenic neurons exhibit a low-threshold, slowly-inactivating transient potassium current (I_A) and that blockade of I_A in the context of normal network activity has deleterious effects on the frequency and discharge pattern of inspiratory activity. Therefore, specific intrinsic currents like I_A play a key role in ensuring stable rhythmogenesis by keeping network activity synchronous and coherent. The third chapter presents a mathematical model of heterogeneous and rhythmogenic neurons that initiate network bursts. We show how this behavior relies on feedback synaptic connections within the network that reinforces activity, i.e., *recurrent-excitation*. We also compare model results to experimental data and make testable predictions. The experimental data includes applications of riluzole, which blocks the persistent Na⁺ current while not preventing rhythmogenesis, and the aforementioned experiments that showed that destruction of NKR⁺ neurons prevents normal breathing. The final chapter elaborates on the discussion of I_{SP} from the first chapter and presents evidence suggesting that a cyclic adenosine monophosphate (cAMP)-modulated non-specific cation channel may account for the depolarizing response in preBötC neurons from several neuromodulators. These channels may be a primary target of convergent mechanisms that alter the respiratory rhythm from different afferent projections. Altogether, this dissertation advances the field's understanding on several fronts. We have distinguished possible functional roles of neurons from electrophysiological characteristics, estimated the number of neurons necessary for rhythmogenesis, characterized I_{SP} , and clarified the distribution of NKRs in inspiratory neurons. We have identified and characterized a voltage-dependent potassium current important for inspiratory activity and analyzed its role. We have also described in detail how rhythmic bursts form from recurrent excitation and how this relates to experimental data. Finally, we have identified and begun characterizing a potentially important and novel mechanism for the modulation of membrane potentials in critical inspiratory neurons.

TABLE OF CONTENTS

	Page
Acknowledgements	iii
List of Figures	iv
Introduction	1
CHAPTER 1: Neurokinin receptor-expressing preBötzinger Complex neurons in neonatal mice studied <i>in vitro</i>	
1.1. Introduction	19
1.2. Methods	21
1.3. Results	29
1.4. Discussion	40
1.5. References	47
CHAPTER 2: 4-aminopyridine-sensitive outward currents promote regular burst discharges within the preBötzinger Complex	
2.1. Introduction	54
2.2. Methods	56
2.3. Results	58
2.4. Discussion	67
2.5. References	70
CHAPTER 3: Network-mediated burst initiation and its role in respiratory rhythm generation	
3.1. Introduction	80
3.2. Methods	83
3.3. Results and Discussion	87
3.4. Appendix 1: Group-Pacemaker Model Equations and Configuration	103
3.5. Appendix 2: Implementation and Operation of <i>neuronetsim</i>	109
3.6. References	122
CHAPTER 4: Modulation of a voltage-insensitive, mixed cation current by cyclic AMP	
4.1. Introduction	130
4.2. Methods	132
4.3. Results and Discussion	132
4.6. References	140
Conclusions	147
Vita	151

This dissertation is dedicated to my parents and brother

ACKNOWLEDGEMENTS

I sincerely thank my advisor, Christopher Del Negro, for all his immeasurable and tireless support: in training, in writing, in data analysis and interpretation -- among many other things. We started this research with a very specific objective in mind, and I thank him for allowing me to diverge from that a bit in order to explore new avenues and put the original goal into context. I also thank him for the corner of the lab to put my paper in, occasional coffee, and the encouraging words.

I thank Gregory Smith for the helpful advice on how to correctly incorporate noise into our model, which is essential for the functioning of the network. I also thank him for advising me on my Master's research. I would also like to thank him for the things I learned in his courses that drove my interest in both the modeling and experimental aspects of biological research.

I thank Maciek Sasinowski, Heather Sasinowska, and the rest of the people at INCOGEN, for getting me to Williamsburg and giving me the opportunity to work at the College of William and Mary.

I thank Margaret Saha for the helpful discussions that influenced how this dissertation was written. Hopefully, her comments were successfully reflected in the final text.

I thank Patrice Guyenet for his helpful comments on this dissertation and for suggesting we perform a very useful control experiment in Chapter 4.

I particularly thank Rex Kincaid and Michael Holroyd for the extensive help providing equations, analysis, and advice for Chapter 3 when we were studying network properties and burst initiation.

I thank my fellow lab member Ryland Pace, for his willingness to talk about his experimental results, and talk about our collective work more generally.

I also thank Jeffrey Mendenhall for suggestions regarding the model and making key contributions to *neuronetsim*. Jeff also had many helpful comments regarding Chapter 3.

I thank our department chair, Eric Bradley, the rest of the members of the Department of Applied Science, the College of William and Mary, and our vice provost, Dennis Manos, for all the indirect support that was necessary to achieve the results of this research.

Finally, I thank our funding sources who make this research possible: the Suzzan Wilson Matthews Faculty Research Award, the Jeffress Memorial Trust, and NSF IOB-0616099.

LIST OF FIGURES

Figure	Page
1.1. The 'breathing slice' preparation	4
1.1. TMR-SP labeling of neurons	24
1.2. Control experiment examining nucleus ambiguus TMR-SP labeling	25
1.3. Intrinsic properties of inspiratory neurons in the preBötC	30
1.4. TMR-SP labeling in preBötC neurons with different phenotypic properties	32
1.5. A TMR-SP ⁺ non-rhythmic neuron near the preBötC	33
1.6. Effects of SP on inspiratory neurons	33
1.7. Effects of SP on inspiratory neurons blocking K ⁺ channels	34
1.8. Effects of SP on inspiratory neurons blocking K ⁺ channels and gap junctions	36
1.9. Simultaneous measurements of inspiratory neurons and TMR-SP ⁺ neurons	38
1.10. Analysis of NKR ⁺ preBötC neuron distribution	40
1.11. Estimates of the composition of the preBötC inspiratory network	45
2.1. Phenotypic behaviors of inspiratory neurons located in the preBötC	59
2.2. Phenotypic behaviors of expiratory neurons located in the preBötC	60
2.3. Biophysics of I_A in inspiratory neurons	61
2.4. I_A attenuation from 2 mM 4-AP	62
2.5. Effects of 4-AP on the preBötC network	64
2.6. Characteristics of phasic synaptic input to inspiratory neurons	64
2.7. Whole-cell effects of 4-AP on inspiratory neurons	65
2.8. Effects of 4-AP on burst frequency in inspiratory neurons	66
2.9. Effects of 4-AP on general burst characteristics	67
3.1. The group-pacemaker is made up of neurons with heterogeneous parameters	87
3.2. The general topology of the model preBötC network	88
3.3. A variety of phenotypic patterns are exhibited by model inspiratory neurons	89
3.4. A raster plot of the population of neurons illustrating network bursts	91
3.5. Comparison of experimental and simulated burst initiation	95
3.6. Dynamics of active component assembly	97
3.7. Blockade of persistent Na ⁺ current does not prevent rhythmogenesis	99
3.8. Simulated SP-saporin lesioning of NKR ⁺ neurons	101
4.1. Forskolin activates a mixed cation current in preBötC neurons by up-regulating adenylyl cyclase	133
4.2. Forskolin occludes the effect of SP in preBötC neurons	134
4.3. Verapamil blocks $I_{\text{forskolin}}$	135
4.4. Verapamil prevents the network-level response to SP	136
4.5. cAMP-gated channels are present in preBötC neurons	138

Introduction

Rhythmic breathing movements in mammals begin *in utero* and the rhythm-generating neural circuits that drive breathing movements must be fully formed and properly configured at birth in order to sustain newborn life. These same circuits then operate continuously for up to, and sometimes more than, 100 years in humans. The body of an average 70 kg adult human male contains a reservoir of about 1000 ml of O₂. At rest, 250 ml of O₂ are consumed every minute and this rate more than triples to 800 ml O₂ per minute during mild exercise. Moreover, low levels of blood O₂ for more than a few minutes can cause irreversible brain damage. To sustain life the brain is relentless in its drive to breathe and regulate respiration. Consequently, the mammalian brain has evolved neural mechanisms to ensure that the respiratory rhythm remains robust and reliable.

These neural mechanisms can go awry, and the resulting diseases afflict both the very young and the aged, and include: congenital central hypoventilation syndrome (CCHS) and sudden infant death syndrome (SIDS) in newborns, sleep apnea in adults, and sudden respiratory failure in Amyotrophic Lateral Sclerosis (ALS) and Multiple Systems Atrophy (MSA) patients (Amir et al. 1999; Arnulf et al. 2000; Barthlen and Lange 2000; Chen and Keens 2004; Gozal 2004; Maria et al. 2003; Munschauer et al. 1990; Stocchi et al. 1998; Vetrugno et al. 2004; Weese-Mayer et al. 2003). Despite its

importance for human health, critical aspects of breathing's neural origins remain unknown.

Breathing behavior consists of pumping movements in the diaphragm and thorax, coordinated with movements in the airways and tongue that affect air flow. Respiratory muscles are controlled by cranial and upper spinal motor nerves that receive motor commands from respiratory networks in the medulla oblongata. Expiration is mainly passive in mammals (Janczewski and Feldman 2006), so at the core of breathing is the rhythm for inspiration. This is advantageous from an experimental perspective because inspiratory motor rhythms can be preserved *in vitro* (Smith and Feldman 1987; Smith et al. 1990; Suzue 1984).

The rhythm and pattern for breathing are generated by networks in the brainstem and spinal cord (Bianchi et al. 1995; Feldman and McCrimmon 2002; Feldman et al. 1986; Feldman et al. 2003; Onimaru et al. 1997; Rekling and Feldman 1998; Richter and Spyer 2001). These networks include the neurons of the dorsal respiratory group (DRG) that participate in afferent feedback and autonomic regulation, and the ventral respiratory group (VRG), which is a bilaterally distributed column of neurons beginning at the level of the facial (VII) nucleus and retrotrapezoid nucleus (Smith and Feldman 1987), which extends caudally to the upper cervical spinal cord. On the caudal end, the VRG contains *bulbospinal premotoneurons* that project to cranial and spinal respiratory motoneurons to carry out breathing movements (Blessing 1997). More importantly, the rostral VRG contains *propriomedullary interneurons*, neurons that form local synaptic connections and do not project to spinal motor nuclei or higher brain centers, which are thought to be specialized for rhythm generation (Connelly et al. 1992; Dobbins and Feldman 1994; Ellenberger and Feldman 1990; Johnson et al. 1994; Schwarzacher et al. 1995; Smith et al. 1991). Although the full set of DRG and VRG neurons are required

to generate the complete motor pattern for breathing, and respond to physiological demands (Feldman et al. 2003), this project aims to describe fundamental interactions of the rhythm-generating circuitry.

To further delineate the brainstem region containing the critical rhythm-generating circuitry, a series of transection experiments were performed in rodents in the early nineties. These seminal experiments functionally identified the region that was necessary and sufficient for inspiratory rhythm generation *in vitro*, subsequently named the preBötzinger Complex (preBötC) (Smith et al. 1991).

The preBötC can be retained in slice preparations and contains a subset of the previously mentioned putatively rhythmogenic propriomedullary interneurons. Consequently, slices remain rhythmically active and inspiratory motor activity is measurable via hypoglossal (XII) nerve output (Fig. 1). During fictive inspiration, neurons in the preBötC generate robust bursts correlated with XII motor output (Fig. 1B). Slices have inherent limitations such as requiring an ionic or pharmacologic 'boost' in excitability, typically accomplished by elevating the extracellular K^+ . Also, slices do not retain the expiratory rhythm-generating circuits located in the Bötzing complex (Bianchi et al. 1995; Feldman and McCrimmon 1999) and the retrotrapezoid/parafacial respiratory group (RTN/pFRG) (Feldman and Del Negro 2006; Janczewski et al. 2002; Mellen et al. 2003; Onimaru and Homma 2003; Vasilakos et al. 2004). Nevertheless, since slices preserve the preBötC and lack peripheral sensory inputs, the XII motor-output pattern primarily reflects the inspiratory rhythm (Lieske et al. 2000; Ramirez and Lieske 2003; Smith et al. 1990). Therefore slices represent a good *in vitro* model in which to examine the neural mechanisms for inspiratory rhythm generation, which we must understand to address mechanisms *in vivo* (Ramirez et al. 2002; Richter and Spyer 2001). Since their inception in 1991 (Smith et al. 1991), slice experiments have motivated critical tests of

hypotheses *in vivo* (Gray et al. 2001; Janczewski and Feldman 2006; Janczewski et al. 2002; Manzke et al. 2003; McKay et al. 2005).

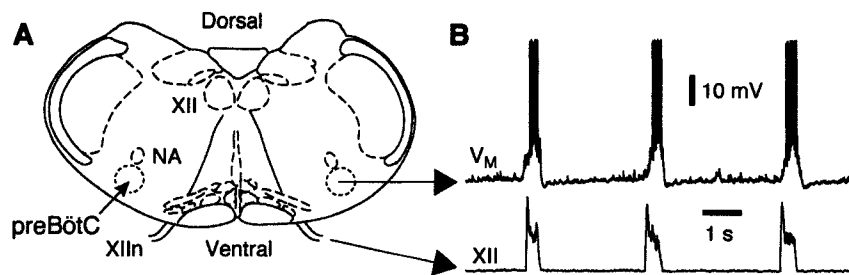


Figure I.1. The ‘breathing slice’ preparation isolates brainstem respiratory circuits and spontaneously generates inspiratory motor rhythm. **A**, Transverse view of the slice containing the preBötC, nucleus ambiguus (NA), hypoglossal motor nucleus (XII) and its nerve rootlets (XIIIn). **B**, Electrical recordings *in vitro* from preBötC inspiratory neurons (V_M) and inspiratory motor output (XII).

One significant outcome of slice experiments was the discovery that substance P (SP), an endogenous neuropeptide long known to increase inspiratory activity (Chen et al. 1991; Chen et al. 1990; Murakoshi et al. 1985), directly excited most inspiratory neurons in the preBötC (Gray et al. 1999; Pena and Ramirez 2004). This led to an anatomical delineation of the boundaries of the preBötC using the neurokinin-1 receptor (NK1R), the principal ligand receptor for SP, as a marker of preBötC neurons (Gray et al. 1999). Further studies, showed that lesioning NK1R-expressing neurons via the ribosomal toxin saporin in intact and behaving adult rats (Gray et al. 2001; McKay et al. 2005) irreversibly resulted in ataxic breathing. This corroborated the results of the earlier transection experiments and showed that the preBötC was necessary for breathing in intact mammals.

NK1R-expressing preBötC neurons are predominantly glutamatergic and propriomedullary (Stornetta et al. 2003; Wang et al. 2001) and glutamate receptors are required to generate inspiratory bursts *in vitro* (Funk et al. 1993; Ge and Feldman 1998; Greer et al. 1991; Lieske and Ramirez 2006; Pace et al. 2007a). Dual intracellular

recordings have provided physiological evidence that putatively rhythmogenic preBötC neurons are coupled with excitatory synaptic connections (Rekling et al. 2000). This suggests that interneuronal glutamatergic preBötC neurons may form excitatory networks that facilitate rhythmic burst generation.

Questions remain with regard to what neurons make up the population of neurons sufficient for rhythm generation. This is because most inspiratory neurons recorded *in vitro* respond to bath-applied SP suggesting they express NK1Rs (Gray et al. 1999; Pena and Ramirez 2004), while the majority of inspiratory neurons recorded *in vivo* do not express detectable NK1R-labeling with immunohistochemistry techniques (Guyenet and Wang 2001). Therefore, there is a discrepancy between the physiological and anatomical means of counting NK1R-expressing neurons of the preBötC, which must be resolved. This has important implications in interpreting how lesioning experiments, that exploit NK1R endocytosis, adversely affects preBötC functioning. Specifically, it is currently unclear if the neurons being destroyed are the only ones necessary for rhythmic behavior and raises the question: is there another set of rhythmogenic neurons that are not destroyed?

Interpreting graded neuronal destruction experiments will provide us with clues regarding the importance of synaptic connections that may impart robustness on the respiratory rhythm in the face of neuronal death.

In addition to synaptic interactions between neurons, the properties and intrinsic roles of currents in rhythm-generating neurons must be considered to gain a full understanding of the mechanism of respiratory rhythmogenesis. Inward currents have been the focus of many studies particularly with respect to two widely expressed inward currents with burst-promoting qualities: persistent Na⁺ current (I_{NaP}) and Ca²⁺-activated non-specific cationic current (I_{CAN}) (Butera et al. 1999a; b; Del Negro et al. 2001; Del

Negro et al. 2002a; Del Negro et al. 2005; Johnson et al. 1994; Pace et al. 2007a; b; Pena et al. 2004; Ptak et al. 2005; Rybak et al. 2003). However, the roles of outward currents in normal inspiratory activity has largely been neglected. The transient K^+ current (I_A) was suggested to be present in inspiratory neurons more than 10 years ago (Rekling et al. 1996), and it has recently been observed under synaptically-isolated conditions (Inyushkin 2005). I_A is important in determining the frequency of other rhythmically-active networks (Byrne 1980; Getting 1983; Tierney and Harris-Warrick 1992), so we speculate that I_A may be important in rhythmic-behavior of I_A -expressing preBötC neurons. We will examine this issue in more detail in Chapter 2.

The properties of intrinsic currents have been used to construct mathematical models of how neurons that make up the respiratory rhythm generator behave. The most influential model has been the Butera preBötC neuron model (1999a; 1999b; Del Negro et al. 2001) which illustrated how heterogeneity was important for flexible rhythmic behaviors (Purvis et al. 2007). This model also set forth predictions that have in some cases been substantiated (Del Negro et al. 2001; Del Negro et al. 2002a), and other cases refuted (Del Negro et al. 2002b; Pace et al. 2007b; Paton et al. 2006). Thus, the development of the model and following experimental developments have had an important influence on the field by illustrating how an iterative approach, alternating between model simulations and experimental tests, can aid our understanding of how basic respiratory rhythmic behavior is generated.

More recently, the limitations of the model have become increasingly apparent and the Butera model is in need of updating. Such limitations include the fact that only 50 neurons made up the rhythm-generating network, every neuron was coupled to every other neuron (i.e., it had very strong positive feedback), and its main utility was in studying the role of I_{NaP} . To properly model the system, which we now know much more

about, will require realistic coupling strategies and population sizes that represent the heterogeneity observed in the real system, and additional intrinsic and synaptic currents that were not considered in the Butera model.

Our framework for analyzing respiratory rhythmogenesis is the *group-pacemaker hypothesis* (Feldman and Del Negro 2006; Reikling and Feldman 1998) which posits that an intrinsic inward current (e.g., I_{CAN}) enhances inspiratory bursts through an activation mechanism coupled to glutamatergic synapses. The synergy of an intrinsic current that amplifies synaptic excitation allows for the creation of robust inspiratory bursts via a positive feedback process dubbed 'recurrent excitation'. Inspiratory bursts are thought to end once all of the preBötC neurons have become fully excited: this activates outward currents extinguishing recurrent excitation which results in burst termination. A small fraction of preBötC neurons spike tonically at low rates and subsequently restarts the cycle, which leads to network rhythmic activity.

This dissertation aims to advance our understanding of the cellular, synaptic, and network mechanisms for breathing behavior in mammals. To this end, we explore the degree of overlap between neurons that have the expected phenotypic behavior of rhythmogenic neurons and those neurons that express NK1Rs (Chapter 1). This was achieved by using the fluorophore, tetramethylrhodamine (TMR), conjugated to SP (Pagliardini et al. 2005). The TMR-SP conjugate is thought to bind to NK1R-expressing neurons and be drawn into them through endocytosis. This allowed us to visually identify which neurons were SP-sensitive after electrophysiologically recording from them. The motivation for this chapter was to gather data needed to develop a realistic model of the rhythm-generating circuitry and later test it. The experimental data incorporated into the model constituted the fraction of rhythmogenic neurons that would be expected to be SP-sensitive. In this study, we also characterized the SP-evoked current in preBötC

neurons as primarily mediated by a voltage-insensitive, mixed cation current and offered a rough estimate of the number of critical neurons necessary for normal inspiratory activity.

In the subsequent analysis, we characterized I_A in inspiratory neurons of the preBötC (Chapter 2). I_A 's characteristics and role in inspiratory activity have remained elusive since it was first suggested to be present in these neurons (Rekling et al. 1996). We used somatic outside-out patch recordings to reliably describe the voltage-dependence and kinetics of the current. We also explored how blockade of I_A affects network rhythm and neuronal behaviors. I_A appears to strongly shape the ascending ("step-like") pattern preceding inspiratory activity as well as providing coincidence detection so that neurons expressing this current only drive postsynaptic neurons if the neuron receives massive convergent input. These data will be important for realistic mathematical models of preBötC neurons and networks but has largely been overlooked thus far in attempts to model respiratory rhythm generation (Butera et al. 1999a; b; Del Negro et al. 2001).

In the third chapter, we present a framework for the composition of the rhythm-generating preBötC population and investigate the collective behavior of these neurons when assembled into a preBötC-like respiratory network model; this is the first explicit model of the group-pacemaker hypothesis. The mathematical model comprises distinct phenotypes of respiratory neurons (which we characterized in Chapter 1), is synaptically coupled in a manner that is consistent with the available data (Pace et al. 2007a; Rekling et al. 2000), and provides for motor output, again according to known data about premotoneurons (Chapter 1). The aim of this chapter was to investigate how a heterogeneous population of neurons can undergo recurrent excitation, and then to investigate how recurrent excitation can drive rhythmic inspiratory-like bursts in a system

like the preBötC. We benchmarked and test the model by trying to replicate key experiments performed in our lab, and by our colleagues, in recent years. For example, we sought to determine whether the model would accurately reproduce *in vitro* and *in vivo* tests of the necessity of I_{Na-P} for rhythmic behavior. And in a more ambitious test, we used the model to test how graded neuronal destruction in the preBötC can abruptly result in loss of rhythmic motor output, which was based on the NKR-cell lesion experiments mentioned above. Here we gain new insights into the mechanisms of cell-death leading to arrhythmic conditions and the origins of apneas following lesions.

The fourth chapter examines evidence suggesting the presence of a potentially important convergent mechanism for modulating the excitability of inspiratory neurons. This objective resulted from the discovery in the first chapter that a particular intrinsic current mediates the response to the agonist for NK1Rs. The aim of this chapter is to further describe the means of activation of this current as well as to discover the sub-cellular molecular mechanisms for this current. Furthermore, we explore the idea that this current may potentially be evoked by multiple neuromessengers that can modulate respiratory activity under different physiological conditions. We begin to analyze the intracellular second messenger systems that affect the recruitment and regulation of these channels and suggest the areas of convergence with other modulatory systems.

We hope that the data and tests contained in this dissertation, which have been designed to bridge *in vivo* as well as *in vitro* and anatomical studies, will be the basis for new tests *in vivo* and in freely behaving adult mammals, rodents especially, to advance our understanding of breathing's neural origins. Furthermore, the new knowledge we provide, may in some small part, enable new approaches for the treatment of breathing disorders with a central nervous system-related etiology.

References

Amir RE, Van den Veyver IB, Wan M, Tran CQ, Francke U, and Zoghbi HY. Rett syndrome is caused by mutations in X-linked MECP2, encoding methyl-CpG-binding protein 2. *Nat Genet* 23: 185-188, 1999.

Arnulf I, Similowski T, Salachas F, Garma L, Mehiri S, Attali V, Behin-Bellhesen V, Meininger V, and Derenne JP. Sleep disorders and diaphragmatic function in patients with amyotrophic lateral sclerosis. *Am J Respir Crit Care Med* 161: 849-856, 2000.

Barthlen GM, and Lange DJ. Unexpectedly severe sleep and respiratory pathology in patients with amyotrophic lateral sclerosis. *Eur J Neurol* 7: 299-302, 2000.

Bianchi AL, Denavit-Saubie M, and Champagnat J. Central control of breathing in mammals: neuronal circuitry, membrane properties, and neurotransmitters. *Physiol Rev* 75: 1-45, 1995.

Blessing WW. *The lower brainstem and bodily homeostasis.* New York: Oxford University Press, 1997, p. 575.

Butera RJ, Jr., Rinzel J, and Smith JC. Models of respiratory rhythm generation in the pre-Bötzinger complex. I. Bursting pacemaker neurons. *J Neurophysiol* 82: 382-397, 1999a.

Butera RJ, Jr., Rinzel J, and Smith JC. Models of respiratory rhythm generation in the pre-Bötzinger complex. II. Populations Of coupled pacemaker neurons. *J Neurophysiol* 82: 398-415, 1999b.

Byrne JH. Analysis of ionic conductance mechanisms in motor cells mediating inking behavior in *Aplysia californica*. *J Neurophysiol* 43: 630-650, 1980.

Chen ML, and Keens TG. Congenital central hypoventilation syndrome: not just another rare disorder. *Paediatr Respir Rev* 5: 182-189, 2004.

Chen ZB, Engberg G, Hedner T, and Hedner J. Antagonistic effects of somatostatin and substance P on respiratory regulation in the rat ventrolateral medulla oblongata. *Brain Res* 556: 13-21, 1991.

Chen ZB, Hedner J, and Hedner T. Local effects of substance P on respiratory regulation in the rat medulla oblongata. *J Appl Physiol* 68: 693-699, 1990.

Connelly CA, Dobbins EG, and Feldman JL. Pre-Bötzinger complex in cats: respiratory neuronal discharge patterns. *Brain Res* 590: 337-340, 1992.

Del Negro CA, Johnson SM, Butera RJ, and Smith JC. Models of respiratory rhythm generation in the pre-Bötzinger complex. III. Experimental tests of model predictions. *J Neurophysiol* 86: 59-74, 2001.

Del Negro CA, Koshiya N, Butera RJ, Jr., and Smith JC. Persistent sodium current, membrane properties and bursting behavior of pre-bötzinger complex inspiratory neurons in vitro. *J Neurophysiol* 88: 2242-2250, 2002a.

Del Negro CA, Morgado-Valle C, and Feldman JL. Respiratory rhythm: an emergent network property? *Neuron* 34: 821-830, 2002b.

Del Negro CA, Morgado-Valle C, Hayes JA, Mackay DD, Pace RW, Crowder EA, and Feldman JL. Sodium and Calcium Current-Mediated Pacemaker Neurons and Respiratory Rhythm Generation. *J Neurosci* 25: 446-453, 2005.

Dobbins EG, and Feldman JL. Brainstem network controlling descending drive to phrenic motoneurons in rat. *J Comp Neurol* 347: 64-86, 1994.

Ellenberger HH, and Feldman JL. Subnuclear organization of the lateral tegmental field of the rat. I: Nucleus ambiguus and ventral respiratory group. *J Comp Neurol* 294: 202-211, 1990.

Feldman JL, and Del Negro CA. Looking for inspiration: new perspectives on respiratory rhythm. *Nat Rev Neurosci* 7: 232, 2006.

Feldman JL, and McCrimmon DR. Neural control of breathing. In: *Fundamental neuroscience*, edited by Zigmond MJ. San Diego: Academic Press, 1999, p. 1063-1090.

Feldman JL, and McCrimmon DR. Neural control of breathing. In: *FUNDAMENTAL NEUROSCIENCE*, edited by Squire LR, Bloom FE, McConnell SK, Roberts JL, Spitzer NC, and Zigmond MJ. Academic Press, 2002, p. Chapter 37.

Feldman JL, McCrimmon DR, Smith JC, Ellenberger HH, and Speck DF. Respiratory pattern generation in mammals. In: *Neurobiology of the Control of Breathing, 10th Nobel Symposium*, edited by von Euler C, and Lagercrantz H. New York: Raven Press, 1986, p. 157-164.

Feldman JL, Mitchell GS, and Nattie EE. Breathing: rhythmicity, plasticity, chemosensitivity. *Annu Rev Neurosci* 26: 239-266, 2003.

Funk GD, Smith JC, and Feldman JL. Generation and transmission of respiratory oscillations in medullary slices: role of excitatory amino acids. *J Neurophysiol* 70: 1497-1515, 1993.

Ge Q, and Feldman JL. AMPA receptor activation and phosphatase inhibition affect neonatal rat respiratory rhythm generation. *J Physiol* 509 (Pt 1): 255-266, 1998.

Getting PA. Mechanisms of pattern generation underlying swimming in Tritonia. III. Intrinsic and synaptic mechanisms for delayed excitation. *J Neurophysiol* 49: 1036-1050, 1983.

Gozal D. New concepts in abnormalities of respiratory control in children. *Curr Opin Pediatr* 16: 305-308, 2004.

Gray PA, Janczewski WA, Mellen N, McCrimmon DR, and Feldman JL. Normal breathing requires preBötzinger complex neurokinin-1 receptor-expressing neurons. *Nat Neurosci* 4: 927-930, 2001.

Gray PA, Rekling JC, Bocchiaro CM, and Feldman JL. Modulation of respiratory frequency by peptidergic input to rhythmogenic neurons in the preBötzinger complex. *Science* 286: 1566-1568, 1999.

Greer JJ, Smith JC, and Feldman JL. Role of excitatory amino acids in the generation and transmission of respiratory drive in neonatal rat. *J Physiol* 437: 727-749, 1991.

Guyenet PG, and Wang H. Pre-Bötzinger Neurons With Preinspiratory Discharges "In Vivo" Express NK1 Receptors in the Rat. *J Neurophysiol* 86: 438-446, 2001.

Inyushkin AN. Thyroliberin blocks the potassium A-current in neurons in the respiratory center of adult rats in vitro. *Neurosci Behav Physiol* 35: 549-554, 2005.

Janczewski WA, and Feldman JL. Distinct rhythm generators for inspiration and expiration in the juvenile rat. *J Physiol* 570: 407-420, 2006.

Janczewski WA, Onimaru H, Homma I, and Feldman JL. Opioid-resistant respiratory pathway from the preinspiratory neurones to abdominal muscles: in vivo and in vitro study in the newborn rat. *J Physiol* 545: 1017-1026, 2002.

Johnson SM, Smith JC, Funk GD, and Feldman JL. Pacemaker behavior of respiratory neurons in medullary slices from neonatal rat. *J Neurophysiol* 72: 2598-2608, 1994.

Lieske SP, and Ramirez JM. Pattern-specific synaptic mechanisms in a multifunctional network. II. Intrinsic modulation by metabotropic glutamate receptors. *J Neurophysiol* 95: 1334-1344, 2006.

Lieske SP, Thoby-Brisson M, Telgkamp P, and Ramirez JM. Reconfiguration of the neural network controlling multiple breathing patterns: eupnea, sighs and gasps [see comment]. *Nat Neurosci* 3: 600-607, 2000.

Manzke T, Guenther U, Ponimaskin EG, Haller M, Dutschmann M, Schwarzacher S, and Richter DW. 5-HT₄(a) receptors avert opioid-induced breathing depression without loss of analgesia. *Science* 301: 226-229, 2003.

Maria B, Sophia S, Michalis M, Charalampos L, Andreas P, John ME, and Nikolaos SM. Sleep breathing disorders in patients with idiopathic Parkinson's disease. *Respir Med* 97: 1151-1157, 2003.

McKay LC, Janczewski WA, and Feldman JL. Sleep-disordered breathing after targeted ablation of preBötzinger complex neurons. *Nat Neurosci* 8: 1142-1144, 2005.

Mellen NM, Janczewski WA, Bocchiaro CM, and Feldman JL. Opioid-induced quantal slowing reveals dual networks for respiratory rhythm generation. *Neuron* 37: 821-826, 2003.

Munschauer FE, Loh L, Bannister R, and Newsom-Davis J. Abnormal respiration and sudden death during sleep in multiple system atrophy with autonomic failure. *Neurology* 40: 677-679, 1990.

Murakoshi T, Suzue T, and Tamai S. A pharmacological study on respiratory rhythm in the isolated brainstem-spinal cord preparation of the newborn rat. *British journal of pharmacology* 86: 95-104, 1985.

Onimaru H, Arata A, and Homma I. Neuronal mechanisms of respiratory rhythm generation: an approach using in vitro preparation. *Jpn J Physiol* 47: 385-403, 1997.

Onimaru H, and Homma I. A novel functional neuron group for respiratory rhythm generation in the ventral medulla. *J Neurosci* 23: 1478-1486, 2003.

Pace RW, Mackay DD, Feldman JL, and Del Negro CA. Inspiratory bursts in the preBötzinger Complex depend on a calcium-activated nonspecific cationic current linked to glutamate receptors. *J Physiol jphysiol*.2007.133660, 2007a.

Pace RW, Mackay DD, Feldman JL, and Del Negro CA. Role of persistent sodium current in mouse preBötzinger Complex neurons and respiratory rhythm generation. *J Physiol* 580: 485-496, 2007b.

Pagliardini S, Adachi T, Ren J, Funk GD, and Greer JJ. Fluorescent Tagging of Rhythmically Active Respiratory Neurons within the Pre-Bötzinger Complex of Rat Medullary Slice Preparations. *J Neurosci* 25: 2591-2596, 2005.

Paton JF, Abdala AP, Koizumi H, Smith JC, and St-John WM. Respiratory rhythm generation during gasping depends on persistent sodium current. *Nat Neurosci* 9: 311-313, 2006.

Pena F, Parkis MA, Tryba AK, and Ramirez JM. Differential Contribution of Pacemaker Properties to the Generation of Respiratory Rhythms during Normoxia and Hypoxia. *Neuron* 43: 105-117, 2004.

Pena F, and Ramirez JM. Substance P-mediated modulation of pacemaker properties in the mammalian respiratory network. *J Neurosci* 24: 7549-7556, 2004.

Ptak K, Zummo GG, Alheid GF, Tkatch T, Surmeier DJ, and McCrimmon DR. Sodium Currents in Medullary Neurons Isolated from the Pre-Bötzinger Complex Region. *J Neurosci* 25: 5159-5170, 2005.

Purvis LK, Smith JC, Koizumi H, and Butera RJ. Intrinsic bursters increase the robustness of rhythm generation in an excitatory network. *J Neurophysiol* 97: 1515-1526, 2007.

Ramirez JM, and Lieske SP. Commentary on the definition of eupnea and gasping. *Respir Physiol Neurobiol* 139: 113-119, 2003.

Ramirez JM, Zuperku EJ, Alheid GF, Lieske SP, Ptak K, and McCrimmon DR. Respiratory rhythm generation: converging concepts from in vitro and in vivo approaches? *Respir Physiol Neurobiol* 131: 43-56, 2002.

Rekling JC, Champagnat J, and Denavit-Saubie M. Electroresponsive properties and membrane potential trajectories of three types of inspiratory neurons in the newborn mouse brain stem in vitro. *J Neurophysiol* 75: 795-810, 1996.

Rekling JC, and Feldman JL. PreBötzinger complex and pacemaker neurons: hypothesized site and kernel for respiratory rhythm generation. *Annu Rev Physiol* 60: 385-405, 1998.

Rekling JC, Shao XM, and Feldman JL. Electrical coupling and excitatory synaptic transmission between rhythmogenic respiratory neurons in the preBötzinger complex. *J Neurosci* 20: RC113, 2000.

Richter DW, and Spyer KM. Studying rhythmogenesis of breathing: comparison of in vivo and in vitro models. *Trends Neurosci* 24: 464-472, 2001.

Rybak IA, Ptak K, Shevtsova NA, and McCrimmon DR. Sodium Currents in Neurons from the Rostroventrolateral Medulla of the Rat. *J Neurophysiol* 90: 1635-1642, 2003.

Schwarzacher SW, Smith JC, and Richter DW. Pre-Bötzinger complex in the cat. *J Neurophysiol* 73: 1452-1461, 1995.

Smith JC, Ellenberger HH, Ballanyi K, Richter DW, and Feldman JL. Pre-Bötzinger complex: a brainstem region that may generate respiratory rhythm in mammals. *Science* 254: 726-729, 1991.

Smith JC, and Feldman JL. In vitro brainstem-spinal cord preparations for study of motor systems for mammalian respiration and locomotion. *J Neurosci Methods* 21: 321-333, 1987.

Smith JC, Greer JJ, Liu GS, and Feldman JL. Neural mechanisms generating respiratory pattern in mammalian brain stem-spinal cord in vitro. I. Spatiotemporal patterns of motor and medullary neuron activity. *J Neurophysiol* 64: 1149-1169, 1990.

Stocchi F, Barbato L, Nordera G, Berardelli A, and Ruggieri S. Sleep disorders in Parkinson's disease. *J Neurol* 245 Suppl 1: S15-18, 1998.

Stornetta RL, Rosin DL, Wang H, Sevigny CP, Weston MC, and Guyenet PG. A group of glutamatergic interneurons expressing high levels of both neurokinin-1 receptors and somatostatin identifies the region of the pre-Bötzinger complex. *J Comp Neurol* 455: 499-512, 2003.

Suzue T. Respiratory rhythm generation in the in vitro brain stem-spinal cord preparation of the neonatal rat. *J Physiol* 354: 173-183, 1984.

Tierney AJ, and Harris-Warrick RM. Physiological role of the transient potassium current in the pyloric circuit of the lobster stomatogastric ganglion. *J Neurophysiol* 67: 599-609, 1992.

Vasilakos K, Wilson RJ, Kimura N, and Remmers JE. Ancient gill and lung oscillators may generate the respiratory rhythm of frogs and rats. *J Neurobiol* 2004.

Vetrugno R, Provini F, Cortelli P, Plazzi G, Lotti EM, Pierangeli G, Canali C, and Montagna P. Sleep disorders in multiple system atrophy: a correlative video-polysomnographic study. *Sleep Med* 5: 21-30, 2004.

Wang H, Stornetta RL, Rosin DL, and Guyenet PG. Neurokinin-1 receptor-immunoreactive neurons of the ventral respiratory group in the rat. *J Comp Neurol* 434: 128-146, 2001.

Weese-Mayer DE, Zhou L, Berry-Kravis EM, Maher BS, Silvestri JM, and Marazita ML. Association of the serotonin transporter gene with sudden infant death syndrome: a haplotype analysis. *Am J Med Genet A* 122: 238-245, 2003.

CHAPTER 1. Neurokinin receptor-expressing preBötzing Complex neurons in neonatal mice studied *in vitro*

1.1. Introduction

Breathing behavior in mammals is generated by respiratory neurons in the medullary brain stem (Ballanyi et al. 1999; Bianchi et al. 1995; Blessing 1997). A critical issue is the role of neurons that both express neurokinin-1 receptors (NK1Rs) and reside in the critical site for inspiratory breathing behavior, the preBötC (Gray et al. 2001; Gray et al. 1999; Guyenet and Wang 2001; Janczewski and Feldman 2006; Smith et al. 1991; Stornetta et al. 2003a; Wang et al. 2001).

Substance P (SP) is an endogenous agonist for NKRs, which is most potent at NK1Rs (Medhurst and Hay 2002), but may also activate other tachykinin receptors. SP accelerates respiratory rhythm *in vitro* and has been shown to depolarize every preBötC neuron recorded intracellularly after pharmacologically silencing network activity (Gray et al. 1999; Murakoshi et al. 1985; Pena and Ramirez 2004). Neurons with *early inspiratory* activity discharge with an ascending ramp-like voltage trajectory, prior to the inspiratory motor output phase of the respiratory cycle, and are widely considered important for rhythmogenesis (Bianchi et al. 1995; Feldman and Del Negro 2006; Onimaru et al. 1989; Onimaru and Homma 1992; Ramirez et al. 2002; Richter and Spyer 2001; Smith et al.

1991). Neurons with early inspiratory activity *in vivo*, which were dubbed *pre-inspiratory* (Guyenet and Wang 2001), express NK1Rs detectable with immunohistochemistry, whereas non-inspiratory neurons that may have other respiratory-related functions are NK1R⁻ (Guyenet and Wang 2001). A large number of bulbospinal premotor neurons in the preBötC, which discharge later in the respiratory cycle compared to early inspiratory neurons, also express NKRs (Guyenet et al. 2002; Stornetta et al. 2003b).

The ribosomal toxin saporin (SAP) conjugated to SP, i.e., SP-SAP, leads to the abolition of normal breathing in otherwise intact and awake rats when injected into the preBötC (Gray et al. 2001; McKay et al. 2005). These observations are consistent with the hypothesis that the preBötC contains NKR⁺ interneurons that respond vigorously to SP and share phenotypic inspiratory discharge properties specialized for rhythm generation (Feldman and Del Negro 2006; Gray et al. 1999). However, the relative number of NKR⁺ and NKR⁻ preBötC neurons that serve rhythmogenic and/or premotor functions remains unknown, and the mechanism underlying the widespread excitatory effects of SP are not well understood.

We examined these issues *in vitro* using fluorescent labeling to identify SP-sensitive neurons that presumably express NKRs, as assessed by their ability to internalize the fluorescent marker tetramethylrhodamine (TMR) conjugated to SP, i.e., TMR-SP (Pagliardini et al. 2005). We recorded TMR-SP⁺ and TMR-SP⁻ neurons and characterized their membrane properties and inspiratory discharge patterns. We examined the ionic mechanism for SP-evoked excitation and may now be able to explain how SP ubiquitously depolarizes preBötC neurons even though only a limited subset appear to express NKRs.

1.2 Methods

The Institutional Animal Care and Use Committee at the College of William and Mary approved all protocols. Transverse slices (550 μm thick) from neonatal (P0-7) C57BL/6 mice were dissected as described previously (Del Negro et al. 2005; Pace et al. 2007). With the neuraxis pinned to a paraffin-coated block, oriented rostral side up with its ventral surface facing forward, we cut into the preBötC at the rostral surface to expose the putatively rhythmogenic neuron population. Based on objective criteria now verified by the 'online histology' atlas published by the Ballanyi group (Ruangkittisakul et al. 2006), we make the first cut above the rostral-most XII nerve roots at the level of the dorsomedial cell column and principal lateral loop of the Inferior Olivary nucleus, thus the preBötC is located at or near the rostral surface (Ruangkittisakul et al. 2006). The caudal cut always captures the obex. Therefore, we record from the rostral side of the slice where the preBötC neurons are exposed and never from the caudal side.

Slices were perfused at 26-28°C with an artificial cerebrospinal fluid (ACSF) containing (in mM): 124 NaCl, 9 KCl, 0.5 NaH_2PO_4 , 25 NaHCO_3 , 30 D-glucose, 1.5 $\text{CaCl}_2 \cdot \text{H}_2\text{O}$, and 1 MgSO_4 . We used 21 slices for the epifluorescence electrophysiology/imaging data (Figs. 1.1, 1.2, 1.3, 1.4, 1.5, 1.10), and report data from 29 slices for the two-photon/confocal imaging experiments (Figs. 1.9, 1.10), and 33 slices for the voltage-clamp experiments (Figs. 1.6-1.8, 1.10). To avoid tachyphylaxis and other consequences of multiple drug applications, each slice was used for one type of experiment: electrophysiological recordings of preBötC neurons following TMR-SP labeling, voltage-clamp experiments to characterize SP-evoked membrane current, or acquisition from a two-photon/confocal imaging experiment.

Electrophysiology

Voltage-clamp and current-clamp experiments were performed with a HEKA EPC-10 patch-clamp amplifier (Lambrecht, Germany). Network activity was monitored from XII nerves with extracellular suction electrodes and a high-gain differential amplifier with band-pass filtering (0.3-1 kHz). The root-mean-square (RMS) of voltage input to the differential amplifier (Dagan Instruments, Minneapolis, MN) was conditioned using a true RMS-to-DC converter (Analog Devices, One Technology Way, Norwood, MA) to provide a full-wave rectified and smoothed XII waveform. Data were acquired digitally and analyzed using Igor Pro 5 (WaveMetrics, OR), Chart 5 (AD Instruments, Colorado Springs, CO), Excel (Microsoft, Redmond, WA) and custom software. An 8 mV liquid junction potential was corrected offline in current-clamp recordings and online in voltage-clamp recordings.

Whole-cell capacitance (C_M) was measured using 50-ms voltage steps from -60 mV to command potentials from -75 mV to -65 mV in a 10-step sequence. Charge (Q) was computed by integrating leak-subtracted capacitive current ($\Delta Q = \int I_C$) and C_M was calculated from $C_M = \Delta Q / \Delta V$. Series (access) resistance (R_S) was monitored throughout voltage-clamp recordings according to the Thevenin equivalent circuit, which allows R_S to be calculated from the decay time constant (τ_m) in response to small voltage steps with $R_S = \tau_m / C_M$ as long as $R_S \ll R_N$. We monitored input resistance (R_N) via P/N online leak protocols. To avoid voltage-clamp errors we discarded experiments in which $R_S > 0.1 \cdot R_N$. We compensated for R_S as much as possible without loss of stability. We also rechecked R_S and R_N before each IV protocol to assess voltage-clamp viability. The average uncompensated R_S was 20.2 ± 2.0 M Ω with an average of $37 \pm 3\%$ R_S compensation, and the average R_N was 355.3 ± 84.2 M Ω ($n=24$). Firing patterns of

recorded neurons were consistent in on-cell and whole-cell and remained constant for the duration of the experiments, which in current clamp could last 40-60 min.

Current-clamp protocols (Figs. 1.4 and 1.5) and some voltage-clamp recordings (Fig. 1.6) used the following patch solution containing (in mM): 140 K-gluconate, 5 NaCl, 0.1 EGTA, 10 HEPES, 2 Mg-ATP, and 0.3 Na(3)-GTP. KOH was used to equilibrate pH at 7.2.

Voltage-clamp experiments in Figs. 1.7 and 1.8 used ACSF containing (in mM): 84 NaCl, 3 KCl, 20-40 TEA-Cl, 25 NaHCO₃, 5 4-AP, 30 D-glucose, 0.5 CaCl₂, 2 MgSO₄, 2 CsCl, 0.2 CdCl₂, 20-40 sucrose (for equimolar balancing with TEA-Cl), and 0.001 TTX. Patch electrodes (4-6 MΩ) contained the following solution (in mM): 140 D-gluconic acid, 140 CsOH monohydrate, 10 TEA-Cl, 10 NaCl, 10 HEPES, 2.5 EGTA, 1.2 CaCl₂ dihydrate, 2 Mg-ATP, and 0.3 Na(3)-GTP, with pH adjusted to 7.2 via HCl.

Epifluorescence microscopy

Slices were incubated in 1 μM TMR-SP (Invitrogen, Carlsbad, CA) for 8-12 minutes at 32°C, and then moved to the perfusion chamber for intracellular recording. We visualized preBötC neurons with Koehler illumination and differential interference contrast (DIC) videomicroscopy, which facilitated patch-clamp recordings, and then switched to epifluorescence (X-cite-120, EXFO, Mississauga, Ontario, Canada) and a rhodamine filter to capture TMR-SP. Positively labeled neurons (TMR-SP⁺) were distinguished by labeling around the somatic border, in a perinuclear area, and occasionally along dendrites (e.g., Figs. 1.1 and 1.5). TMR-SP labeling became more diffuse over time (>1-2 hrs) (Grady et al. 1995).

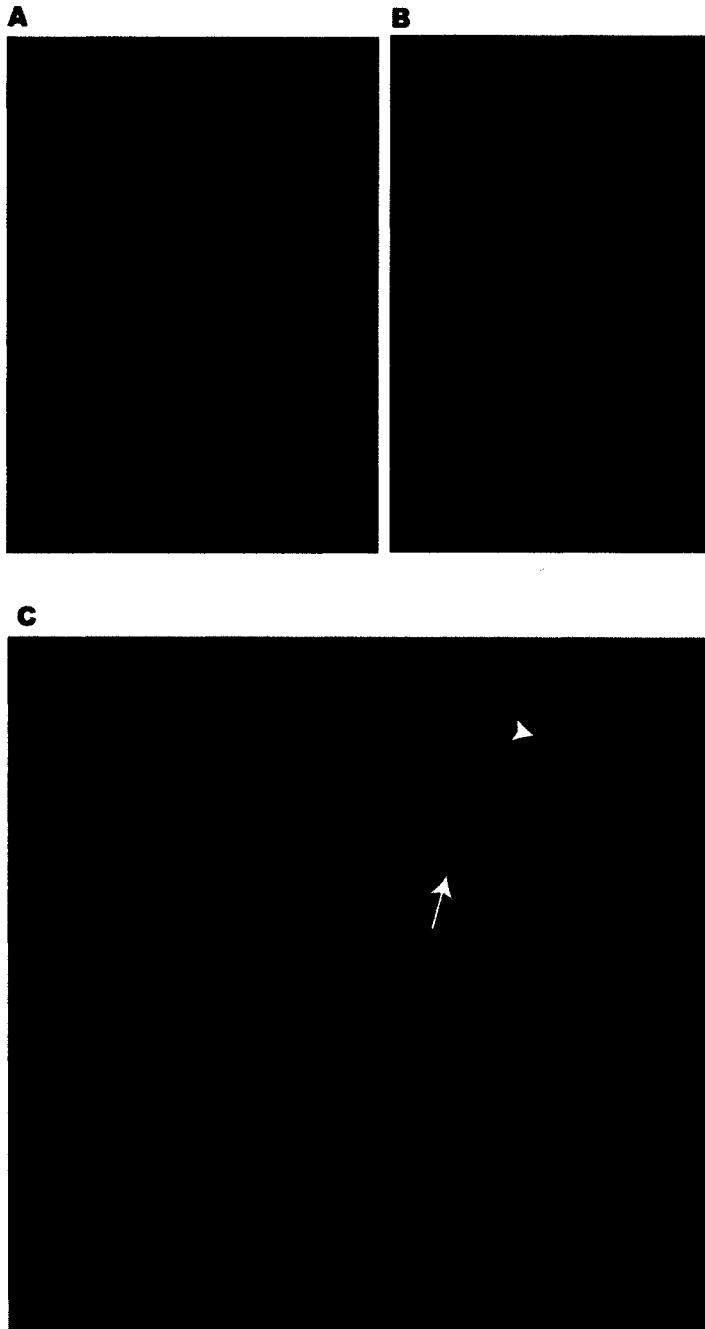


Figure 1.1. **A**, TMR-SP labeling with epifluorescence illustrating the punctate labeling of cells in the preBötC region. **B**, A higher magnification picture of the cell from **A** to emphasize punctate features of the labeling. **C**, TMR-SP labeling observed with TPLSM in the absence of fluo-4. Nucleus ambiguus is oriented in the bottom-left and the preBötC with TMR-SP⁺ cells shown in the top-right region. The arrow-head shows labeling in vesicles around the nucleus of the neuron, while the arrow shows labeling on the surface of another neuron.

Control experiments

were performed (Fig. 1.2) by pre-incubating a slice in 10 μ M unconjugated SP for 5 minutes at 32 $^{\circ}$ C, and then applying 1 μ M TMR-SP following the protocol described above. After exposure to both forms of SP, only sparse TMR-SP labeling could be detected in regions that included the preBötC; the extent of the labeling was

dramatically less than when TMR-SP was applied without prior exposure to unconjugated SP. This is most apparent in the nucleus ambiguus (NA, Bieger and Hopkins 1987), which is heavily populated by NK1R⁺ neurons and is adjacent to the preBötC dorsally (Gray et al. 1999; Pagliardini et al. 2005). In the control experiments, the NA

showed substantially less TMR-SP labeling (Fig. 1.2A) than using the standard TMR-SP loading protocol (Fig. 1.2B).

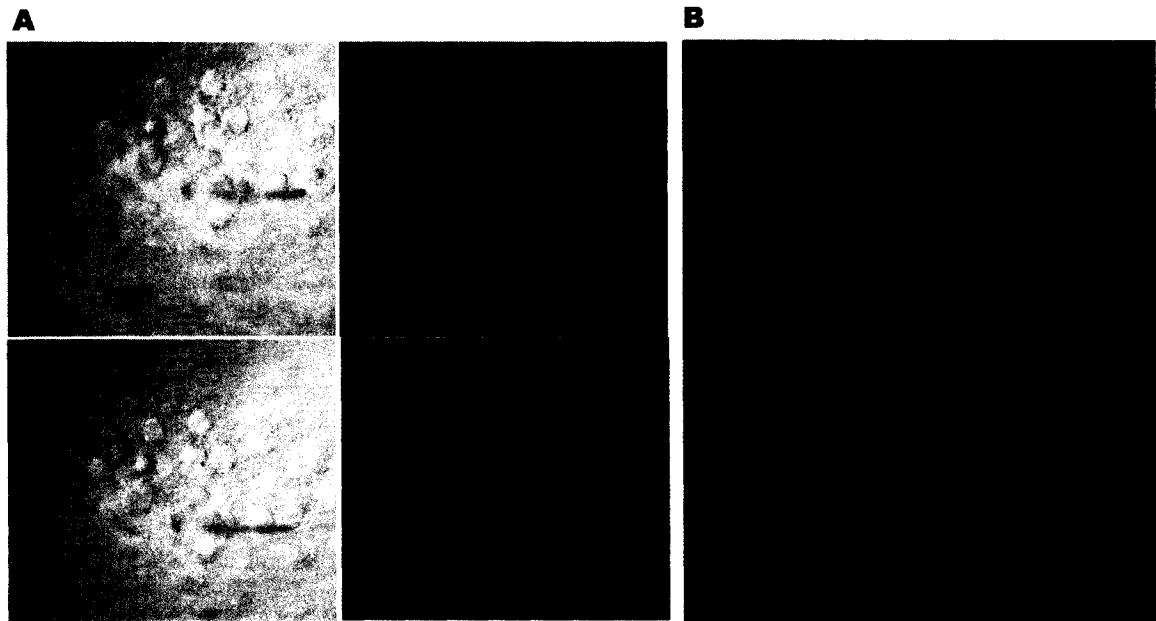


Figure 1.2. A, IR-DIC (left) and TMR-SP (right) images of the NA in tissue that was pre-incubated for 5 min with 10 μM SP before applying 1 μM TMR-SP. Top row shows NA on the left side of the slice, and bottom row shows NA on the right. B, NA from a separate slice that was just incubated in 1 μM TMR-SP.

Epifluorescence images were acquired with a 12-bit charge-coupled device (CCD) monochromatic camera, the QImaging Retiga 1300i (Surrey, British Columbia, Canada) using a long-working distance water immersion 40x objective with a 0.80 numerical aperture. Before image acquisition the pipette tip or somatic border was focused with IR-DIC videomicroscopy; IR-DIC images were typically exposed for 150-250 ms with 1x1 binning. Epifluorescence images were exposed for 10 s with 1x1 binning at maximum fluorescence intensity. The images were pseudocolored with a black-to-red look-up table in iVision software (Biovision Technologies, Exton, PA). Background subtraction was performed by plotting a histogram of pixel intensities and then truncating all values less than the lowest peak. For publication figures, we copied

images to Photoshop (Adobe Systems Inc., San Jose, CA) and enhanced contrast and applied a 1 pixel radius Gaussian blur.

Confocal and two-photon microscopy

Fifty μg of fluo-4 acetoxymethyl ester (fluo-4 AM) (Invitrogen, Carlsbad, CA) was dissolved in 50 μL of pluronic (20%) + DMSO (Invitrogen, Carlsbad, CA) and vortexed for 10 min. After that, 750 μL of 30 °C 9 mM $[\text{K}^+]$ ACSF was added to the dye solution and vortexed until the dye was evenly distributed. Then, the solution was divided into two tubes (~375 μL each) and an additional 375 μL of 30 °C 9 mM $[\text{K}^+]$ ACSF was added to each tube for a final concentration of 29.4 μM fluo-4-AM. Slices were incubated 40-50 minutes in 29.4 μM fluo-4 AM at 32°C, and then incubated in a separate chamber of 1 μM TMR-SP at 32°C for 10-14 min. We imaged cellular Ca^{2+} fluctuations using an inverted Nikon Radiance microscope (Nikon USA, Melville, NY) and a Mai-Tai Ti:sapphire femtosecond laser (Spectraphysics, Mountain View, CA) tuned to 800-nm excitation wavelength. Data were acquired digitally and saved to disk on a PC running Windows NT and LaserSharp software by Zeiss Microimaging (Thornwood, NY).

TMR-SP labeling was measured at the same workstation (without moving the slice) using a 543-nm Green HeNe laser at full intensity (1.5 mW), a pinhole size of 2.2 Airy units, at 512x512 pixels scanned with 25 lines per second (lps) using an accumulate feature to optimize the signal-to-noise ratio. This involved 30 scans per image where the pixel intensities of each scan were divided by two and added to the previous scans (~10 min acquisition time). We used a Nikon 40x Plan Fluor objective with a numerical aperture of 0.75 which resulted in a 5 μm depth of field. We acquired one green (500-530 nm) and one red (600-650 nm) channel for TMR-SP images. For each image, background correction was accomplished by subtracting the RMS of the pixel intensity

across the image from every pixel value. Then we renormalized each image and subtracted 8% of the green signal (the fluo-4 channel) from the red channel to correct for the overlap of the emission spectra, i.e., the portion of fluo-4 emission expected in the 600-650 nm band. Images were analyzed using iVision and ImageJ (NIH, Bethesda, MD). Like the epifluorescence data, for publication figures we copied images to Photoshop and enhanced contrast and applied a 1 pixel radius Gaussian blur.

Peak acquisitions (i.e., Fig. 1.9A fluo-4) were achieved by scanning the focal plane repeatedly at 25 lps (1024x1024 pixels) until at least one pixel saturated. Time-series recordings of Ca^{2+} activity (Fig. 1.9B) were scanned at 256x256 pixels and 500 lps (~2 Hz) for ~125 frames. Summed Ca^{2+} activity of time-series two-photon experiments (i.e., small inset panels in Fig. 1.9C) was plotted by taking the minimum pixel value for the whole time course of the acquisition bout and then subtracted this baseline from the entire time series. Then, we summed all the fluorescence measurements for the whole time series collapsed on to one aggregate image. This produces an image that convolves expiratory and inspiratory neurons (and other transiently active cells), highlighted in warm colors.

We scanned one plane per slice preparation for experiments that contained both TMR-SP and fluo-4; the imaging plane was <5 μm in thickness. Using the two-photon (Ti:Sapphire) laser to detect Ca^{2+} transients via fluo-4 fluorescence changes, we first probed for inspiratory neurons. If we detected inspiratory neurons in a given plane, then we applied a long-duration confocal scan to detect TMR-SP labeling using the 543 nm laser (HeNe). This long-lasting exposure at high intensity bleached TMR-SP thus we terminated the experiment after acquiring these data in the selected plane. If in a given plane we failed to detect inspiratory neurons, then we did not apply the long-duration

confocal scan but instead we incremented our z-axis by 5 μm (up to 30–40 μm into the tissue) to probe for inspiratory neurons in the adjacent tissue layer.

Some pilot experiments with just TMR-SP were performed using the Ti:Sapphire laser to investigate the viability of the labeling technique (Fig. 1.1C).

Statistics

We compared neurons on the basis of drive potential latency (see Fig. 1.4B), C_M , and TMR-SP labeling. We tested for normality and then applied Student's t-test or Wilcoxon signed ranks tests as appropriate to detect statistically significant differences. Mean values are reported with standard error (mean \pm SE).

We compared NKR expression in six different experimental approaches using a resampling method (Manley 1996). We used the fraction of NKR⁺ neurons detected in a given experiment as our benchmark, and then counted the number of times a uniformly distributed randomly generated number in the interval [0,1] fell below that fraction when drawing the same number of samples. We repeated this algorithm in 10,000 simulated experiments and tallied the outcomes to generate a histogram that reports the likelihood of each experimental sample drawn by chance. Removing the highest and lowest 250 counts yields the 95% credible interval for the experiment.

We tested whether the fraction of SP-sensitive neurons detected in voltage clamp (Fig. 1.7, 86.7%) was significantly higher than the TMR-SP⁺ fraction detected with other techniques. This was performed by comparing the SP-sensitive fraction detected in voltage-clamp (control) to the fraction of TMR-SP⁺ neurons found using epifluorescence imaging (Fig. 1.5) and confocal imaging (Fig. 1.9), SP-sensitive fraction in voltage-clamp with carbenoxolone (CBX, obtained from Sigma-Aldrich, St. Louis, MO) (Fig. 1.8), and we meta-analyzed the NK1R immunoreactive (NK1R-ir) data set taken from adult rats

(Guyenet and Wang 2001) and single-cell RT-PCR evidence for NK1Rs in inspiratory neurons of neonatal rats (Manzke et al. 2003). Altogether, the pooled fraction of neurons that show evidence of NK1R expression was 40% (Fig. 1.10). To calculate the likelihood of the voltage clamp experiment being different from the other experiments by chance, we used the above resampling technique and calculated a p-value by dividing the number of samples drawn that equaled or exceeded 86.7% (the SP-sensitive fraction in this experiment) by 10,000 simulated experiments.

1.3. Results

Electrical properties and TMR-SP labeling in inspiratory neurons

Inspiratory neurons were separable on the basis of multiple phenotypic properties (Figs. 1.3, 1.4). We measured C_M in preBötC neurons satisfying reliable voltage-clamp conditions (see Methods). We also characterized *inspiratory drive latency* in all neurons with reliable current-clamp recordings, defined as the difference between the onset of inspiratory EPSPs and the beginning of the XII motor output (Rekling et al. 1996). Figure 1.3A plots inspiratory drive latency versus C_M in neurons that had both reliable voltage- and current-clamp recordings. We found a subset of *early inspiratory* neurons with significantly longer latency (241.2 ± 8.4 ms, $n=8$) and lower C_M (45.6 ± 1.5 pF, $n=8$) compared to a subset of *late inspiratory* neurons that had significantly larger C_M (85.9 ± 6.5 pF, $n=5$) (t-test: $p < 0.01$) and shorter latency (103.7 ± 8.2 ms, $n=5$) (Wilcoxon: $p < 0.01$). Early inspiratory neurons showed an incremental discharge pattern (Fig. 1.3B left, note arrow) whereas late inspiratory neurons exhibited a rapid onset with decrementing discharge pattern (Fig. 1.3B right, note arrow).

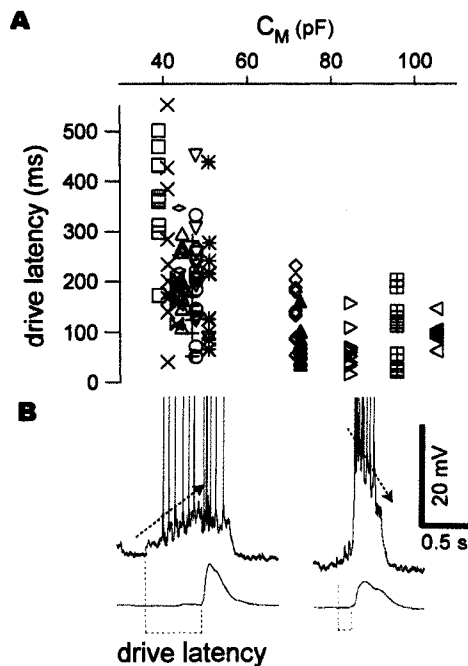


Figure 1.3. Intrinsic properties of inspiratory neurons in the preBötC. **A**, Inspiratory drive latency plotted versus C_M . Each symbol shows drive latency in a preBötC neuron for several consecutive cycles. **B**, A representative early inspiratory neuron is shown in the left with broken lines illustrating the measured latency. Arrow shows ascending voltage trajectory. A representative late inspiratory neuron is shown in the right, also with illustrated drive latency and an arrow showing decremting voltage trajectory.

Once we recognized the correlation between C_M and inspiratory drive latency we divided preBötC neurons into the two classes: (1) early inspiratory neurons had an average drive latency of 201.5 ± 8.1 ms ($n=22$, with a total of 256 latency measurements) and (2) late inspiratory neurons had an average drive latency of 88.9 ± 6.5 ms ($n=6$, with a total of 66 latency measurements). Inspiratory drive latency was significantly different between these two classes (t-test: $p < 0.05$).

Nine early inspiratory neurons showed a low baseline membrane potential and thus a silent interburst phase (Fig. 1.4A), whereas 13 spiked at low rates during the inter-inspiratory burst interval (Fig. 1.4B). One neuron exhibited ectopic bursts at depolarized baseline membrane potentials (Fig. 1.4C), suggesting voltage-dependent pacemaker properties (Del Negro et al. 2002; Del Negro et al. 2005; Ramirez et al. 2004; Smith et al. 1991; Thoby-Brisson and Ramirez 2001). These factors in early inspiratory neurons did not correlate with C_M so we did not further subdivide the early inspiratory data set.

After patch-recording we tested for TMR-SP labeling. TMR-SP labeled 8 of 22 (36.4%) early inspiratory neurons. Figure 1.4 shows one TMR-SP⁺ inspiratory neuron (A)

and two TMR-SP⁺ inspiratory neurons (B,C) with discharge properties described above. Four out of 6 late inspiratory neurons exhibited TMR-SP labeling (66.6%) as shown in Fig. 1.4D. For the combined sample of 28 early and late inspiratory neurons, 42.8% were TMR-SP⁺.

We also recorded TMR-SP⁺ expiratory neurons, which discharge at high rates throughout the interburst interval but are actively inhibited during the inspiratory phase (Fig. 1.4E, n=18). These data were surprising since adult rat expiratory neurons showed no NK1R immunoreactivity (Guyenet and Wang 2001). Finally, non-rhythmic TMR-SP⁺ cells were detected within the preBötC region but were not counted because their identity could not be verified *in vitro* (Fig. 1.5).

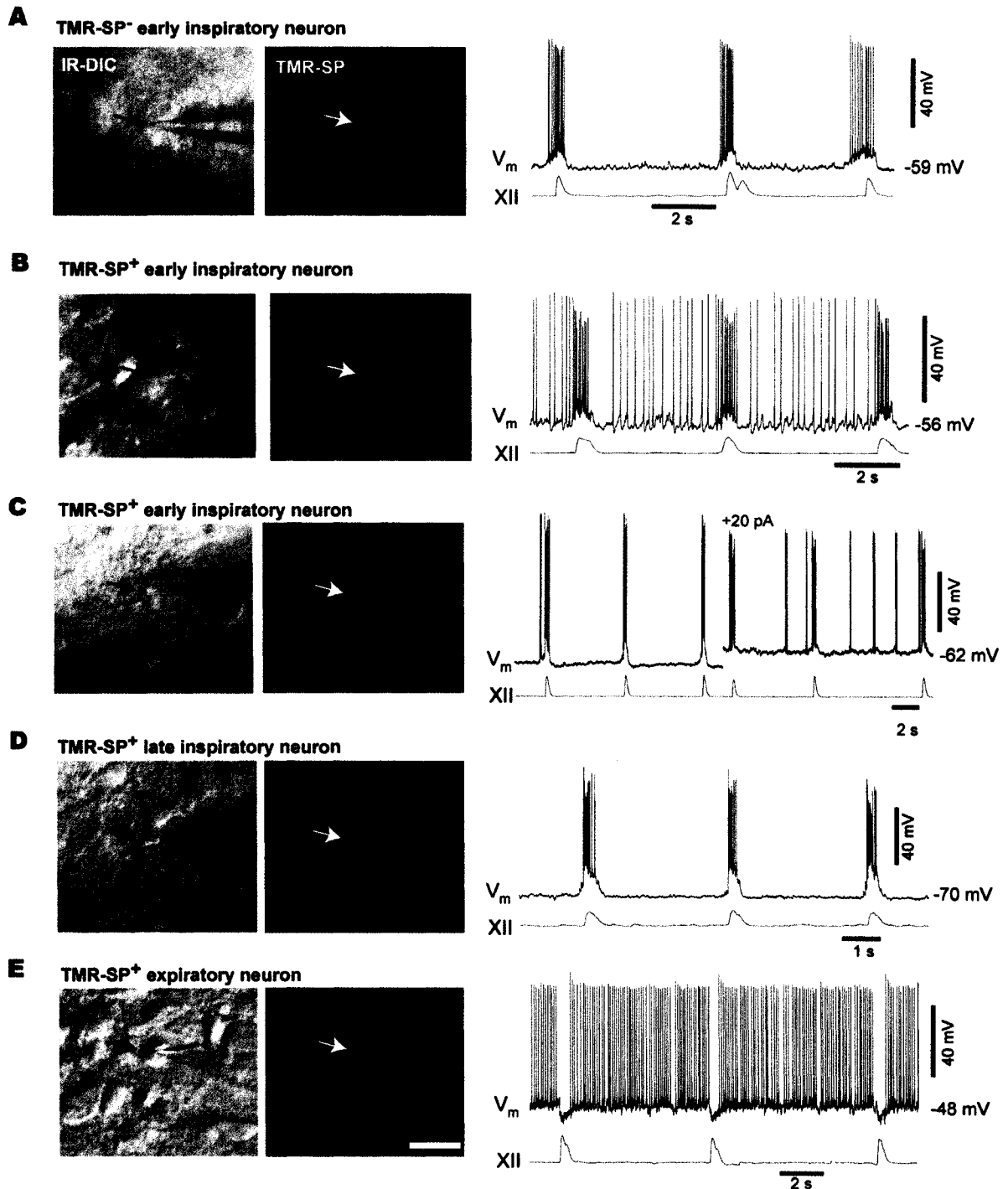


Figure 1.4. TMR-SP labeling in preBötC neurons with different phenotypic properties. IR-DIC and epifluorescence images are shown in left columns, with corresponding intracellular traces to the right. **A**, A TMR-SP⁻ early inspiratory neuron with silent interburst intervals. **B**, A TMR-SP⁺ early inspiratory neuron with tonic low-frequency spiking properties. **C**, A TMR-SP⁺ early inspiratory neuron with voltage-dependent pacemaker properties. **D**, A TMR-SP⁺ late inspiratory neuron. **E**, A TMR-SP⁺ expiratory neuron. Scale bar (25 μ m) applies to all images in A-E.

TMR-SP⁺ non-rhythmic neuron

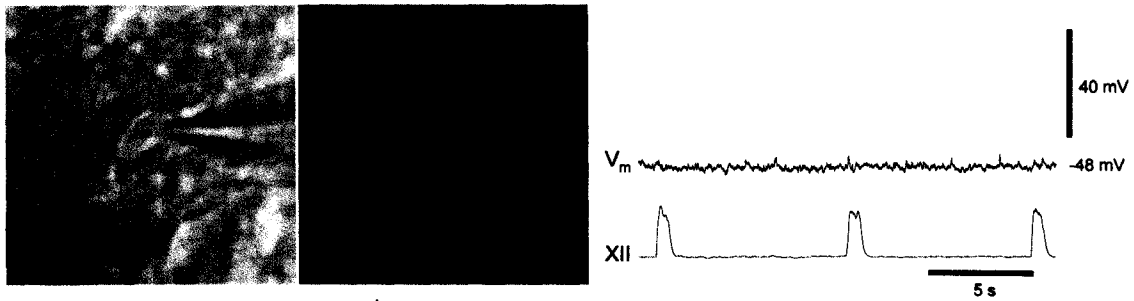


Figure 1.5. A TMR-SP⁺ non-rhythmic neuron near the preBötC.

Excitation of inspiratory neurons by substance P

SP has been hypothesized to excite preBötC inspiratory neurons by evoking a low-threshold, voltage-dependent, and TTX-insensitive Na⁺ current (Pena and Ramirez 2004). Since we were interested in SP-evoked excitation we did not pre-label neurons with TMR-SP to avoid NKR desensitization. We measured the steady-state current-voltage (IV) relationship with a K-gluconate patch solution and standard ACSF while blocking TTX-sensitive Na⁺ currents and Cd²⁺-sensitive voltage-gated Ca²⁺ currents (Fig. 1.6). The slope of the IV curve increased in 0.5-1 μ M SP and crossed the control IV curve at approximately -20 mV, which suggests the opening of a mixed cation channel (n=4).

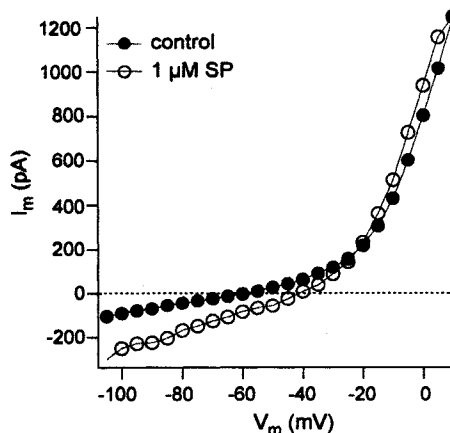


Figure 1.6. Effects of 1 μ M SP on inspiratory neurons. The steady-state IV relationship is shown for a typical experiment using K-gluconate patch solution and standard ACSF with 200 μ M Cd²⁺ and 1 μ M TTX.

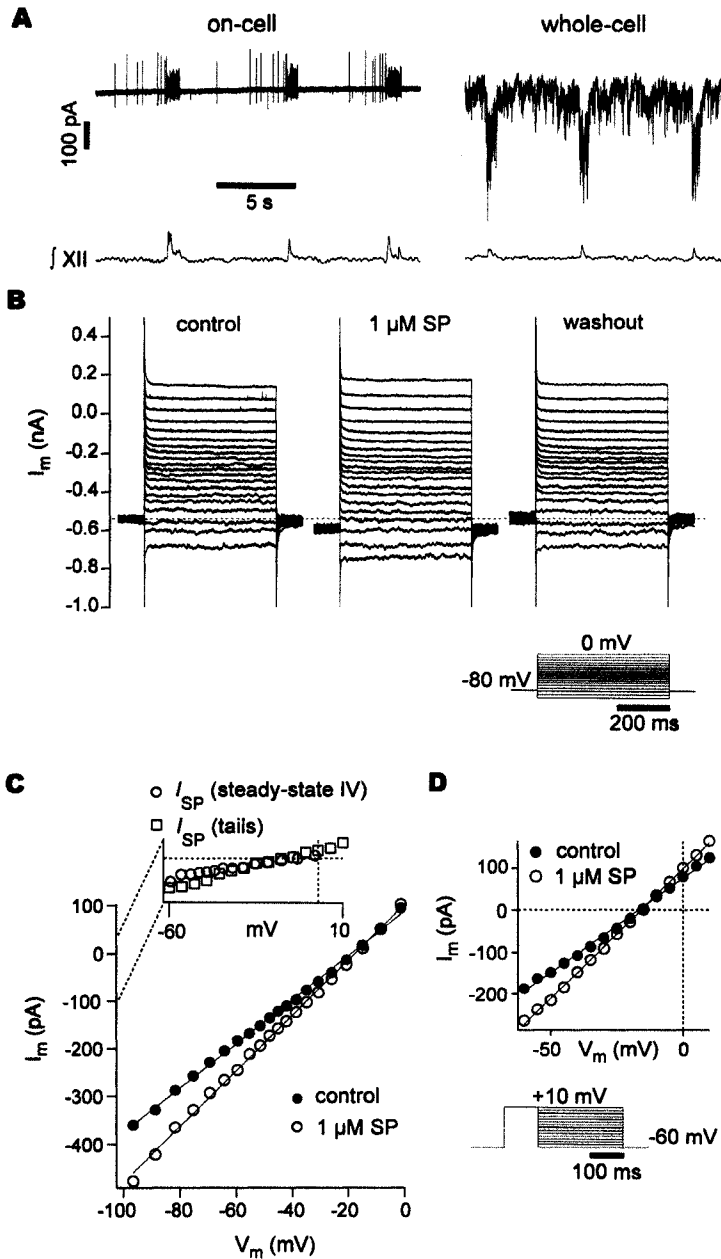


Figure 1.7. Effects of 1 μM SP on inspiratory neurons with additional blockade of K^+ channels. 200 μM Cd^{2+} and 1 μM TTX were present in the bath (as in Fig. 3) but the patch solution was based on Cs-gluconate and the ACSF contained a cocktail of K^+ channel antagonists (see Methods). **A**, On-cell and whole-cell recordings of a typical inspiratory neuron. **B**, Steady-state IV protocols showing the reversibility of the SP-evoked response. **C**, The steady-state IV curve and effects of SP. The inset shows I_{SP} obtained by subtraction (SP - control). **D**, Tail current analysis, protocol shown below the IV curve. I_{SP} obtained by subtraction using the tail protocol is also plotted in the inset of panel C.

To isolate the SP-induced current (I_{SP}) we used patch solution containing Cs^+ and TEA, with Cs^+ , TEA, and 4-AP in the ACSF to block K^+ currents and hyperpolarization-

activated cation current (I_{h}). We identified inspiratory neurons in the on-cell configuration (Fig. 1.7A) by observing the onset latency of inspiratory discharge. It was impossible to determine early vs. late inspiratory phenotypes because Cs^+ -patch solution elevates input resistance and depolarizes the reversal potential for chloride. Nevertheless, C_{M} ranged from 23.3-78.9 pF, (the mean C_{M} was 49.2 ± 7.0 pF, $n=9$), which suggests both

early and late inspiratory phenotypes were sampled (see Fig. 1.3). We measured the IV relationship in control and 1 μ M SP, and then obtained I_{SP} by subtraction (Fig. 1.7B,C). I_{SP} was linear (n=13) and reversed at $E_{SP} = -19.4 \pm 0.02$ mV (n=9), similar to the I_{SP} reversal potential measurement with the K-gluconate patch solution (Fig. 1.7).

Next, we examined whether I_{SP} expressed any voltage-dependent properties. Since the IV protocol could cause voltage-dependent inactivation of I_{SP} during 500-ms-long voltage steps, we analyzed tail currents from -60 to $+10$ mV following a prepulse to $+10$ mV for 100 ms (Fig. 1.7D). I_{SP} was computed by subtraction. We compared I_{SP} tail currents to steady-state I_{SP} in the range -60 to 0 mV. In both cases I_{SP} was identical throughout the voltage range (Fig. 1.7C inset) suggesting no voltage-dependent inactivation of I_{SP} .

We detected I_{SP} in 13/15 neurons (87%). These data are consistent with current clamp studies showing that SP depolarizes every inspiratory neuron tested *in vitro* (Gray et al. 1999; Pena and Ramirez 2004). However, TMR-SP labeling was only present in 42.8% of inspiratory neurons in our previous experiments. This disparity could reflect a failure to detect TMR-SP labeling in some NKR^+ neurons, or that SP-sensitive glial cells play some role in exciting inspiratory preBötC neurons that are otherwise SP-insensitive and NKR^- .

An alternative explanation for the disparity between the large number of preBötC neurons with measurable I_{SP} and the smaller TMR-SP⁺ subset is that gap junctions (Rekling et al. 2000) might confer the effects of SP to NKR⁻ neurons. To test whether gap junctions were required to evoke I_{SP} , we repeated the voltage-clamp protocols from Fig. 1.7 after >15 min exposure to 100 μ M CBX to block gap junctions. Our intra- and extracellular solutions minimized undesired effects of CBX on intrinsic membrane properties such as leak currents (Rekling et al. 2000; Rouach et al. 2003). We evoked I_{SP} in 7 of 14 inspiratory neurons with CBX present, whereas 7 inspiratory neurons did

not respond to SP either in IV or tail-current protocols (Fig. 1.8).

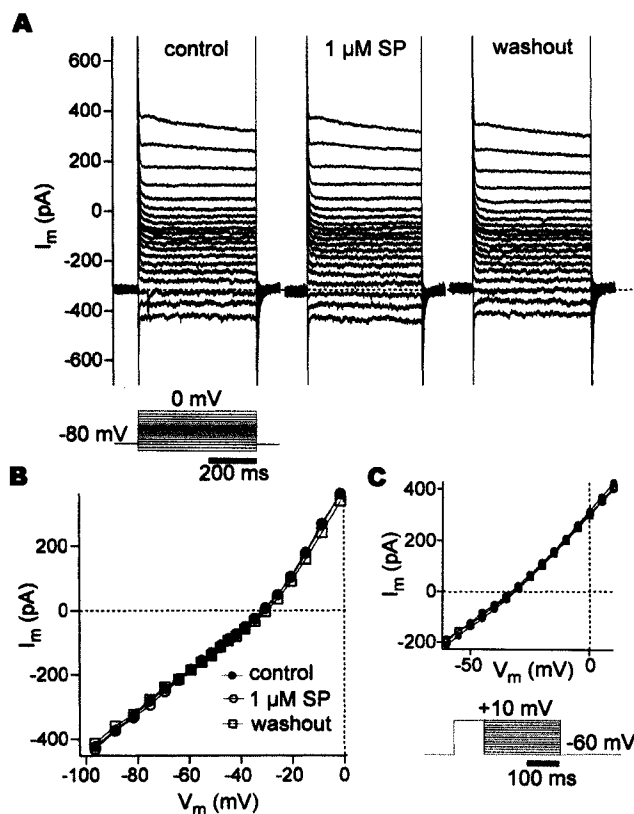


Figure 1.8. Effects of 1 μ M SP on preBötC neurons with blockade of K^+ channels and gap junctions. 100 μ M CBX was added in control to attenuate gap junction-mediated transmission. **A**, Steady-state IV protocols. **B**, Steady-state IV curves. **C**, Tail-current analysis. SP had no effect on membrane properties in 100 μ M CBX.

TMR-SP labels respiratory phasic and non-rhythmic neurons in the mouse preBötC

We measured the rhythmic Ca^{2+} activity of inspiratory neurons using two-photon laser-scanning microscopy (TPLSM), which enabled us to scan 5- μ m-thick focal planes in a defined 293x293 μ m area within the preBötC. In 49 planes from 29 slices, we observed 344 inspiratory neurons and detected a maximum of 11 and a

minimum of 1 inspiratory neuron per plane (average 6) which is commensurate with inspiratory neuron counts recently reported using TPLSM in neonatal rats (Ruangkittisakul et al. 2006). Fluorescence changes could not differentiate early versus late inspiratory phenotypes; with drive latencies typically less than 500 ms (see Fig. 1.3) our maximum 4 Hz sampling rate was too low to make reliable distinctions.

Figure 1.9A (top) illustrates the peak acquisition of Ca^{2+} emission over several respiratory cycles in a typical experiment. Figure 1.9A (bottom) illustrates TMR-SP emission in the same region detected with confocal laser-scanning microscopy (CLSM). Cycle-to-cycle activity from neurons in Fig. 1.9A are plotted with XII activity in panel B: 1-7 were inspiratory, whereas neuron 8 was expiratory. Neurons 4, 7, and 8 are shown at higher magnification in Fig. 1.9C. We detected 13/31 (41.9%) TMR-SP⁺ inspiratory neurons with TPLSM/CLSM and 3/3 (100%) TMR-SP⁺ expiratory neurons in a total of 4 imaging planes acquired in 4 slices. Several non-rhythmic cells were situated among the inspiratory neurons (such as 9-11, Fig. 1.9C) that appeared TMR-SP⁺. They may have been damaged and saturated with cytosolic Ca^{2+} which may have led to fluo-4 bleedthrough into the TMR-SP channel.

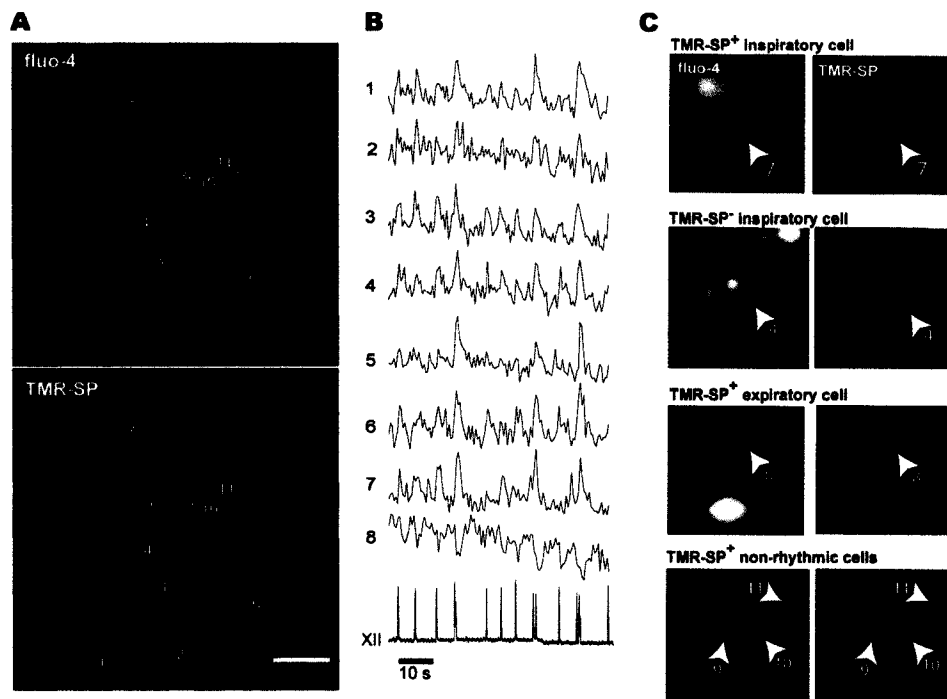


Figure 1.9. Simultaneous measurements of inspiratory activity and TMR-SP labeling in preBötC neurons. **A**, The fluo-4 image shows a peak acquisition of the Ca^{2+} -labeling that illustrates where the regions of interest (ROIs) were selected (the numbers are immediately above the ROIs); the TMR-SP image shows TMR-SP⁺ cells in the same region. Scale bar is 50 μm . **B**, Changes in fluorescence intensity from ROIs indicated by numerals in **A**, plotted with synchronized XII activity. The maximum $\Delta F/F$ range for each ROI was used for illustrative purposes (1: 50%, 2: 26%, 3: 39%, 4: 49%, 5: 50%, 6: 32%, 7: 54%, 8: 57%). **C**, Magnified images shows background subtracted and summed Ca^{2+} activity of a TMR-SP⁺ inspiratory neuron (#7), a TMR-SP⁻ inspiratory neuron (#4), an TMR-SP⁺ expiratory neuron (#8), and the peak acquired view of 3 TMR-SP⁺ non-rhythmic neurons (#9, #10, #11).

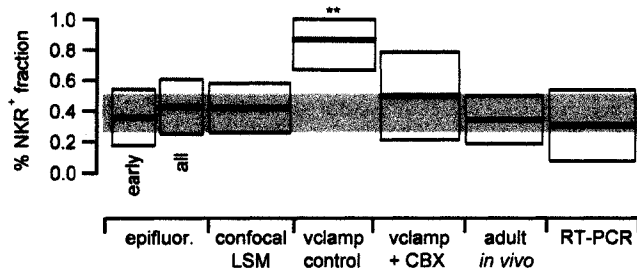
Comparing the relative fraction of preBötC neurons with evidence for NKR expression in several experimental conditions

Altogether we used three methods to quantify the fraction of NKR⁺ inspiratory neurons in the preBötC: epifluorescence yielded 12/28 (42.9%) TMR-SP⁺, TPLSM/CLSM yielded 13/31 (41.9%) TMR-SP⁺, and I_{SP} was measured in voltage clamp in 7/14 (50%) inspiratory neurons in the presence of 100 μM CBX. These measurements in the neonatal mouse preBötC are comparable to the fraction of early inspiratory neurons, dubbed pre-inspiratory (pre-I) by the authors, which were recorded in adult rats *in vivo*

and subsequently found to be NK1R⁺ by immunohistochemistry: 11/32 (34.4%) (Guyenet and Wang 2001). Additionally, our results are consistent with the fraction of inspiratory neurons (4/13, 30.7%) with NK1R expression measured via single-cell reverse transcriptase-polymerase chain reaction (RT-PCR) methods (Manzke et al. 2003) and qualitatively similar to the conclusion by Manzke et al. that there is a large presence of non-inspiratory NK1R-ir neurons in the preBötC.

We tested the null hypothesis that these independent measurements reflect the same underlying fraction of NKR⁺/NK1R⁺ neurons in the preBötC. A virtual preBötC *in silico* containing 40% NKR⁺/NK1R⁺ neurons (the pooled fraction of NKR⁺/NK1R⁺ neurons detected using all methods excluding the control I_{SP} experiment) and 60% NKR⁻/NK1R⁻ neurons was used to randomly sample 14, 28, 31, 32, and 13 neurons (with replacement) corresponding to the experiments above. Each sample was repeated 10,000 times. We tallied the results in a frequency histogram and found that for a population containing 40% NKR⁺/NK1R⁺ neurons, drawing empirical samples of 42.9%, 41.9%, 50%, 34.4%, and 30.7% were statistically indistinguishable ($p \gg 0.05$). Finally, we considered the possibility that the early inspiratory neurons we found in the neonatal mouse preBötC are phenotypically the same as the pre-I neurons recorded in adult rats *in vivo* (Guyenet and Wang 2001); again, the fraction of NKR⁺/NK1R⁺ neurons were statistically indistinguishable (8/22, 36.4% vs. 11/32 (34.4%), $p \gg 0.5$).

In contrast, we evoked I_{SP} in 13/15 (86.7%) inspiratory neurons with gap junctions intact (Fig. 1.7). In resampling simulations, this outcome (i.e., drawing a sample fraction of 86.7% NKR⁺ neurons) occurred by chance less than 1% of the time, so we reject the null hypothesis at $p < 0.01$. Figure 1.10 plots the sample mean fraction of NKR⁺ neurons with 95% credible intervals to illustrate the consistency between the fraction of NKR⁺ neurons detected with imaging experiments, immunohistochemistry,



RT-PCR, and voltage-clamp experiments in the presence of CBX, compared to the much larger number of NK1R⁺ neurons with measurable I_{SP} with gap junctions unblocked.

Figure 1.10. Analysis of NK1R⁺ preBötC neuron distribution. Box plot shows: the fraction of TMR-SP⁺ neurons measured with conventional epifluorescence (*epifluor.*) displayed for the early inspiratory neurons (*early*) and for the entire sample of all inspiratory neurons (*all*); the fraction of TMR-SP⁺ inspiratory neurons measured with confocal laser-scanning microscopy (*confocal LSM*); the fraction of neurons with measurable I_{SP} in control (*vclamp control*) and in the presence of 100 μ M CBX (*vclamp + CBX*). The fraction of NK1R-ir neurons detected in adult rats are also shown (*adult in vivo*) meta-analyzed from (Guyenet and Wang 2001). Meta-analyzed data from (Manzke et al. 2003) using single-cell RT-PCR (*RT-PCR*) to determine NK1R⁺ inspiratory neurons is also included. Bold horizontal lines in each category show the mean and thin lines show the 95% credible intervals. Overlapping regions of *epifluor.*, *confocal LSM*, *vclamp + CBX*, *adult in vivo*, and *RT-PCR* data are bounded by the gray rectangle. Statistical significance at $p < 0.01$ is shown with double asterisks.

1.4. Discussion

Our data suggest that the preBötC comprises approximately 40% NK1R⁺ inspiratory neurons in rodents. Nonetheless, SP may exert widespread excitatory effects due to gap junctions that activate I_{SP} in both NK1R⁺ and NK1R⁻ neurons. The functional roles of NK1R⁺ and NK1R⁻ neurons may overlap because both subsets showed early and late inspiratory phenotypes, and both respond to SP-mediated modulation (Gray et al. 1999) in the absence of gap junction blockers. Therefore, the NK1R expression *per se* may not be a reliable means to classify preBötC neurons functionally. Destruction of NK1R⁺ neurons disrupts normal respiratory physiology (Gray et al. 2001; McKay et al. 2005). Since NK1R⁺ neurons exhibit both early inspiratory and late inspiratory phenotypic properties, as well as expiratory and non-respiratory phenotypes, the loss of all of these neuron types must be considered when interpreting the functional consequences of lesion or natural NK1R⁺ cell death.

The biophysics of I_{SP} in inspiratory neurons

I_{SP} is measurable in early and late inspiratory neurons using doses of SP that have clear respiratory effects in previous studies (Gray et al. 1999; Pagliardini et al. 2005; Pena and Ramirez 2004). I_{SP} does not depend on extracellular Ca^{2+} , is TTX-insensitive, and Na^+ is the dominant inward charge carrier (Pena and Ramirez 2004). Its reversal potential (E_{SP}) is -19 mV so we conclude that K^+ is also a charge carrier. E_{SP} was the same with K-gluconate patch solution and Cs^+ -based patch solution that substantially raised the Cl^- reversal potential, so Cl^- is not a charge carrier for I_{SP} . We observed I_{SP} in the presence of combined Na^+ , Ca^{2+} , and K^+ -blockers, which suggests that I_{SP} arises from a single type of mixed cation channel.

Tail current analysis would enable detection of any component of I_{SP} that slowly inactivates during the steady-state IV protocol. Since I_{SP} tail currents and the steady-state I_{SP} were identical (Fig. 1.7C inset), we conclude that there was no significant voltage-dependent component of I_{SP} that inactivates on the time scale of 100-500 ms. This contradicts the hypothesis that I_{SP} is a TTX-insensitive voltage-activated Na^+ current (Pena and Ramirez 2004) that can give rise to negative slope resistance and bursting properties (Delmas et al. 1997).

SP increases excitability via the closure of K^+ channels in hypoglossal motoneurons (Yasuda et al. 2001) and C1 neurons that are situated at the ventral border of the preBötC (Blessing 1997; Li and Guyenet 1997). Our data set did not contain C1 neurons because I_{SP} never reversed at E_K and was unaffected by intracellular and extracellular K^+ channel blockers.

SP has widespread excitatory effects on inspiratory neurons *in vitro* (Gray et al. 1999; Pena and Ramirez 2004; Yamamoto et al. 1992) and we evoked I_{SP} in 86.7% of inspiratory neurons in the absence of CBX. However, NKR expression appears to be

much less prevalent: approximately 42% of both early and late inspiratory neurons in neonatal mice were TMR-SP⁺, 34% of pre-I neurons identified in adult rats *in vivo* were NK1R-ir (Guyenet and Wang 2001), and 31% of preBötC inspiratory neurons were NK1R⁺ as identified with single-cell RT-PCR (Manzke et al. 2003). The latter measurements are consistent with our ability to evoke I_{SP} in only 50% of inspiratory neurons after blocking gap junctions, suggesting that gap junctions are involved in evoking I_{SP} in NK1R⁻ neurons. It is conceivable that the slightly higher (but not statistically significant) difference between our TMR-SP⁺ fraction and the meta-analyzed NK1R-expression data can be attributed to other tachykinin receptors that can bind TMR-SP but do not show NK1R immunoreactivity. However, this is unlikely since respiratory-related neurons in NK1R^{-/-} mice do not respond to SP (Ptak et al. 2000).

A cationic current that reverses at -11 mV (in ACSF with 9 mM external $[K^+]$) is coupled to muscarinic receptor activation in preBötC inspiratory neurons (Shao and Feldman 2000). This current is very similar to I_{SP} : it is TTX-insensitive, its activation is voltage- and Ca^{2+} -independent, and Na^+ and K^+ are the principal charge carriers. This suggests that muscarinic and neurokinin receptors may open the same underlying class of cation channels (Pena and Ramirez 2004; Shao and Feldman 2000), but this remains to be tested.

The putative roles of NK1R⁺ and NK1R⁻ inspiratory neurons in respiratory rhythmogenesis

The majority of our neurons showed early inspiratory activity patterns and small C_M . The early latency, small size, and incremental discharge trajectory are characteristic of propriomedullary glutamatergic interneurons that putatively serve in a rhythmogenic capacity (Guyenet and Wang 2001; Stornetta et al. 2003a; Wallen-Mackenzie et al.

2006). 36% of these early inspiratory neurons were NKR⁺. Given their discharge pattern and NKR expression, these neurons are probably glutamatergic and are unlikely to be GABA- or glycinergic (Stornetta et al. 2003a; Stornetta et al. 2003b; Wang et al. 2001), although we cannot rule out some of these NKR⁺ neurons belonging to a class of GABAergic neurons involved in sympathetic control of blood pressure (Wang et al. 2002). NKR⁺ early inspiratory neurons are unlikely to contain cardiovagal preganglionic motoneurons in the external division of the nucleus ambiguus because choline acetyltransferase was never co-detected with NK1R expression in adult rat preBötC neurons (Wang et al. 2001). The fraction of NK1R-ir early inspiratory-like neurons (called 'pre-I' by the authors) in adult rats *in vivo* is also near 36% (Guyenet and Wang 2001), so we conclude that the fraction of NKR⁺ rhythmogenic neurons in the preBötC is consistent in neonates and adults.

Large C_M and late inspiratory discharge pattern are characteristics consistent with glutamatergic bulbospinal neurons that putatively serve in a premotor capacity (Guyenet et al. 2002; Rekling et al. 1996; Stornetta et al. 2003b). Since 67% of late inspiratory neurons were NKR⁺, SP-SAP lesions may ablate a larger percentage of late inspiratory (putative premotoneurons) compared to early inspiratory neurons. However, because early inspiratory neurons are more numerous and show membrane properties consistent with a role in rhythmogenesis, NKR-targeted lesions will probably cause a greater total reduction in NKR⁺ rhythmogenic-like neurons. However, the destruction of a large fraction of NKR⁺ respiratory premotoneurons must be considered as a factor in explaining apneas resulting from SP-SAP lesions (Gray et al. 2001; McKay et al. 2005).

NKR⁻ neurons with early and late inspiratory discharge properties probably incorporate some cardiovagal preganglionic and pharyngeal motoneurons (Bieger and Hopkins 1987; Rekling et al. 1996; Rekling and Feldman 1997), as well as respiratory

premotoneurons (Guyenet et al. 2002). Inspiratory neurons within the preBötC may also be GABAergic (Kuwana et al. 2006) or glycinergic (Shao and Feldman 1997). Therefore, some NKR⁻ neurons are either inhibitory or motor-related neurons that presumably do not directly contribute to rhythmogenesis.

Nevertheless, because of their discharge phenotype and sensitivity to SP (with gap junctions intact), we propose that many early inspiratory NKR⁻ neurons are also rhythmogenic interneurons analogous to NKR⁺ glutamatergic early inspiratory interneurons (Guyenet et al. 2002; Stornetta et al. 2003a). However, we cannot be certain of the transmitter type in NKR⁻ early inspiratory neurons and thus cannot exclude the possibility that some of these neurons have non-rhythmogenic functions.

Furthermore, it is difficult to ascertain how our early and late inspiratory phenotypes map to respiratory phenotypes in larger brainstem preparations or *in vivo*, which is problematic from the standpoint of nomenclature, since the pattern of activity may change with further levels of embedded neural circuitry. However, we provide simple names for distinct phenotypes in slices and our dichotomy may be useful to distinguish putatively rhythmogenic and premotor neurons in this context.

Estimating the size and composition of the neonatal preBötC

The preBötC in rats is remarkably constant in size during early neonatal development and extends for approximately 200 μm in the rostral-caudal axis of rats (Ruangkittisakul et al. 2006; Smith et al. 1991). Given somatic diameter of approximately 10 μm for preBötC neurons (Stornetta et al. 2003a; Wang et al. 2001), we can offer a rough estimate of the population size of inspiratory neurons in the preBötC. If we assume 1 neuron-layer per 10 μm of tissue in the sagittal plane, account for a bilaterally distributed preBötC, and employ our measured average of 6 inspiratory neurons per plane, then the

neonatal rodent preBötC contains approximately 240 inspiratory neurons. This assumes that the rostro-caudal extent of the neonatal mouse preBötC matches that of the rat.

We counted 22/28 (78.6%) neurons with early inspiratory discharge pattern and small C_M , in which 8/22 (36.3%) were TMR-SP⁺. We found 6/28 (21.4%) neurons with late inspiratory pattern and large C_M in which 4/6 (66.7%) were TMR-SP⁺. We thus estimate that the preBötC contains approximately 189 early inspiratory neurons of which 69 are NKR⁺ and 120 are NKR⁻, and 51 late inspiratory neurons of which 34 are NKR⁺ and 17 are NKR⁻ (Fig. 1.11).

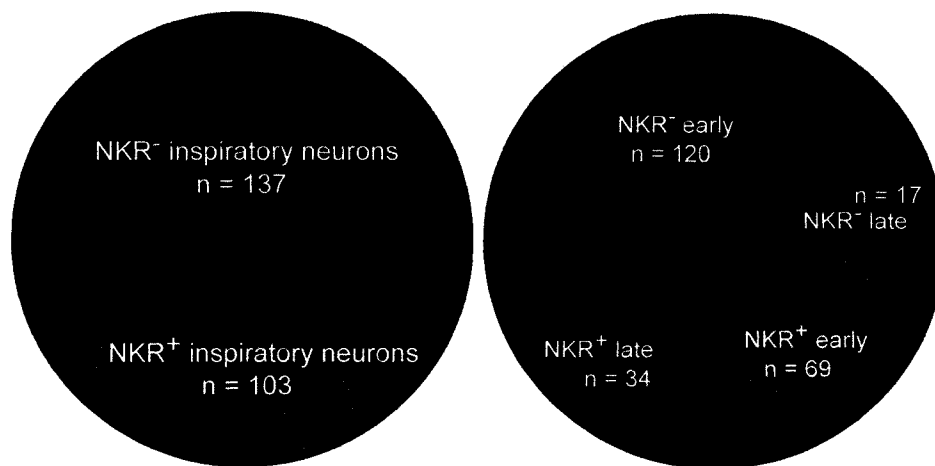


Figure 1.11. Estimates of the composition of the preBötC inspiratory network. **Left,** The estimated number of NKR⁺ and NKR⁻ inspiratory neurons. **Right,** The same fraction of NKR⁺/NKR⁻ inspiratory neurons separated by the estimated number of early and late inspiratory phenotypes.

Physiological significance: a prediction for recovering respiratory function after

NKR⁺ neuron loss

In neonatal mice (our results) and adult rats (Guyenet and Wang 2001), ~36% of rhythmogenic-like neurons showed evidence of NKR expression. We postulate that ~64% of putative rhythmogenic inspiratory neurons, and ~33% of premotor-like neurons, may survive SP-SAP lesions or diseases that ablate NKR⁺ neurons and impair breathing (Gray et al. 2001; McKay et al. 2005). Our estimates for population sizes (above) will

facilitate graded cell-destruction simulations in mathematical models of the preBötC that reflect the approximate numbers of NKR^+ and NKR^- neurons with respective rhythmogenic-like and premotor-like phenotypes. Models of this type may elucidate the mechanism by which graded neuron destruction perturbs rhythmogenesis and may help clarify the different effects of destroying rhythmogenic versus premotor neurons.

Stable breathing behavior is impaired by NKR^+ neuron loss in the preBötC and may be a result of a breakdown in fundamental rhythmogenic mechanisms. However, strengthening the excitatory synaptic transmission between NKR^- preBötC neurons may restore respiratory function, assuming that NKR^- preBötC neurons are glutamatergic and interconnected (Guyenet et al. 2002; Rekling et al. 2000; Stornetta et al. 2003a; Stornetta et al. 2003b). Augmenting excitatory synaptic strength could be accomplished using cyclothiazide (Funk et al. 1995) or ampakines (Ren et al. 2006) that enhance ionotropic glutamate receptors, or by enhancing the role of metabotropic glutamate receptors by targeting specific intracellular signaling cascades coupled to their activation. This prediction arises from the hypothesis that a limited number of synaptically interconnected constituent neurons in the preBötC can maintain rhythmic function by periodically evoking burst-generating intrinsic membrane properties that are only available in the context of behavior via ionotropic and metabotropic glutamate receptors (Feldman and Del Negro 2006; Rekling et al. 1996; Rekling and Feldman 1998; Wallen-Mackenzie et al. 2006).

1.5. References

Ballanyi K, Onimaru H, and Homma I. Respiratory network function in the isolated brainstem-spinal cord of newborn rats. *Prog Neurobiol* 59: 583-634, 1999.

Bianchi AL, Denavit-Saubie M, and Champagnat J. Central control of breathing in mammals: neuronal circuitry, membrane properties, and neurotransmitters. *Physiol Rev* 75: 1-45, 1995.

Bieger D, and Hopkins DA. Viscerotopic representation of the upper alimentary tract in the medulla oblongata in the rat: the nucleus ambiguus. *J Comp Neurol* 262: 546-562, 1987.

Blessing WW. *The lower brainstem and bodily homeostasis.* New York: Oxford University Press, 1997, p. 575.

Del Negro CA, Koshiya N, Butera RJ, Jr., and Smith JC. Persistent sodium current, membrane properties and bursting behavior of pre-botzinger complex inspiratory neurons in vitro. *J Neurophysiol* 88: 2242-2250, 2002.

Del Negro CA, Morgado-Valle C, Hayes JA, Mackay DD, Pace RW, Crowder EA, and Feldman JL. Sodium and Calcium Current-Mediated Pacemaker Neurons and Respiratory Rhythm Generation. *J Neurosci* 25: 446-453, 2005.

Delmas P, Raggenbass M, and Gola M. Low-threshold Na⁺ currents: a new family of receptor-operated inward currents in mammalian nerve cells. *Brain Res Brain Res Rev* 25: 246-254, 1997.

Feldman JL, and Del Negro CA. Looking for inspiration: new perspectives on respiratory rhythm. *Nat Rev Neurosci* 7: 232, 2006.

Funk GD, Smith JC, and Feldman JL. Modulation of neural network activity in vitro by cyclothiazide, a drug that blocks desensitization of AMPA receptors. *J Neurosci* 15: 4046-4056, 1995.

Grady EF, Garland AM, Gamp PD, Lovett M, Payan DG, and Bunnett NW. Delineation of the endocytic pathway of substance P and its seven-transmembrane domain NK1 receptor. *Mol Biol Cell* 6: 509-524, 1995.

Gray PA, Janczewski WA, Mellen N, McCrimmon DR, and Feldman JL. Normal breathing requires preBötzinger complex neurokinin-1 receptor-expressing neurons. *Nat Neurosci* 4: 927-930, 2001.

Gray PA, Rekling JC, Bocchiaro CM, and Feldman JL. Modulation of respiratory frequency by peptidergic input to rhythmogenic neurons in the preBötzinger complex. *Science* 286: 1566-1568, 1999.

Guyenet PG, Sevigny CP, Weston MC, and Stornetta RL. Neurokinin-1 receptor-expressing cells of the ventral respiratory group are functionally heterogeneous and predominantly glutamatergic. *J Neurosci* 22: 3806-3816, 2002.

Guyenet PG, and Wang H. Pre-Bötzinger Neurons With Preinspiratory Discharges "In Vivo" Express NK1 Receptors in the Rat. *J Neurophysiol* 86: 438-446, 2001.

Hayes JA, and Del Negro CA. Neurokinin Receptor-Expressing Pre-Bötzinger Complex Neurons in Neonatal Mice Studied In Vitro. *J Neurophysiol* 97: 4215-4224, 2007.

Janczewski WA, and Feldman JL. Distinct rhythm generators for inspiration and expiration in the juvenile rat. *J Physiol* 570: 407-420, 2006.

Kuwana S, Tsunekawa N, Yanagawa Y, Okada Y, Kuribayashi J, and Obata K. Electrophysiological and morphological characteristics of GABAergic respiratory neurons in the mouse pre-Bötzinger complex. *Eur J Neurosci* 23: 667-674, 2006.

Li YW, and Guyenet PG. Effect of substance P on C1 and other bulbospinal cells of the RVLM in neonatal rats. *Am J Physiol* 273: R805-813, 1997.

Manley BFJ. *Randomization, Bootstrap and Monte Carlo methods in biology.* 1996.

Manzke T, Guenther U, Ponimaskin EG, Haller M, Dutschmann M, Schwarzacher S, and Richter DW. 5-HT₄(a) receptors avert opioid-induced breathing depression without loss of analgesia. *Science* 301: 226-229, 2003.

McKay LC, Janczewski WA, and Feldman JL. Sleep-disordered breathing after targeted ablation of preBötzinger complex neurons. *Nat Neurosci* 8: 1142-1144, 2005.

Medhurst A, and Hay D. Tachykinin receptors. In: *Understanding G protein-coupled receptors and their role in the CNS*, edited by Pangalos M, and Davies C. New York: Oxford University Press, 2002, p. 483-502.

Murakoshi T, Suzue T, and Tamai S. A pharmacological study on respiratory rhythm in the isolated brainstem-spinal cord preparation of the newborn rat. *British journal of pharmacology* 86: 95-104, 1985.

Onimaru H, Arata A, and Homma I. Firing properties of respiratory rhythm generating neurons in the absence of synaptic transmission in rat medulla in vitro. *Exp Brain Res* 76: 530-536, 1989.

Onimaru H, and Homma I. Whole cell recordings from respiratory neurons in the medulla of brainstem-spinal cord preparations isolated from newborn rats. *Pflugers Arch* 420: 399-406, 1992.

Pace RW, Mackay DD, Feldman JL, and Del Negro CA. Role of Persistent Sodium Current in Mouse PreBötzing Neurons and Respiratory Rhythm Generation. *J Physiol (Lond)* jphysiol.2006.124602, 2007.

Pagliardini S, Adachi T, Ren J, Funk GD, and Greer JJ. Fluorescent Tagging of Rhythmically Active Respiratory Neurons within the Pre-Bötzing Complex of Rat Medullary Slice Preparations. *J Neurosci* 25: 2591-2596, 2005.

Pena F, and Ramirez JM. Substance P-mediated modulation of pacemaker properties in the mammalian respiratory network. *J Neurosci* 24: 7549-7556, 2004.

Ptak K, Hunt SP, and Monteau R. Substance P and central respiratory activity: a comparative in vitro study in NK1 receptor knockout and wild-type mice. *Pflugers Arch* 440: 446-451, 2000.

Ramirez JM, Tryba AK, and Pena F. Pacemaker neurons and neuronal networks: an integrative view. *Curr Opin Neurobiol* 14: 665-674, 2004.

Ramirez JM, Zuperku EJ, Alheid GF, Lieske SP, Ptak K, and McCrimmon DR.

Respiratory rhythm generation: converging concepts from in vitro and in vivo approaches? *Respir Physiol Neurobiol* 131: 43-56, 2002.

Rekling JC, Champagnat J, and Denavit-Saubie M. Electroresponsive properties and membrane potential trajectories of three types of inspiratory neurons in the newborn mouse brain stem in vitro. *J Neurophysiol* 75: 795-810, 1996.

Rekling JC, and Feldman JL. Calcium-dependent plateau potentials in rostral ambiguous neurons in the newborn mouse brain stem in vitro. *J Neurophysiol* 78: 2483-2492, 1997.

Rekling JC, and Feldman JL. PreBötzinger complex and pacemaker neurons: hypothesized site and kernel for respiratory rhythm generation. *Annu Rev Physiol* 60: 385-405, 1998.

Rekling JC, Shao XM, and Feldman JL. Electrical coupling and excitatory synaptic transmission between rhythmogenic respiratory neurons in the preBötzinger complex. *J Neurosci* 20: RC113, 2000.

Ren J, Poon BY, Tang Y, Funk GD, and Greer JJ. Ampakines Alleviate Respiratory Depression in Rats. *Am J Respir Crit Care Med* 2006.

Richter DW, and Spyer KM. Studying rhythmogenesis of breathing: comparison of in vivo and in vitro models. *Trends Neurosci* 24: 464-472, 2001.

Rouach N, Segal M, Koulakoff A, Giaume C, and Avignone E. Carbenoxolone blockade of neuronal network activity in culture is not mediated by an action on gap junctions. *J Physiol* 553: 729-745, 2003.

Ruangkittisakul A, Schwarzacher SW, Secchia L, Poon BY, Ma Y, Funk GD, and Ballanyi K. High Sensitivity to Neuromodulator-Activated Signaling Pathways at Physiological $[K^+]$ of Confocally Imaged Respiratory Center Neurons in On-Line-Calibrated Newborn Rat Brainstem Slices. *J Neurosci* 26: 11870-11880, 2006.

Shao XM, and Feldman JL. Acetylcholine modulates respiratory pattern: effects mediated by M3-like receptors in preBötzinger complex inspiratory neurons. *J Neurophysiol* 83: 1243-1252, 2000.

Shao XM, and Feldman JL. Respiratory rhythm generation and synaptic inhibition of expiratory neurons in pre-Botzinger complex: differential roles of glycinergic and GABAergic neural transmission. *J Neurophysiol* 77: 1853-1860, 1997.

Smith JC, Ellenberger HH, Ballanyi K, Richter DW, and Feldman JL. Pre-Bötzinger complex: a brainstem region that may generate respiratory rhythm in mammals. *Science* 254: 726-729, 1991.

Stornetta RL, Rosin DL, Wang H, Sevigny CP, Weston MC, and Guyenet PG. A group of glutamatergic interneurons expressing high levels of both neurokinin-1 receptors and somatostatin identifies the region of the pre-Bötzinger complex. *J Comp Neurol* 455: 499-512, 2003a.

Stornetta RL, Sevigny CP, and Guyenet PG. Inspiratory augmenting bulbospinal neurons express both glutamatergic and enkephalinergic phenotypes. *J Comp Neurol* 455: 113-124, 2003b.

Thoby-Brisson M, and Ramirez JM. Identification of two types of inspiratory pacemaker neurons in the isolated respiratory neural network of mice. *J Neurophysiol* 86: 104-112, 2001.

Wallen-Mackenzie A, Gezelius H, Thoby-Brisson M, Nygard A, Enjin A, Fujiyama F, Fortin G, and Kullander K. Vesicular glutamate transporter 2 is required for central respiratory rhythm generation but not for locomotor central pattern generation. *J Neurosci* 26: 12294-12307, 2006.

Wang H, Germanson TP, and Guyenet PG. Depressor and Tachypneic Responses to Chemical Stimulation of the Ventral Respiratory Group Are Reduced by Ablation of Neurokinin-1 Receptor-Expressing Neurons. *J Neurosci* 22: 3755-3764, 2002.

Wang H, Stornetta RL, Rosin DL, and Guyenet PG. Neurokinin-1 receptor-immunoreactive neurons of the ventral respiratory group in the rat. *J Comp Neurol* 434: 128-146, 2001.

Yamamoto Y, Onimaru H, and Homma I. Effect of substance P on respiratory rhythm and pre-inspiratory neurons in the ventrolateral structure of rostral medulla oblongata: an in vitro study. *Brain Res* 599: 272-276, 1992.

Yasuda K, Robinson DM, Selvaratnam SR, Walsh CW, McMorland AJ, and Funk GD. Modulation of hypoglossal motoneuron excitability by NK1 receptor activation in neonatal mice in vitro. *J Physiol* 534: 447-464, 2001.

CHAPTER 2. 4-aminopyridine-sensitive outward currents in inspiratory neurons promote regular burst discharges within the preBötzinger Complex

2.1. Introduction

Rhythmic motor behaviors originate from central pattern generator (CPG) networks in the brain stem and spinal cord (Marder 2001). A key issue is to what degree proper network function (i.e., rhythmogenesis) depends on specific ion channels and intrinsic properties in constituent rhythm-generating neurons (Stein 1997). The respiratory CPG is an excellent model for examining this question because its constituent rhythmogenic neurons are contained within the preBötzinger Complex (preBötC) (Feldman and Del Negro 2006; Gray et al. 2001; Gray et al. 1999; Rekling and Feldman 1998; Smith et al. 1991) and the network output is measurable *in vitro*. Transverse medullary slices containing the preBötC spontaneously generate behaviorally relevant rhythmic motor activity that can be monitored via the hypoglossal nerve (XII) *in vitro*.

Most studies of respiratory rhythm generation have focused on the role of voltage-dependent inward currents (Del Negro et al. 2001; Del Negro et al. 2002a; Del Negro et al. 2002b; Del Negro et al. 2005; Mironov et al. 2000; Mironov and Richter 1998; Onimaru et al. 2003; Pace et al. 2007c; Pena et al. 2004; Pierrefiche et al. 1999;

Ptak et al. 2005; Thoby-Brisson et al. 2000), neuromodulation (Johnson et al. 1996; Onimaru et al. 1998; Pena and Ramirez 2002; 2004; Reklings et al. 1996b; Ruangkittisakul et al. 2006; Shao and Feldman 2000), as well as excitatory and inhibitory synaptic currents (Brockhaus and Ballanyi 1998; Funk et al. 1993; 1995; Greer et al. 1991; Paarmann et al. 2005; Pace et al. 2007a; Pierrefiche et al. 1998; Shao et al. 2003). Apart from an ATP-inhibited K^+ current primarily activated during hypoxia (Haller et al. 2001a; Haller et al. 2001b; Mironov et al. 1998; Mironov et al. 1999; Mironov and Richter 2000; 2001; Pierrefiche et al. 1996), outward currents have not been well-characterized in the preBötC of neonatal rodents, nor have their contributions to rhythmogenesis been analyzed.

Reklings et al. (1996a) described a subset of inspiratory neurons that depolarized with a ramp-like trajectory and started spiking ~400 ms prior to XII output, dubbed *type 1* neurons, which are putatively rhythmogenic (Gray et al. 1999; Reklings and Feldman 1998). In addition to their ramp-like trajectory prior to XII output, type 1 neurons exhibited delayed excitation in response to 400-ms step pulses of depolarizing current from hyperpolarized membrane potentials (Reklings and Feldman 1998). Delayed excitation is often attributed to transient outward currents (i.e., A-currents, I_A) (Dekin and Getting 1987; Dekin et al. 1987; Getting 1983; Hagiwara et al. 1961; Nisenbaum et al. 1994), thus Reklings and colleagues proposed that rhythmogenic preBötC neurons expressed I_A (Reklings et al. 1996a; Reklings and Feldman 1998). This was recently confirmed by Inyushkin (2005) who recorded I_A in whole-cell voltage clamp and blocked it with 4-aminopyridine (4-AP) in the preBötC, but did not analyze its contributions to rhythmogenesis. Therefore, we sought to measure the biophysical properties of I_A in more detail in order to and test its specific role(s) in respiratory rhythm generation.

2.2. Methods

The Institutional Animal Care and Use Committee at the College of William and Mary approved all protocols. Transverse slices (550 μm thick) from neonatal (P0-7) C57BL/6 mice were dissected as described previously (Chapter 1, Hayes and Del Negro 2007).

Slices were perfused at 26-28°C with an artificial cerebrospinal fluid (ACSF) containing (in mM): 124 NaCl, 9 KCl, 0.5 NaH_2PO_4 , 25 NaHCO_3 , 30 D-glucose, 1.5 $\text{CaCl}_2 \cdot \text{H}_2\text{O}$, and 1 MgSO_4 . We used 45 slices for the electrophysiology data.

Voltage- and current-clamp experiments were performed with a HEKA EPC-10 patch-clamp amplifier and Patchmaster software (Lambrecht, Germany). Respiratory-related motor output was monitored from XII nerves with extracellular suction electrodes and a high-gain differential amplifier with band-pass filtering (0.3-1 kHz) (Dagan Instruments, Minneapolis, MN). Raw XII activity was conditioned using a true RMS-to-DC converter (Analog Devices, One Technology Way, Norwood, MA) to provide a full-wave rectified and smoothed XII waveform. Data were acquired digitally and analyzed using Igor Pro 5 (WaveMetrics, OR), Chart 5 (AD Instruments, Colorado Springs, CO), Excel (Microsoft, Redmond, WA) and custom software. An 8 mV liquid junction potential was corrected online in both current- and voltage clamp.

Whole-cell capacitance (C_M) was measured using 50-ms voltage steps from -60 mV to command potentials from -75 mV to -65 mV in a 10-step sequence. Charge (Q) was computed by integrating leak-subtracted capacitive current ($\Delta Q = \int I_C$) and C_M was calculated from $C_M = \Delta Q / \Delta V$. Series (access) resistance (R_S) was monitored throughout voltage-clamp recordings according to the Thevenin equivalent circuit, which allows R_S to be calculated from the decay time constant (τ_m) in response to small voltage steps with $R_S = \tau_m / C_M$ as long as $R_S \ll R_N$. We monitored input resistance (R_N) via P/N online

leak protocols. To avoid voltage-clamp errors we discarded experiments in which $R_S > 0.1 \cdot R_N$. We compensated for R_S using analog feedback circuitry within the EPC-10 as much as possible without causing clamp oscillations that jeopardize stable recording. We rechecked R_S and R_N before bouts of episodic voltage-clamp protocols to assess voltage-clamp viability, ensuring the reliability of the acquired data.

We used the following standard patch solution containing (in mM): 140 K-gluconate, 5 NaCl, 0.1 EGTA, 10 HEPES, 2 Mg-ATP, and 0.3 Na(3)-GTP. KOH was used to equilibrate pH at 7.2. To isolate I_A in voltage clamp (Figs. 1B-C, 1E-F, 2, 3) we used a low Ca^{2+} /high Mg^{2+} extracellular ACSF with contents (in mM): 124 NaCl, 9 KCl, 25 $NaHCO_3$, 30 D-glucose, 0.5 $CaCl_2 \cdot H_2O$, and 2 $MgSO_4$.

We measured the voltage dependence and kinetics of I_A using Fitmaster software by HEKA (Lambrecht, Germany) and Igor Pro (v. 5.02, Wavemetrics, Lake Oswego, OR). Activation and inactivation functions took the form:

$$x_{\infty}(V) = \frac{1}{1 + e^{\left(\frac{V - \theta_x}{\sigma_x}\right)}}$$

where x_{∞} is the steady-state activation (m_{∞}) or inactivation (h_{∞}) function, θ_x is the membrane potential of half-activation (θ_m) or half-inactivation (θ_h), and σ_x is the slope factor.

Characteristic features of inspiratory drive potentials were measured during rhythmic activity *in vitro* using the Peak Parameters extension in Chart software (v. 5, ADInstruments, Colorado Springs, CO). Regarding the role of I_A , leading and trailing slopes of drive potentials were particularly relevant (Fig. 7,9). Leading and trailing slopes were calculated from digitally smoothed traces (Fig. 8) to minimize spikes but preserve the underlying drive potential characteristics (Pace et al. 2007b). Peak amplitude and

baseline were automatically detected and the leading slope was computed from 20% of peak amplitude to 80% peak amplitude and trailing slope is calculated from 80% to 20%.

2.3. Results

Inspiratory preBötC neurons express I_A

Rhythmogenic inspiratory neurons in the preBötC characteristically discharge several hundred milliseconds prior to XII motor activity with an incremental pattern of depolarization (Fig. 2.1A) (Bianchi et al. 1995; Richter and Spyer 2001). We frequently observed I_A in these neurons. We isolated K^+ currents in whole-cell voltage-clamp using low Ca^{2+} ACSF containing 3 mM extracellular $[K^+]$, 1 μM TTX, and 200 μM Cd^{2+} . Step commands from -100 mV to higher voltages (up to $+10$ mV) evoked sustained K^+ currents in addition to I_A (Fig. 2.1B). I_A could also be evoked by depolarizing step commands from a -60 mV holding potential (Fig. 2.1B, inset), suggesting that I_A does not completely inactivate at baseline membrane potentials observed during normal inspiratory activity *in vitro* (e.g., Fig. 2.1A). In current clamp, depolarizing current steps from a holding potential of -70 mV evoked a ramping depolarization ($\Delta V/\Delta t = 3.6$ mV/200 ms), whereas steps from -40 mV resulted in largely passive responses that quickly achieved steady-state (Fig. 2.1C), which is indicative of I_A that is de-inactivated at hyperpolarized potentials, but steady-state inactivated at voltages above spike threshold.

Expiratory neurons in the preBötC are inhibited during XII motor activity but otherwise spike tonically (Fig. 2.2A). Outward currents were typically smaller overall, and none expressed I_A (compare Fig. 2.1B to 2.2B, note scale bars are the same, $n=4$). In current clamp, depolarizing step commands did not evoke a ramping depolarization from any holding potential (Fig. 2.2C), which is consistent with the lack of I_A .

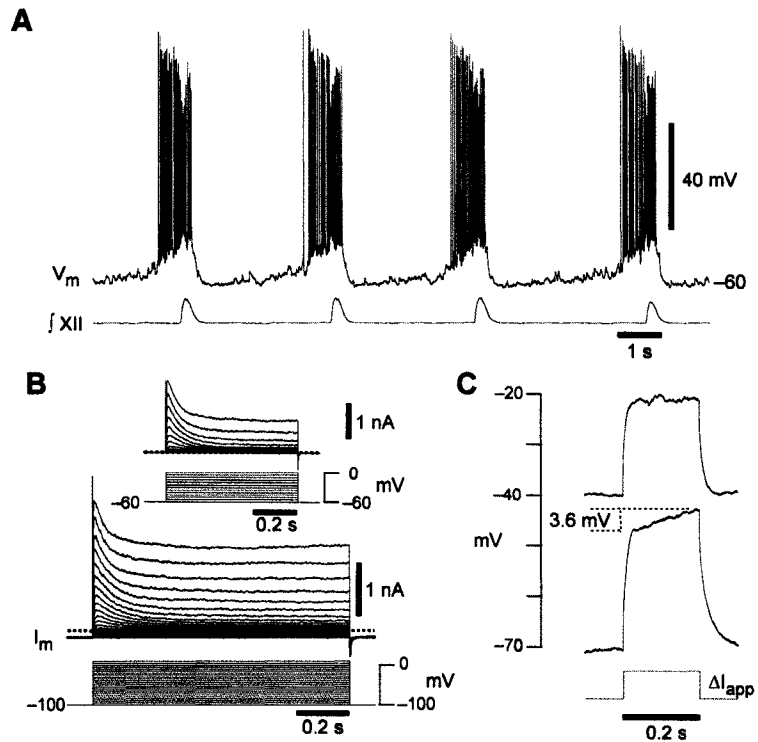


Figure 2.1. Phenotypic behaviors of inspiratory neurons located in the preBötC. **A**, A current-clamp recording of an inspiratory neuron that activates before the integrated XII nerve recording (f_{XII}). **B**, A voltage-clamp recording from a holding potential of -100 mV illustrating the transient outward current evoked at high membrane potentials. *Inset*, a different neuron's voltage-clamp recording from a holding potential of -60 mV. **C**, The same neuron as in A and B illustrating voltage-dependent delayed excitation where ΔI_{app} was 95 pA. Recordings in B and C were in the presence of $1 \mu\text{M}$ TTX, $200 \mu\text{M}$ Cd^{2+} , and 3 mM extracellular $[\text{K}^+]$.

Biophysical properties of I_A

We separated I_A from non-inactivating K^+ currents by subtraction. Using the same conditions as Fig. 2.1B and 2.2B, we applied a sequence of 1-s step commands from -80 to $+10$ mV from a holding potential of -100 mV and then repeated these steps from -40 mV (Fig. 2.3A [lower traces] superimposes the protocol from both -100 and -40 mV holding potentials). The difference current was defined as I_A (Fig. 2.3A, upper traces). I_A activated at -60 mV and its maximum amplitude exceeded 1 nA at voltages greater than 0 mV. A detailed analysis of voltage dependence was precluded in the whole-cell

configuration, however, due to inherent space-clamp limitations and series resistance errors attributable to large magnitude membrane currents (Armstrong et al. 1992).

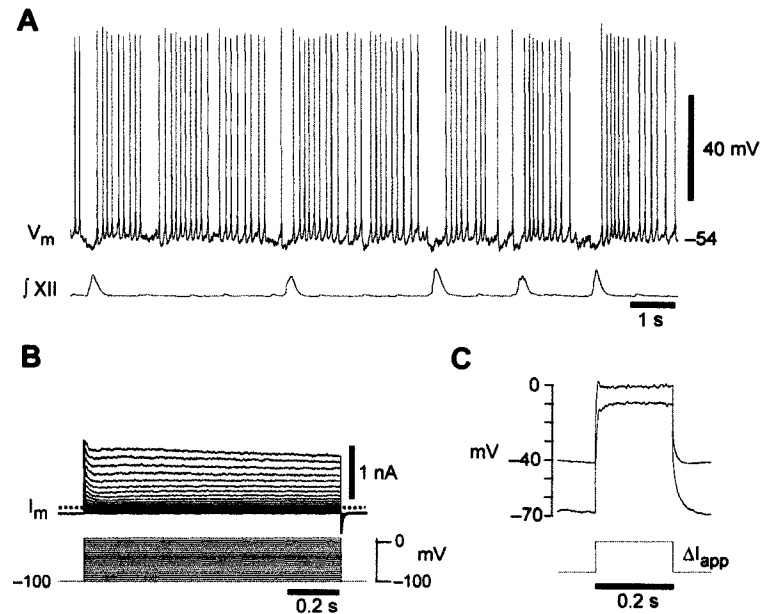


Figure 2.2. Phenotypic behaviors of expiratory neurons located in the preBötC. **A**, A current-clamp recording of an expiratory neuron that is inhibited during XII activity. **B**, The corresponding voltage-clamp recording of the expiratory neuron showing only minimal transient outward currents. **C**, Likewise, prominent delayed excitation is not exhibited by the expiratory neuron where ΔI_{app} was 379 pA. Recordings in B and C were in the presence of 1 μM TTX, 200 μM Cd^{2+} , and 3 mM extracellular $[\text{K}^+]$.

To accurately measure voltage dependence and kinetics, we isolated somatic outside-out patches and repeated the subtraction protocol described above with step commands that reached +30 mV (Fig. 2.3B). The I_A activation function was fit with the parameters $\theta_m = -16.3$ mV and $\sigma_m = 14.9$ mV. Even in patches I_A generally exceeded 200 pA with a mean conductance of 1.14 ± 0.36 nS ($n=6$). In 3/3 patches, 2 mM 4-AP substantially attenuated I_A (Fig. 2.4); 4-AP similarly attenuates I_A in whole-cell recordings ($n=5$) as previously shown (Inyushkin 2005).

We measured the steady-state inactivation of I_A at +10 mV for 500 ms following 1-s conditioning prepulses from -100 to +10 mV. The inactivation function reached its

minimum above -40 mV and had the parameters $\theta_h = -85.6$ mV and $\sigma_h = -13.8$ mV. These data explain why I_A can be evoked from a holding potential of -60 mV (e.g., Fig. 2.1B, inset). I_A is not fully inactivated at that potential, $h_\infty(-60) = 0.135$, (Fig. 2.3B).

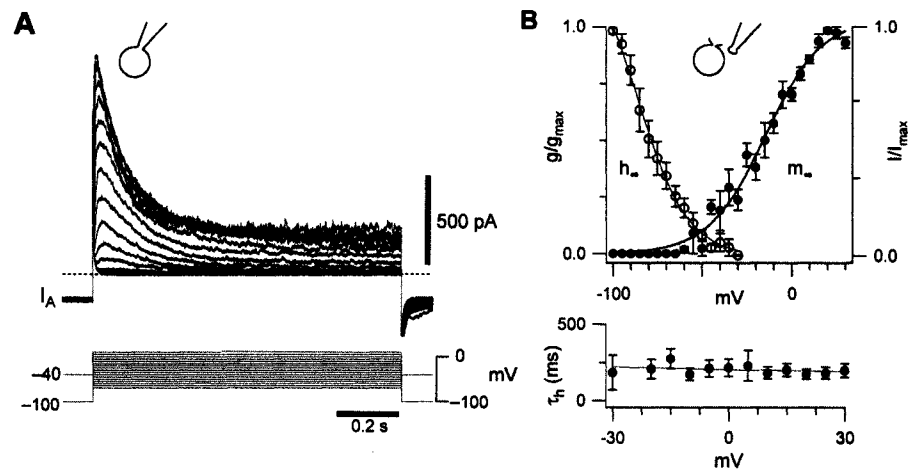


Figure 2.3. Biophysics of I_A in inspiratory neurons. **A**, The voltage-dependency of activation was measured by subtracting currents at holding potentials of -100 mV from evoked currents at -40 mV. **B**, Steady-state activation curve (m_∞) and inactivation curve (h_∞) from outside-out patches. **C**, The time constant of inactivation (τ_h) as a function of voltage.

I_A exhibits a small window current extending from -60 to -30 mV that peaks at -52.2 mV with only 0.6% of the current active. These data suggest that I_A does not substantially influence the baseline membrane potential during the majority of the quiescent (i.e., expiratory) phase of network activity but resides in a de-inactivated state and can be evoked by depolarization.

Over the range -30 to $+30$ mV, the time constant of inactivation was 200-300 ms and could be empirically fit with a line in the form, $\tau_h(V) = 201.95 - 0.42V$ (Fig. 2.3B, bottom), which is consistent with weak voltage dependence for the slow inactivation time constant of approximately 200 ms in mouse spinal cord and rat hippocampus (among others), as well as in Kv4.1, Kv4.2, and Kv4.3 channels

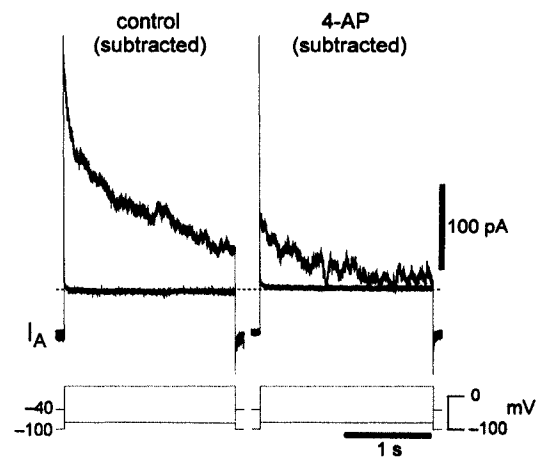


Figure 2.4. I_A attenuation from 2 mM 4-AP.

expressed in oocytes. (Koch 1999; Segal et al. 1984; Serodio et al. 1994; Serodio et al. 1996). Interestingly, $\tau_h(V)$ of ~ 200 ms is commensurate with both the ramping depolarization responses observed in current clamp from baseline voltages of -70 mV (e.g., Fig. 2.1C) and the transient ramp-like depolarization seen during endogenous network activity (e.g., Fig. 2.1A), suggesting the involvement of I_A in these membrane behaviors.

The prevalence of I_A in rhythmogenic preBötC neurons

As one way to classify inspiratory neurons as rhythmogenic, Rekling et al. (1996a) measured the difference between the onset of inspiratory-related EPSPs and the upstroke of XII activity, i.e., the *drive latency*, and proposed that the earliest neurons to activate during the respiratory cycle are important for rhythmogenesis. Furthermore we recently showed that membrane capacitance (C_M) of ~ 30 -65 pF is correlated with early drive latency in rhythmogenic preBötC neurons (Chapter 1, Hayes and Del Negro 2007). Using these criteria we quantified I_A expression in the preBötC. Eighteen of 28 (64.3%)

inspiratory neurons expressed measurable I_A . The average C_M was 54.0 ± 7.4 pF ($n=15$) and the average drive latency was 304.5 ± 14.9 ms, consistent with a role in rhythmogenesis. The average whole-cell conductance for I_A (g_A) normalized to C_M was 0.289 ± 0.047 nS/pF ($n=11$). Thus for a typical preBötC neuron with a whole-cell capacitance of 50 pF, the whole-cell g_A would be about 15 nS and I_A would be expected to generate 0.5-1.5 nA of outward current during standard rhythmic activity *in vitro*.

The 10 of 28 (35.7%) preBötC neurons without measurable I_A exhibited drive latencies of 312.4 ± 15.7 ms and C_M of 42.9 ± 3.7 pF ($n=10$), which were indistinguishable from I_A -expressing neurons (t-test: $p > 0.35$ and t-test: $p > 0.19$). These data suggest that rhythmogenic neurons do not uniformly express I_A as originally suggested (Rekling et al. 1996a).

Nevertheless, I_A is expressed in more than half of the preBötC neurons classified as rhythmogenic, in which it is available at typical baseline membrane potentials and generates large magnitude outward currents lasting several hundred milliseconds (Figs. 1,3,4). These data suggest that I_A might have an important role in influencing respiratory rhythmogenesis.

4-AP affects rhythmic activity in the preBötC

In the context of respiratory network activity we found that 4-AP caused XII output to become erratic and essentially uninterpretable. Therefore, we sought to determine whether the disorganized XII output reflected a breakdown in rhythmogenesis by performing field recordings within the preBötC (\int preBötC) while recording the contralateral XII activity (Fig. 2.5A). The \int preBötC and \int XII activity patterns were well correlated and rhythmic in control and washout, whereas 4-AP caused noisy \int preBötC activity that fluctuated in amplitude and period (Fig. 2.5B). 4-AP (as stated above)

induced irregular \int XII activity. These data suggest that pharmacological attenuation of I_A affected rhythmic preBötC neurons directly or indirectly.

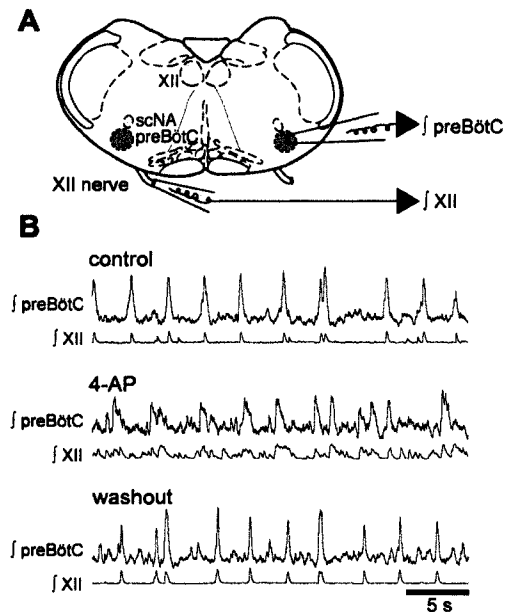


Figure 2.5. Effects of 4-AP on the preBötC network. **A**, A cartoon showing the configuration of the preBötC field-recording pipette (\int preBötC) and \int XII. **B**, \int preBötC (top traces) and \int XII (bottom traces) under control conditions, in the presence of 2 mM 4-AP, and washout.

To explain the role of I_A we examined the transformation of network activity from the perspective of single preBötC neurons in the presence of 4-AP. The respiratory rhythm generating network is active before the XII burst. During on-cell recordings accelerating spike discharge in the 400-600 ms prior to XII output suggested temporal summation of network drive (Fig. 2.6A). We obtained direct evidence for such drive in whole-cell current clamp by comparing zero bias conditions (Fig. 2.6B) to hyperpolarized membrane potentials below spike threshold (Fig. 2.6C), and in voltage clamp (Fig. 2.6D). All of these records illustrate spiking

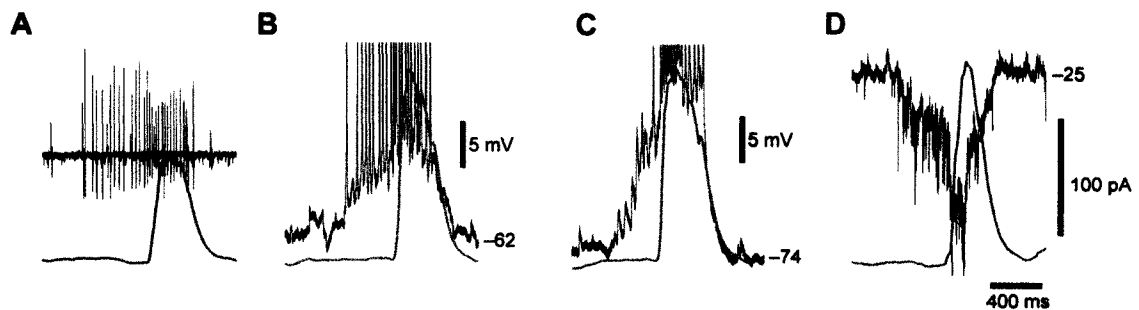


Figure 2.6. Characteristics of phasic synaptic input to inspiratory neurons. **A**, On-cell unit recordings of an inspiratory neuron that activates early relative to the \int XII. **B**, A current-clamp recording at 0 pA holding current illustrating similar activity as in **A**. **C**, A current-clamp recording at -40 pA holding current. **D**, Voltage-clamp recording at a holding potential of -60 mV. Traces in **A**, **C**, **D**, and **E** were all recorded in the same neuron.

and/or temporal summation of EPSPs/EPSCs for several hundred milliseconds preceding inspiratory bursts, which did not change as a function of membrane voltage.

We applied 2 mM 4-AP to examine cellular changes induced by I_A attenuation. Delayed excitation was eliminated in 4-AP and recovered in washout (Fig. 2.7A). 4-AP modified the inspiratory burst pattern, which reversibly changed from incrementing in control to decrementing in the presence of 4-AP (Fig. 2.7C). We quantified this change by measuring the leading slope of the burst, which changed significantly in 4-AP from 53.1 ± 7.4 mV/s to 80.2 ± 5.3 mV/s ($p < 0.05$, $n=8$, Fig. 9). However, the trailing slope did not change significantly: -52.7 ± 2.5 mV/s in control versus -65.5 ± 6.0 mV/s in 4-AP ($p > 0.05$, $n=8$, Fig. 2.9). These data suggest that orderly recruitment of inspiratory activity prior to XII output depends on I_A .

To analyze the network-level bursting pattern from the perspective of a single constituent neuron we applied a 5 Hz low-pass filter, which facilitates measurements of synaptic drive activity while filtering out spikes (Fig. 2.8). The average period of drive potentials did not change significantly between control and 4-AP application (Figs. 2.8 and 2.9) while the coefficient of variation (CV) of the period approximately doubled, which is a very significant change ($p < 0.001$, $n=8$, Fig. 2.9). The

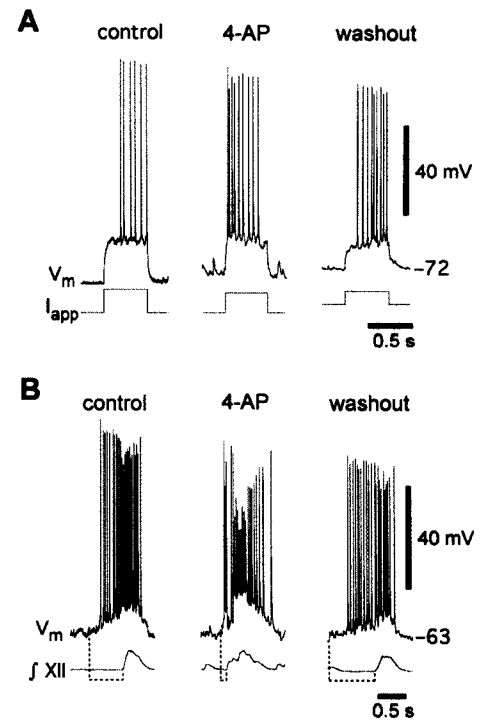


Figure 2.7. Whole-cell effects of 4-AP on inspiratory neurons. **A**, The presence of voltage-dependent delayed excitation was tested between bursts of activity and was abolished in 4-AP and recovered in washout. **B**, The burst discharge pattern changes from predominantly incremental (left) to decremental (middle) and back to incremental in washout (right). Dashed lines at the bottom indicate the change in drive latency of these specific bursts. Recordings were at 0 pA bias current.

average amplitude of the drive potential did not significantly change (Figs. 2.8 and 2.9) but the CV for amplitude changed significantly ($p < 0.05$, $n=8$, Fig. 2.9).

4-AP did not change the baseline membrane (bias current is 0 pA in Figs. 2.7B and 2.8), which is consistent with the lack of significant window current measured in voltage clamp (see Fig. 2.3B).

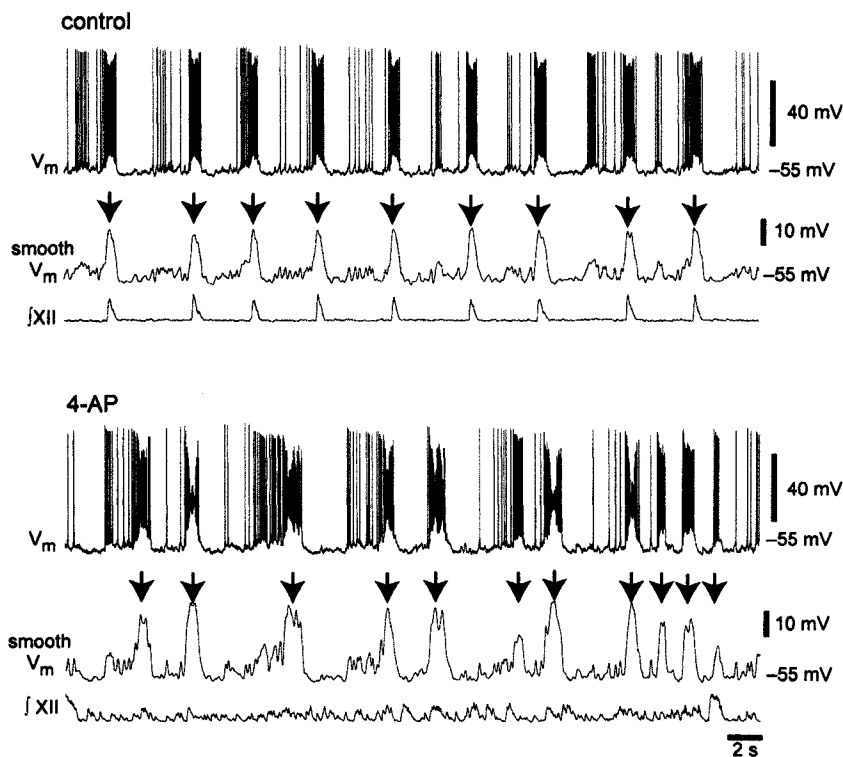


Figure 2.8. Effects of 4-AP on burst frequency in inspiratory neurons. All recordings were at 0 pA bias current. Vertical arrowheads indicate the type of bursts analyzed in Fig. 2.9.

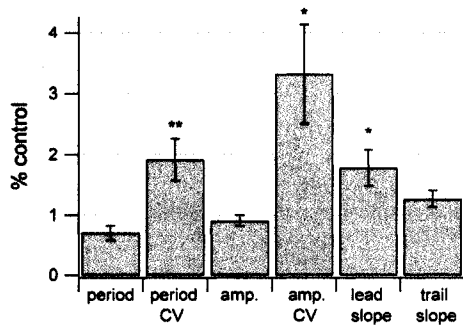


Figure 2.9. Effects of 4-AP on general burst characteristics expressed as fraction of control. Peak amplitude of bursts are indicated by "amp." Statistical significance at $p < 0.05$ is shown with * and $p < 0.01$ is shown with **.

2.4. Discussion

I_A in preBötC neurons resembles the canonical I_A found throughout the brain of mammals and other organisms (Birnbaum et al. 2004; Connor and Stevens 1971; Gustafsson et al. 1982; Hagiwara et al. 1961; Neher 1971). With regard to respiration, I_A has been observed in synaptically isolated preBötC neurons (Inyushkin 2005), and its role has been studied in mathematical models of the ventral respiratory group in the medulla (Rybak et al. 1997). However, this is the first detailed characterization of I_A from putatively rhythmogenic preBötC neurons. More importantly, we offer the first analysis of the role of I_A during endogenous respiratory network activity *in vitro*.

Role of I_A in vitro

We characterized the voltage-dependence and kinetics of I_A in somatic outside-out patches, which allowed us to minimize space-clamp limitations and series-resistance errors. I_A activates below -60 mV and is not fully inactivated until approximately -30 mV. These activation and inactivation functions encompass the range of membrane potentials visited during the interval between inspiratory bursts. This implies that I_A resides in a de-inactivated state at baseline membrane potentials and can be quickly recruited by synaptic depolarization during the respiratory cycle.

I_A has a small window current, but does this affect baseline membrane potential?

In 9 mM extracellular $[K^+]$, I_A attenuation via 4-AP application did not depolarize preBötC

neurons, suggesting that the window current was small and perhaps irrelevant. However, Rekling et al. (1996a) used a lower extracellular $[K^+]$ solution (6.2 mM) that would enhance the driving force for I_A . The window current may be large enough to account for their observation that neurons with evidence of I_A expression (i.e., type 1 neurons) had lower baseline membrane potentials than respiratory neurons without evidence for I_A .

A membrane behavior widely associated with I_A can be described as 'delayed excitation', wherein depolarization evoked by current pulses gets delayed for several hundred milliseconds (or longer) by the transient influence of I_A (Dekin and Getting 1987; Gabel and Nisenbaum 1998; Getting 1989; 1983; Hagiwara et al. 1961). This behavior can affect synaptic integration as demonstrated in hippocampal and neocortical pyramidal neurons (Gulledge et al. 2005; Hoffman et al. 1997; Storm 1988). Synaptic excitation builds up over several hundred milliseconds preceding XII output in rhythmogenic preBötC neurons (Hayes and Del Negro 2007; Rekling et al. 1996a; Rekling and Feldman 1998, also see Figs. 2.1A, 2.6 and 2.7B). Since I_A gives rise to delayed excitation in preBötC neurons in dedicated current-clamp protocols, is deactivated at baseline membrane potentials (Fig. 2.1B inset and 2.3B), and has a 200-ms inactivation time constant, we conclude that I_A plays a major role in shaping the ramp-like incremental discharge pattern characteristic of rhythmogenic neurons. Supporting evidence for this role is the dramatic increase in the leading slope of inspiratory activity following 4-AP application (Fig. 2.7B and 2.9).

In invertebrate CPGs, I_A regulates the order in which rhythmogenic neurons discharge (Byrne 1980; Getting 1983; Tierney and Harris-Warrick 1992). With regard to respiration, in spite of the fact that 4-AP caused uninterpretable XII discharge, network rhythms continued within the preBötC and could be detected and measured in whole-cell

and field recordings. 4-AP did not affect the mean period or amplitude of inspiratory burst-like discharges, but it did significantly increase period and amplitude variability (Fig. 2.9). Since the increase in variability was correlated with the diminished ramp-like incremental discharge pattern in 4-AP, this suggests that I_A influences the orderly recruitment of rhythm-generating neurons in the build-up to the inspiratory burst, which promotes regularity in respiratory network behavior.

Role of I_A in vivo

In the context of endogenous network activity, the E_K in our system is calculated to be approximately -71 mV, while *in vivo* this is probably closer to -98 mV (assuming ~ 3 mM $[K^+]$ in the cerebrospinal fluid, c.f. (Richter et al. 1978)). Under *in vivo* conditions we expect the driving force of I_A to be much higher, and thus the window current would have a larger hyperpolarizing influence on baseline membrane potential. This may bring I_A to an even more de-inactivated state between inspiratory bursts than our *in vitro* conditions. In this environment, where inspiratory neurons are expected to be under intensive bombardment of excitatory and inhibitory input, I_A may play an even more substantial role in the orderly recruitment of respiratory rhythmic activity through its ability to rapidly activate with a large outward current and quench spurious depolarizations.

2.5. References

Armstrong CM, Gilly WF, and Bernardo R. [5] Access resistance and space clamp problems associated with whole-cell patch clamping. In: *Methods in Enzymology* Academic Press, 1992, p. 100-122.

Bianchi AL, Denavit-Saubie M, and Champagnat J. Central control of breathing in mammals: neuronal circuitry, membrane properties, and neurotransmitters. *Physiol Rev* 75: 1-45, 1995.

Birnbaum SG, Varga AW, Yuan LL, Anderson AE, Sweatt JD, and Schrader LA. Structure and function of Kv4-family transient potassium channels. *Physiol Rev* 84: 803-833, 2004.

Brockhaus J, and Ballanyi K. Synaptic inhibition in the isolated respiratory network of neonatal rats. *Eur J Neurosci* 10: 3823-3839, 1998.

Byrne JH. Analysis of ionic conductance mechanisms in motor cells mediating inking behavior in *Aplysia californica*. *J Neurophysiol* 43: 630-650, 1980.

Connor JA, and Stevens CF. Voltage clamp studies of a transient outward membrane current in gastropod neural somata. *J Physiol* 213: 21-30, 1971.

Dekin MS, and Getting PA. In vitro characterization of neurons in the ventral part of the nucleus tractus solitarius. II. Ionic basis for repetitive firing patterns. *J Neurophysiol* 58: 215-229, 1987.

Dekin MS, Getting PA, and Johnson SM. In vitro characterization of neurons in the ventral part of the nucleus tractus solitarius. I. Identification of neuronal types and repetitive firing properties. *J Neurophysiol* 58: 195-214, 1987.

Del Negro CA, Johnson SM, Butera RJ, and Smith JC. Models of respiratory rhythm generation in the pre-Bötzinger complex. III. Experimental tests of model predictions. *J Neurophysiol* 86: 59-74, 2001.

Del Negro CA, Koshiya N, Butera RJ, Jr., and Smith JC. Persistent sodium current, membrane properties and bursting behavior of pre-bötzinger complex inspiratory neurons in vitro. *J Neurophysiol* 88: 2242-2250, 2002a.

Del Negro CA, Morgado-Valle C, and Feldman JL. Respiratory rhythm: an emergent network property? *Neuron* 34: 821-830, 2002b.

Del Negro CA, Morgado-Valle C, Hayes JA, Mackay DD, Pace RW, Crowder EA, and Feldman JL. Sodium and Calcium Current-Mediated Pacemaker Neurons and Respiratory Rhythm Generation. *J Neurosci* 25: 446-453, 2005.

Feldman JL, and Del Negro CA. Looking for inspiration: new perspectives on respiratory rhythm. *Nat Rev Neurosci* 7: 232, 2006.

Funk GD, Smith JC, and Feldman JL. Generation and transmission of respiratory oscillations in medullary slices: role of excitatory amino acids. *J Neurophysiol* 70: 1497-1515, 1993.

Funk GD, Smith JC, and Feldman JL. Modulation of neural network activity in vitro by cyclothiazide, a drug that blocks desensitization of AMPA receptors. *J Neurosci* 15: 4046-4056, 1995.

Gabel LA, and Nisenbaum ES. Biophysical characterization and functional consequences of a slowly inactivating potassium current in neostriatal neurons. *J Neurophysiol* 79: 1989-2002, 1998.

Getting PA. Emerging principles governing the operation of neural networks. *Annu Rev Neurosci* 12: 185-204, 1989.

Getting PA. Mechanisms of pattern generation underlying swimming in Tritonia. III. Intrinsic and synaptic mechanisms for delayed excitation. *J Neurophysiol* 49: 1036-1050, 1983.

Gray PA, Janczewski WA, Mellen N, McCrimmon DR, and Feldman JL. Normal breathing requires preBötzinger complex neurokinin-1 receptor-expressing neurons. *Nat Neurosci* 4: 927-930, 2001.

Gray PA, Rekling JC, Bocchiaro CM, and Feldman JL. Modulation of respiratory frequency by peptidergic input to rhythmogenic neurons in the preBötzinger complex. *Science* 286: 1566-1568, 1999.

Greer JJ, Smith JC, and Feldman JL. Role of excitatory amino acids in the generation and transmission of respiratory drive in neonatal rat. *J Physiol* 437: 727-749, 1991.

Gulledge AT, Kampa BM, and Stuart GJ. Synaptic integration in dendritic trees. *J Neurobiol* 64: 75-90, 2005.

Gustafsson B, Galvan M, Grafe P, and Wigstrom H. A transient outward current in a mammalian central neurone blocked by 4-aminopyridine. *Nature* 299: 252-254, 1982.

Hagiwara S, Kusano K, and Saito N. Membrane changes of Onchidium nerve cell in potassium-rich media. *J Physiol* 155: 470-489, 1961.

Haller M, Mironov SL, Karschin A, and Richter DW. Dynamic activation of K(ATP) channels in rhythmically active neurons. *J Physiol* 537: 69-81, 2001a.

Haller M, Mironov SL, and Richter DW. Intrinsic optical signals in respiratory brain stem regions of mice: neurotransmitters, neuromodulators, and metabolic stress. *J Neurophysiol* 86: 412-421, 2001b.

Hayes JA, and Del Negro CA. Neurokinin Receptor-Expressing Pre-Bötzinger Complex Neurons in Neonatal Mice Studied In Vitro. *J Neurophysiol* 97: 4215-4224, 2007.

Hayes JA, Mendenhall JM, Brush BR, and Del Negro CA. Transient K⁺ currents in preBötzinger Complex neurons shape inspiratory discharge and promote coherent network activity. *Journal of Neurophysiology* submitted: 2007.

Hoffman DA, Magee JC, Colbert CM, and Johnston D. K⁺ channel regulation of signal propagation in dendrites of hippocampal pyramidal neurons. *Nature* 387: 869-875, 1997.

Inyushkin AN. Thyroliberin blocks the potassium A-current in neurons in the respiratory center of adult rats in vitro. *Neurosci Behav Physiol* 35: 549-554, 2005.

Johnson SM, Smith JC, and Feldman JL. Modulation of respiratory rhythm in vitro: role of Gi/o protein-mediated mechanisms. *J Appl Physiol* 80: 2120-2133, 1996.

Koch C. Biophysics of computation : information processing in single neurons. In: *Computational neuroscience*. New York: Oxford University Press, 1999, p. 221.

Marder E. Moving rhythms. *Nature* 410: 755, 2001.

Mironov SL, Langohr K, Haller M, and Richter DW. Hypoxia activates ATP-dependent potassium channels in inspiratory neurones of neonatal mice. *J Physiol* 509 (Pt 3): 755-766, 1998.

Mironov SL, Langohr K, and Richter DW. A1 adenosine receptors modulate respiratory activity of the neonatal mouse via the cAMP-mediated signaling pathway. *J Neurophysiol* 81: 247-255, 1999.

Mironov SL, Langohr K, and Richter DW. Hyperpolarization-activated current, I_h , in inspiratory brainstem neurons and its inhibition by hypoxia. *Eur J Neurosci* 12: 520-526, 2000.

Mironov SL, and Richter DW. Intracellular signalling pathways modulate K(ATP) channels in inspiratory brainstem neurones and their hypoxic activation: involvement of metabotropic receptors, G-proteins and cytoskeleton. *Brain Res* 853: 60-67, 2000.

Mironov SL, and Richter DW. L-type Ca^{2+} channels in inspiratory neurones of mice and their modulation by hypoxia. *J Physiol* 512 (Pt 1): 75-87, 1998.

Mironov SL, and Richter DW. Oscillations and hypoxic changes of mitochondrial variables in neurons of the brainstem respiratory centre of mice. *J Physiol* 533: 227-236, 2001.

Neher E. Two fast transient current components during voltage clamp on snail neurons. *J Gen Physiol* 58: 36-53, 1971.

Nisenbaum ES, Xu ZC, and Wilson CJ. Contribution of a slowly inactivating potassium current to the transition to firing of neostriatal spiny projection neurons. *J Neurophysiol* 71: 1174-1189, 1994.

Onimaru H, Ballanyi K, and Homma I. Contribution of Ca²⁺-dependent conductances to membrane potential fluctuations of medullary respiratory neurons of newborn rats in vitro. *J Physiol* 552: 727-741, 2003.

Onimaru H, Shamoto A, and Homma I. Modulation of respiratory rhythm by 5-HT in the brainstem-spinal cord preparation from newborn rat. *Pflugers Arch* 435: 485-494, 1998.

Paarmann I, Frermann D, Keller BU, Villmann C, Breitingner HG, and Hollmann M. Kinetics and subunit composition of NMDA receptors in respiratory-related neurons. *J Neurochem* 93: 812-824, 2005.

Pace RW, Mackay DD, Feldman JL, and Del Negro CA. Inspiratory bursts in the preBötzinger Complex depend on a calcium-activated nonspecific cationic current linked to glutamate receptors. *J Physiol* jphysiol.2007.133660, 2007a.

Pace RW, Mackay DD, Feldman JL, and Del Negro CA. Role of persistent sodium current in mouse preBötzinger Complex neurons and respiratory rhythm generation. *J Physiol* 580: 485-496, 2007b.

Pace RW, Mackay DD, Feldman JL, and Del Negro CA. Role of Persistent Sodium Current in Mouse PreBotzinger Neurons and Respiratory Rhythm Generation. *J Physiol (Lond)* jphysiol.2006.124602, 2007c.

Pena F, Parkis MA, Tryba AK, and Ramirez J-M. Differential Contribution of Pacemaker Properties to the Generation of Respiratory Rhythms during Normoxia and Hypoxia. *Neuron* 43: 105, 2004.

Pena F, and Ramirez JM. Endogenous activation of serotonin-2A receptors is required for respiratory rhythm generation in vitro. *J Neurosci* 22: 11055-11064, 2002.

Pena F, and Ramirez JM. Substance P-mediated modulation of pacemaker properties in the mammalian respiratory network. *J Neurosci* 24: 7549-7556, 2004.

Pierrefiche O, Bischoff AM, and Richter DW. ATP-sensitive K⁺ channels are functional in expiratory neurones of normoxic cats. *J Physiol* 494 (Pt 2): 399-409, 1996.

Pierrefiche O, Haji A, Bischoff A, and Richter DW. Calcium currents in respiratory neurons of the cat in vivo. *Pflugers Arch* 438: 817-826, 1999.

Pierrefiche O, Schwarzacher SW, Bischoff AM, and Richter DW. Blockade of synaptic inhibition within the pre-Bötzinger complex in the cat suppresses respiratory rhythm generation in vivo. *J Physiol* 509 (Pt 1): 245-254, 1998.

Ptak K, Zummo GG, Alheid GF, Tkatch T, Surmeier DJ, and McCrimmon DR. Sodium Currents in Medullary Neurons Isolated from the Pre-Bötzinger Complex Region. *J Neurosci* 25: 5159-5170, 2005.

Rekling JC, Champagnat J, and Denavit-Saubie M. Electroresponsive properties and membrane potential trajectories of three types of inspiratory neurons in the newborn mouse brain stem in vitro. *J Neurophysiol* 75: 795-810, 1996a.

Rekling JC, Champagnat J, and Denavit-Saubie M. Thyrotropin-releasing hormone (TRH) depolarizes a subset of inspiratory neurons in the newborn mouse brain stem in vitro. *J Neurophysiol* 75: 811-819, 1996b.

Rekling JC, and Feldman JL. PreBötzinger complex and pacemaker neurons: hypothesized site and kernel for respiratory rhythm generation. *Annu Rev Physiol* 60: 385-405, 1998.

Richter DW, Camerer H, and Sonnhof U. Changes in extracellular potassium during the spontaneous activity of medullary respiratory neurones. *Pflugers Arch* 376: 139-149, 1978.

Richter DW, and Spyer KM. Studying rhythmogenesis of breathing: comparison of in vivo and in vitro models. *Trends Neurosci* 24: 464-472, 2001.

Ruangkittisakul A, Schwarzacher SW, Secchia L, Poon BY, Ma Y, Funk GD, and Ballanyi K. High Sensitivity to Neuromodulator-Activated Signaling Pathways at Physiological $[K^+]$ of Confocally Imaged Respiratory Center Neurons in On-Line-Calibrated Newborn Rat Brainstem Slices. *J Neurosci* 26: 11870-11880, 2006.

Rybak IA, Paton JF, and Schwaber JS. Modeling neural mechanisms for genesis of respiratory rhythm and pattern. I. Models of respiratory neurons. *J Neurophysiol* 77: 1994-2006, 1997.

Segal M, Rogawski MA, and Barker JL. A transient potassium conductance regulates the excitability of cultured hippocampal and spinal neurons. *J Neurosci* 4: 604-609, 1984.

Serodio P, Kentros C, and Rudy B. Identification of molecular components of A-type channels activating at subthreshold potentials. *J Neurophysiol* 72: 1516-1529, 1994.

Serodio P, Vega-Saenz de Miera E, and Rudy B. Cloning of a novel component of A-type K⁺ channels operating at subthreshold potentials with unique expression in heart and brain. *J Neurophysiol* 75: 2174-2179, 1996.

Shao XM, and Feldman JL. Acetylcholine modulates respiratory pattern: effects mediated by M3-like receptors in preBötzinger complex inspiratory neurons. *J Neurophysiol* 83: 1243-1252, 2000.

Shao XM, Ge Q, and Feldman JL. Modulation of AMPA receptors by cAMP-dependent protein kinase in preBötzinger complex inspiratory neurons regulates respiratory rhythm in the rat. *J Physiol* 547: 543-553, 2003.

Smith JC, Ellenberger HH, Ballanyi K, Richter DW, and Feldman JL. Pre-Bötzinger complex: a brainstem region that may generate respiratory rhythm in mammals. *Science* 254: 726-729, 1991.

Stein PSG. *Neurons, networks, and motor behavior.* Cambridge: MIT Press, 1997, p. 305.

Storm JF. Temporal integration by a slowly inactivating K⁺ current in hippocampal neurons. *Nature* 336: 379-381, 1988.

Thoby-Brisson M, Telgkamp P, and Ramirez JM. The role of the hyperpolarization-activated current in modulating rhythmic activity in the isolated respiratory network of mice. *J Neurosci* 20: 2994-3005, 2000.

Tierney AJ, and Harris-Warrick RM. Physiological role of the transient potassium current in the pyloric circuit of the lobster stomatogastric ganglion. *J Neurophysiol* 67: 599-609, 1992.

CHAPTER 3. Network-mediated burst initiation and its role in respiratory rhythm generation

3.1. Introduction

Attempts to understand rhythmogenesis *in vitro* have focused on canonical mechanisms including *reciprocal inhibition* or *pacemaker neurons* (Grillner 2003; Marder 2001; Marder and Calabrese 1996; Orlovsky et al. 1999; Stein 1997). Early models of respiration based on reciprocal inhibition (Feldman 1986) were ruled out by the demonstration that a respiratory-like rhythmic output persists after blocking synaptic inhibition *in vitro* (Brockhaus and Ballanyi 1998; Feldman and Smith 1989). This bolstered the idea, originally speculative (Feldman and Cleland 1982), that voltage-dependent pacemaker neurons drive rhythmogenesis, i.e., the *pacemaker hypothesis*.

The putative pacemaker neurons in neonates (ages P0-15) depend on persistent Na^+ current (I_{NaP}) (Butera et al. 1999a; Del Negro et al. 2002a; Del Negro et al. 2002b; Del Negro et al. 2005; Thoby-Brisson and Ramirez 2001). However, riluzole (RIL) and tetrodotoxin (TTX), applied at dosages that selectively block I_{NaP} (Doble 1996; Urbani and Belluzzi 2000), do not prevent rhythmogenesis *in vitro* (Del Negro et al. 2002b; Del

Negro et al. 2005; Pace et al. 2007b; Pena et al. 2004), which contradicts an essential role for pacemaker neurons in rhythmogenesis.

In older neonates (P7-15) another form of bursting utilizes calcium- and calcium-activated cationic currents and is RIL-insensitive (Pena et al. 2004). Neurons with this property are not present, or comprise a minuscule fraction, of the preBötC in neonates P0-6, and thus are unlikely to be rhythmogenic, especially in newborns. Therefore, we have argued that neurons with pacemaker properties probably do not drive rhythmogenesis.

Our favored hypothesis for the mechanism of rhythmogenesis is based on emergent network properties. The *group pacemaker hypothesis* proposed by Rekling and Feldman (1996a; 1998) posits that recurrent synaptic excitation convolved with intrinsic cellular properties gives rise to periodic network-wide bursts. It is predicated on a functional hierarchy of electrophysiological phenotypes and their synaptic connectivity (Rekling et al. 1996a; Rekling and Feldman 1998), not subpopulations of pacemaker neurons. Pacemaker properties, to the extent that they utilize intrinsic currents such as I_{NaP} and I_{CAN} , participate in rhythm generation but are not obligatory.

Under Rekling et al.'s original classification (1996a), the neurons that initiate large amplitude inspiratory bursts earliest in the respiratory cycle (i.e., similar to Fig. 1.4A, Fig. 2.1A) were referred to as 'type 1 neurons'. Bursts terminate with an after-hyperpolarization that recovers during the first half of the inter-inspiratory interval. Because of their early drive latency (see Chapter 1 and 2) and sensitivity to SP, type 1 neurons were hypothesized to be the crucial population of NK1R⁺ neurons that comprise the rhythmogenic kernel (Gray et al. 1999; Rekling et al. 1996a; b).

Rekling et al.'s (1996a) 'type 2' neurons have high input resistance and discharge tonically at a low frequency during the inter-inspiratory interval (i.e., similar to

Fig. 1.4B). Notwithstanding their high excitability, type 2 neurons initiate inspiratory bursts later in the cycle compared to type 1 neurons and therefore were classified as downstream targets that receive inspiratory synaptic drive from the rhythmogenic type 1 population (Rekling et al. 1996a). This synaptic coupling arrangement is logical except that type 2 neurons selectively express the hyperpolarization-activated cationic current I_h (Rekling et al. 1996a; Thoby-Brisson et al. 2000). Pharmacological attenuation of I_h has no effect on type 1 neurons yet accelerates respiratory frequency, which suggests that type 2 neurons have feedback interactions with the type 1 population and play some role in rhythm generation, or are themselves part of the rhythmogenic core.

Finally, Rekling et al.'s (1996a) 'type 3' neurons have relatively low input resistance and depolarize latest in the respiratory cycle (i.e. similar to Fig. 1.4D). These neurons were proposed to be respiratory premotoneurons or motoneurons in the nucleus ambiguus (Bieger and Hopkins 1987; Rekling et al. 1996a).

In the previous two chapters we discussed early inspiratory neurons (Fig. 1.3) which seem to share many of the aforementioned properties of type 1 (Fig. 1.4A) and type 2 neurons (Fig. 1.4B) including the A-current that can give rise to delayed excitation (Chapter 2). Likewise, our description of late inspiratory neurons (Figure 1.3, 1.4D) appear to be generally consistent with the type 3 phenotype. Our data suggest that early inspiratory neurons are a heterogeneous population made up of some neurons similar to type 1 neurons and others similar to type 2 neurons, but there is no discrete separation based on drive latency or NKR-expression. Therefore, throughout the remainder of this chapter we will continue to use the terminology early and late inspiratory populations unless specifically discussing Rekling's earlier nomenclature.

As the group pacemaker hypothesis predicts, anatomical evidence shows that rhythmogenic neurons are predominantly glutamatergic and form locally interconnected

networks within the preBötC (Guyenet et al. 2002; Guyenet and Wang 2001; Rekling et al. 2000; Stornetta et al. 2003; Wang et al. 2001) although how many average synaptic connections between the neurons is still speculative.

In this manuscript we evaluate the group pacemaker hypothesis of respiratory rhythm generation. Our approach was to construct a mathematical model that unifies the pacemaker/non-pacemaker, type 1-3, and early/late-inspiratory classification schemes, incorporates realistic numbers of neurons that are synaptically interconnected in a manner that may accurately reflect the general composition and function of the mouse preBötC. To this end, voltage-dependent pacemaker neurons with I_{NaP} are randomly dispersed throughout the early-inspiratory population, and calcium-activated non-specific cationic current (I_{CAN}) is expressed within all phenotypes. We show how excitatory synaptic coupling among early inspiratory neurons plays a crucial role in burst generation through recurrent excitation (Ballanyi et al. 1999; Bianchi et al. 1995; Rekling et al. 2000; Smith et al. 2000) and make testable predictions that rely on this recurrent excitation.

3.2. Methods

Differential equations were integrated using the 4th order Runge-Kutta method in custom C/C++ software run on Apple Macintosh G5 computers under OS 10.4 (See Appendices 3.4,3.5). Model experiments were performed for 2-3 simulated minutes. Integration step size was 0.1 ms.

Running-time histograms of late inspiratory neurons, believed to be premotoneurons, were plotted in lieu of, and to mimic, XII output in experiments (bin size=25 ms). Burst duration and cycle period were computed from the running-time histogram using the threshold 10 spikes/bin as the beginning and end point of model network bursts.

Several standard currents were included in the preBötC cellular model such as fast sodium current (I_{Na-F}), delayed-rectifier potassium current (I_{K-DR}), potassium leakage current (I_{K-LEAK}), persistent sodium current (I_{NaP}), AMPAR-mediated synaptic current (I_{AMPA}), and a tonic excitatory current ($I_{tonic-e}$). These currents are very similar to the ones in the preBötC neuron model developed by Butera and colleagues (Butera et al. 1999a; b; Del Negro et al. 2001). Other currents included:

Electrogenic Na^+/K^+ -ATPase ($I_{Na/K-APTase}$). $I_{Na/K-APTase}$ may contribute to burst termination in the preBötC, consistent with similar contributions in other rhythmic networks (Ballerini et al. 1997; Darbon et al. 2003; Del Negro et al. 1999; Johnson et al. 1992; Li et al. 1996; Seutin et al. 1996).

Hyperpolarization-activated mixed cation current (I_h). I_h causes 'sag' potentials in respiratory neurons (Mironov et al. 2000; Reikling et al. 1996a; Thoby-Brisson et al. 2000). In the model, I_h also contributes to $I_{Na/K-APTase}$ activation by fluxing Na^+ inward.

A-current (I_A). I_A causes 'delayed excitation' in more than half of inspiratory neurons (see Chapter 2). I_A also provides a slight hyperpolarizing window current, limits spike frequency, and will shunt incoming EPSPs during the onset of inspiratory bursts (Chapter 2).

SK-type calcium-dependent potassium current (I_{SK-Ca}). The I_{SK-Ca} underlies spike-frequency adaptation (Stocker 2004). This current mimics the role of the hypothetical ensemble of activity-dependent outward currents that terminate inspiratory bursts.

Calcium-activated non-specific cation current (I_{CAN}). We incorporated I_{CAN} , which was simulated with an intracellular $[Ca^{2+}]_i$ half-activation of 0.5 μM . This value is approximately half the value for the probable channel that gives rise to this current, TRPM4b or TRPM5 (Crowder et al. 2007; Ullrich et al. 2005). We coupled I_{CAN} in an *ad hoc* fashion to a mean synaptic gating variable, which approximately models the

synaptically generated sources of calcium entry that are not explicitly contained in the single-compartment formulation (Koch and Segev 1998). Ongoing studies suggest that I_{CAN} activates predominantly in dendritic sites and boosts excitatory synaptic input (Feldman and Del Negro 2006; Pace et al. 2007a). A full and complete description of I_{CAN} will require multi-compartment modeling at the cellular level, which is beyond the scope of the present project but is being pursued (Mendenhall et al. 2006). In this model, I_{CAN} fluxes Na^+ and K^+ and has a reversal potential (E_{CAN}) of 0 mV which, due to the relation to synaptic activity, boosts burst drive potentials. I_{CAN} also moderately contributes to $I_{Na/K-APTase}$ activation by fluxing Na^+ inward.

Calcium current (I_{Ca}). A generic high threshold calcium current with an effective inactivation time constant estimated at 15 ms (Elsen and Ramirez 1998) was incorporated that provided intracellular Ca^{2+} to activate the I_{CAN} and I_{SK-Ca} and provide a depolarizing current during bursts.

NMDA receptor-mediated synaptic current (I_{NMDA}). An I_{NMDA} was implemented to capture the voltage-dependent Mg^{2+} -block (Jahr and Stevens 1990a; b). The decay time constant was estimated from data to be approximately 30 ms. In addition to enhancing EPSPs, I_{NMDA} also contributes a small Ca^{2+} current to activate I_{CAN} and I_{SK-Ca} .

Electrical synaptic current ($I_{electrical}$). Electrical coupling via gap junctions was incorporated according to experimental measurements in preBötC neurons (Rekling et al. 2000). $I_{electrical}$ promotes homogenous baseline potentials among neurons with otherwise disparate leakage conductances (Koch and Segev 1998).

Noise current (I_{noise}). I_{noise} is a random low amplitude current input that is not captured by $I_{tonic-e}$ (Fall 2002).

The network is composed of the two phenotypes we have described and encapsulate many characteristic membrane properties described by Rekling et. al.

(1996a). Some of these neurons express low amounts of I_h , but express large I_A (similar to type 1 neurons) or high amounts of I_h , and low I_A (similar to type 2 neurons). Some neurons also experience a significant after-hyperpolarization at the end of the inspiratory phase, and thus recover from refractoriness with ramp-like trajectories during the expiratory phase (Chapter 2, Rekling et al. 1996a; Thoby-Brisson and Ramirez 2001). We also have neurons with large I_{NaP} that lead to voltage-dependent pacemakers in the early inspiratory population that represent up to 25% of that population. Finally, some of these neurons spike at low frequency during the interburst interval.

Late inspiratory neurons were assigned significantly lower input resistance (R_N) and are typically larger cells, reflected by their larger capacitance (Chapter 1). In the model, the late inspiratory neurons act as a threshold detector because they are the least excitable and the last to discharge prior to XII output. We use the late inspiratory spiking activity as an analogue to the XII output in simulations, since they may make up a portion of respiratory premotoneurons, but otherwise have the same currents as early inspiratory neurons.

Model Size and Topology. We simulated the bilaterally distributed preBötC as a single network with 1125 neurons and the following coupling topology: 975 early inspiratory neurons are sparsely coupled with feedback chemical and electrical connections among the rest of the early inspiratory population and then are also chemically connected to 150 late inspiratory neurons. Late inspiratory cells do not feed back into the early inspiratory population because we presume they project to motoneurons not explicitly modeled here and do not directly contribute to rhythmogenesis. All model equations and the details of the coupling topology are described in section 3.4 (Appendix 1).

3.3. Results and Discussion

Our previous data (Chapter 1 and 2) suggests that the population of preBötC inspiratory neurons are made up of heterogeneous subpopulations of putatively rhythmogenic (early inspiratory neurons) and premotoneurons (late inspiratory neurons). We were interested in testing the hypothesis that a heterogeneous population of model preBötC neurons could generate rhythmic activity through recurrent excitation by simulating the proposed group-pacemaker as realistically as possible[‡].

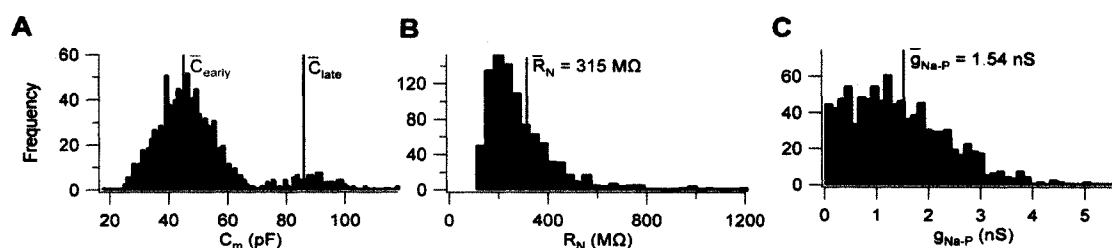


Figure 3.1. The group-pacemaker is made up of neurons with heterogeneous parameters. **A**, The distribution of membrane capacitances for early and late inspiratory neurons. **B**, The distribution of input resistances for all inspiratory neurons. **C**, The distribution of maximum persistent sodium conductance in all inspiratory neurons.

We first started out with varying the membrane capacitance (C_M) of model neurons to replicate experimental results where early inspiratory neurons had a mean C_M of 45 pF and late inspiratory neurons had a mean C_M of 86 pF. Since membrane capacitance is related to neuron size (Hille 2001), we related all our neurons' conductances to the magnitude of the capacitance by a factor that also varied (see section 3.4, Appendix 1). Figure 3.1 illustrates how the cellular capacitance (Fig. 3.1A), input resistance (R_N , Fig. 3.1B), and maximum persistent sodium conductance (g_{Na-P} , Fig. 3.1C) are distributed among the neurons. Figure 3.2 then illustrates how the two

[‡] Note that the work in this chapter was performed before most of the experimental results in Chapters 1 and 2 was completed and motivated us to perform that work. Therefore, the network size, fraction of NKR^+ neurons, and characteristics of I_A used here are not consistent with that data.

groups of inspiratory neurons were arranged into a network (see section 3.4., Appendix 1, for details on how connections were arranged).

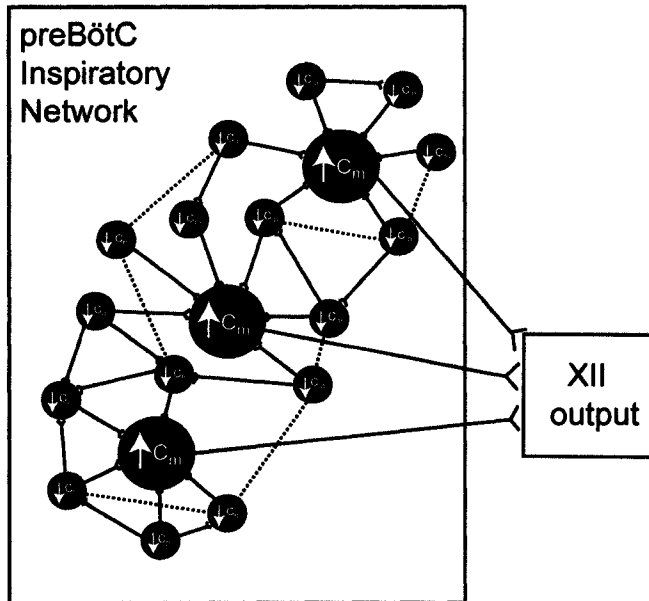


Figure 3.2. The general topology of the model preBötC network. Red circles represent early inspiratory neurons with relatively low C_M , while blue circles represent the late inspiratory neurons with relatively large C_M . Early neurons project with excitatory AMPAR- and NMDAR-mediated synapses to late neurons and also to other early neurons (solid lines). Early neurons are also coupled by electrical synapses mediated by gap junctions (dotted lines). The late neurons are hypothesized to project to XII neurons, so they represent the model XII output. See Section 3.4, Appendix 1, for details on how the network topology was generated.

Dynamics of rhythm generation

When the neurons are connected through excitatory synapses, the model generates respiratory-like oscillations resembling neonatal rodent *in vitro* preparations (Fig. 3.3)

Some inspiratory neurons are silent during the interburst interval and have monotonic current-voltage (IV) curves (Fig. 3.3A), while other early inspiratory neurons recover rapidly from inspiration and approach a steady state where they spontaneously discharge action potentials at a low rate that depends on the resting potassium conductance (R_N^{-1}) and noise (Fig. 3.3B). Collective tonic spiking of these neurons produces a steady stream of excitatory synaptic potentials that are 'broadcast' to the other early inspiratory neurons and these neurons also typically have a monotonic IV curve. A subset of the early inspiratory neurons have an IV curve with a negative-slope region (Fig. 3.3C) that leads to voltage-dependent pacemaker properties. Finally, late

inspiratory neurons (Fig. 3.3D) that have a substantially larger cellular capacitance (Fig. 3.1A) and low resting membrane potential are only activated when they receive massive convergent input from early inspiratory neurons.

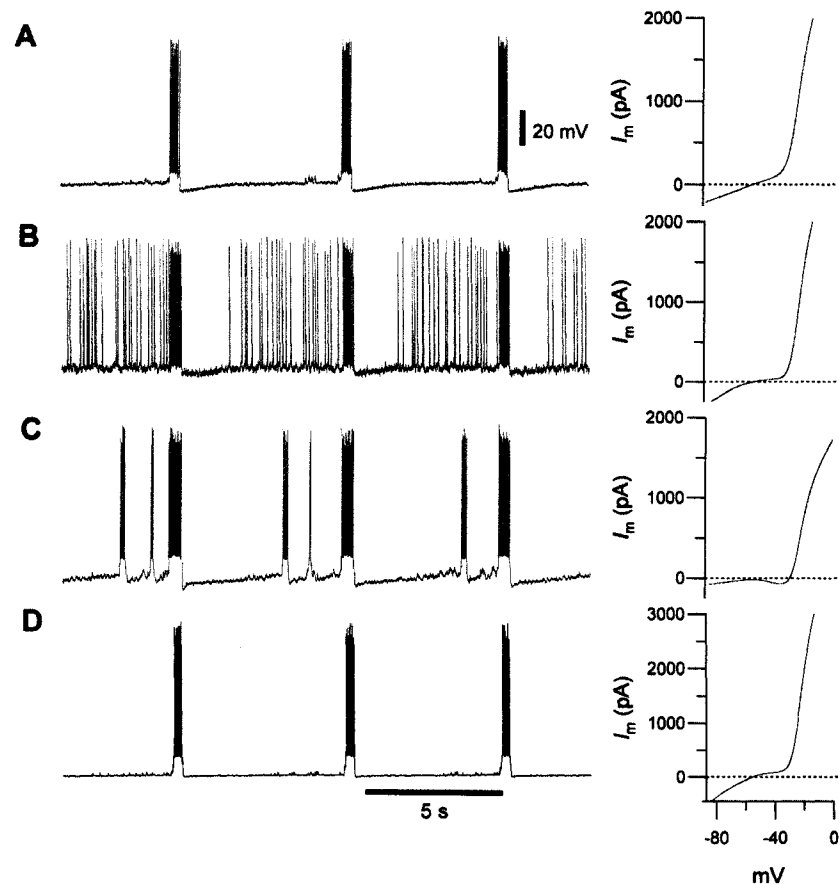


Figure 3.3. A variety of phenotypic patterns are exhibited by model inspiratory neurons. To the right of each voltage trace is a simulated IV curve for that neuron. **A**, A silent early inspiratory neuron similar to Fig. 1.4A and Fig. 2.1A. **B**, A tonically active early inspiratory neuron similar to Fig. 1.4B. **C**, An early inspiratory neuron with voltage-dependent pacemaker properties indicated by the negative slope region in the right IV curve. **D**, A silent late inspiratory neuron similar to the one in Fig. 1.4D.

To understand the cellular and synaptic mechanisms of rhythmogenesis, we begin by analyzing the respiratory cycle shortly after an inspiratory burst. Neurons such as the ones in Fig. 3.3B recover quickly from the inspiratory phase and spike at low frequency during the interburst interval. At first this synaptic broadcast fails to register in

the other neurons that remain hyperpolarized in a *refractory* state where even spatial and temporal summation of coincident EPSPs cannot cause these neurons to cross spike threshold. But as neurons recover from refractoriness they approach baseline potentials that we define as *susceptible* since a single EPSP can cause suprathreshold depolarization. Susceptible neurons become *active* when they commence spiking.

Neurons recover from refractoriness and relax toward the susceptible state. Then, spontaneous spiking from the broadcaster neurons promotes susceptible silent neurons into the active state. The highly interconnected nature of the early inspiratory neurons begins to dominate the dynamic evolution of network activity soon after in a cycle of recurrent excitation.

Figure 3.4A illustrates that burst onset is extremely sudden and cascade-like, overwhelmingly dependent on positive feedback. Burst onset is much faster than the slow recovery from refractoriness that dominates the majority of the expiratory phase. Recurrent excitation can only take place once a critical fraction of early inspiratory neurons attain the susceptible state. Otherwise, positive feedback cannot spread and will shortly be extinguished from lack of susceptible cells. The tipping point where a cascade is inevitable depends entirely on the number of active and synaptically interconnected early inspiratory neurons, but is very difficult to determine analytically. Neurons are high-dimensional dynamical systems and their trajectories are determined by a complement of ionic currents. Moreover, the state of connectivity in the network changes constantly as neurons evolve independently and flow into and out of the discrete classes we dub *active* and *susceptible*.

For the moment, we continue with a qualitative description focusing on the neurophysiology of the burst. Burst initiation depends on recurrent excitation. Thereafter, recurrent loops of positive feedback assist in sustaining the burst. Early inspiratory neurons project to other early inspiratory neurons, reinforcing their mutual excitation. Intrinsic inward currents, such as I_{NaP} and I_{CAN} , activate within constituent neurons due to

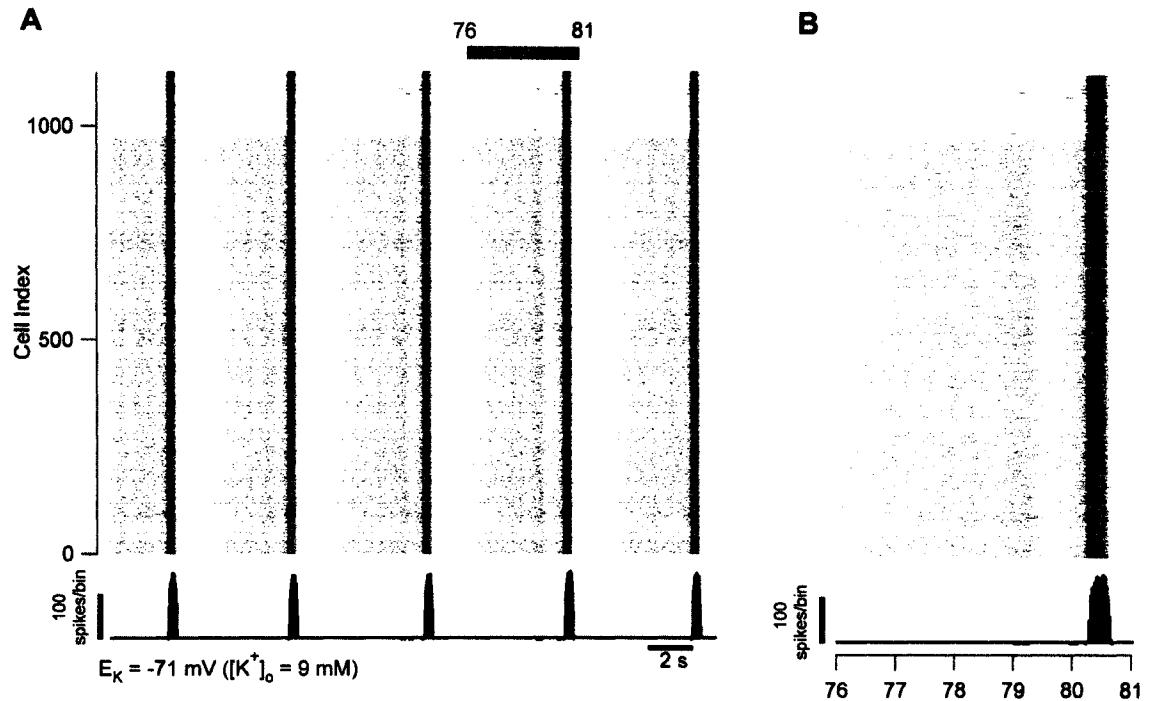


Figure 3.4. A raster plot of the population of neurons illustrating network bursts. Each dot represents an individual neuron's spike. Red dots indicate spikes from the early inspiratory neuron indicated on the ordinate. Blue dots represent late inspiratory neurons. The blue histogram represents the number of spikes in a 25 ms bin from late inspiratory neurons. **A**, Five simulated network bursts. **B**, A detail of one burst represented by the grey bar in A showing a network-mediated ectopic burst.

depolarization and calcium influx. I_{NaP} causes greater numbers of spikes per burst and I_{CAN} amplifies the magnitude of the inspiratory drive potential (Pace et al. 2007a; b). These intrinsic mechanisms further enhance the positive feedback, allowing the inspiratory burst to last up to several hundred milliseconds. During this time the early inspiratory neurons deliver massive synaptic drive to the late inspiratory neurons, which would otherwise remain silent. The late inspiratory neurons have high input conductance

and large capacitance and thus tend to remain in a state of very low excitability. However, there are fewer of them so when the rhythmogenic kernel of early inspiratory neurons becomes fully active during inspiration, the input to the late inspiratory neurons is massively convergent (975 rhythmogenic neurons projecting to 150 motor relays), which evokes robust bursts in the late inspiratory population. One can envision the late inspiratory cells as a threshold element.

The burst terminates because high frequency spiking recruits activity-dependent outward currents that gradually hyperpolarize early inspiratory neurons. The activity-dependent outward currents in this model include calcium-dependent potassium currents (I_{SK-Ca}) and Na^+/K^+ ATPase pump current ($I_{Na/K-ATPase}$). In the real system this effect may occur because of the activation of other important outward currents which have not yet been fully elucidated. In this model, I_{SK-Ca} and $I_{Na/K-ATPase}$ currents cause spiking cessation in early inspiratory neurons and the consequent breakup of feedback loops, which very rapidly disassembles the network activity. Since neither calcium nor sodium clearance exceeds the rate of breakup of the feedback loops, the early inspiratory neurons continue to be influenced by I_{SK-Ca} and $I_{Na/K-ATPase}$ for several hundred milliseconds after synaptic inputs stop and the inspiratory burst terminates, which is the ionic explanation for the post-inspiratory after-hyperpolarization, i.e., what causes the early inspiratory neurons to enter a hyperpolarized refractory state.

The broadcasting early inspiratory neurons also enter a transient refractory state after feedback loops are broken because they also express I_{SK-Ca} and $I_{Na/K-ATPase}$ (Fig. 3.3B). These neurons recover relatively fast and begin spiking with their characteristic low frequency rate, which then returns us to the point in the cycle where our analysis began.

Since the recovery process in silent early inspiratory neurons is the limiting factor in generating a subsequent burst they function as *refractors*. That is, in the context of network rhythmogenesis their primary role is to control the duration of the inter-inspiratory interval via their rate of recovery to the susceptible state. The dominant role of early inspiratory neurons with low frequency interburst spiking is to seed the network with a steady stream of excitatory synaptic potentials that can activate susceptible neurons, so we refer to them as *broadcasters*, which cannot and do not alone control when their stream of excitation will cause the refractors to coalesce and initiate the next burst. This illustrates one possible reason heterogeneous properties are important in the network.

Burst initiation

Recurrent excitation begins in the early inspiratory population, so this fraction of the full inspiratory population encapsulates the dynamics of burst initiation.

First we examine 'ectopic' bursts where the kernel partially assembles but fails to evoke motor output (Fig. 3.5). This phenomenon is frequently observed in the preBötC and illustrated in a field recording of the preBötC in Fig. 3.5A. Figure 3.5B plots an analogous behavior in simulated data by plotting snapshots of active early inspiratory neurons and the susceptible neurons. The point at which the peak number of active neurons in the ectopic burst (a) corresponds to the peak number of active neurons in the full burst (b). These two points differ only insofar as many more susceptible neurons are available prior to the full burst (b). The ectopic burst fails because positive feedback cannot occur; a sufficient number of early inspiratory population have not recovered from refractoriness. Also, note that the slope of both the preBötC field-recording (indicated by dashed lines) and simulated data is rather shallow in the ectopic bursts while

substantially steeper in the full burst. This suggests that additional neurons are more easily recruited when the full burst occurs in both the model and the experimental data.

We now define an *active component* as a contiguous set of active neurons that share either inbound or outbound synaptic connections. At any time, the network can contain refractory or susceptible neurons (which are inactive) as well as isolated active neurons, and finally active components comprising several synaptically interconnected active neurons. A *giant component* exists when all the active neurons in the network are contained within one active component. The giant component can grow or contract as neurons become active and join the giant component or become inactive and leave the component, respectively.

The presence of a giant component can be analytically determined using the Molloy-Reed criterion (Molloy and Reed 1995). If we treat the network as a graph, by analyzing its state in snapshots of time, we can consider the fraction of active neurons and their respective connectivity at every time point using the following equation:

$\sum_k k(k-2)p_k$, where k is the number of output connections between active neurons (mathematicians refer to this number as the *degree* of a node in the graph) and p_k is the fraction of neurons with a given k . A giant component has formed when the Molloy-Reed criterion crosses zero (indicated with vertical dashed lines in Fig. 3.5B-D).

The giant component is formed from an agglomeration of smaller active components. Figure 3.5D shows the size of all the active component sizes at each snapshot of the network (black dots). At each time step there can be 0, 1 or more active components. As the Molloy-Reed criterion progresses toward crossing zero (Fig. 3.5C), the active components converge to form one giant component and the burst is spread throughout the population.

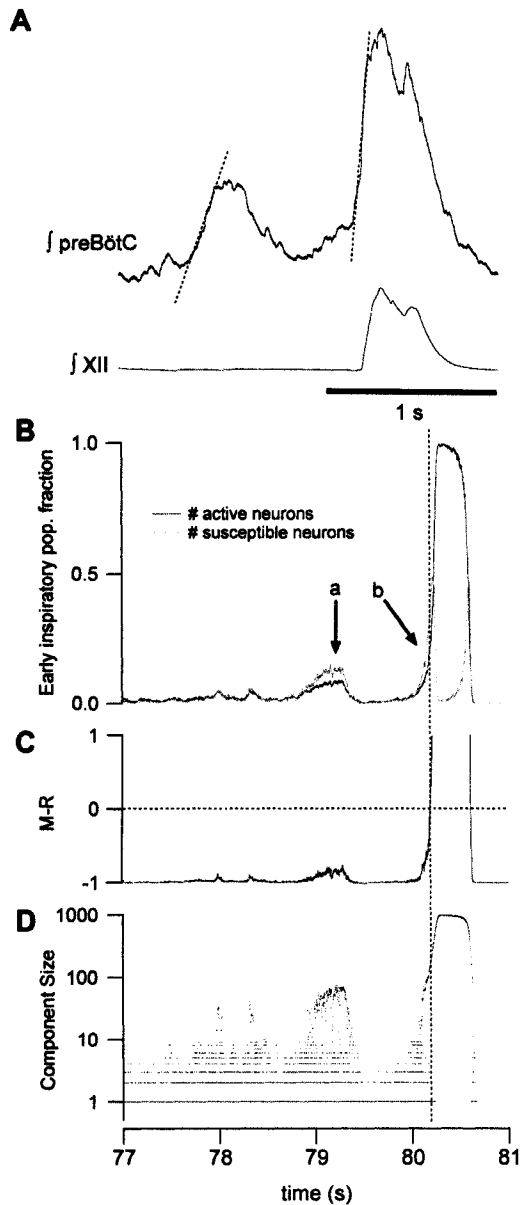


Figure 3.5. Comparison of experimental and simulated burst initiation. **A**, Field recording (see Fig. 2.5) of the preBötC with XII activity. Dashed lines highlight the change in slope between the ectopic and inspiratory bursts. **B**, The fraction of simulated neurons plotted during an ectopic burst (*a*) and the beginning of an inspiratory burst (*b*). **C**, The Molloy-Reed criterion calculated at each snapshot. The time it crosses zero is indicated by a vertical dashed line through B-D indicating when a giant active component has formed. **D**, The size of every active component at each snapshot illustrating that as they cross the vertical dashed line they merge into one component (the giant component).

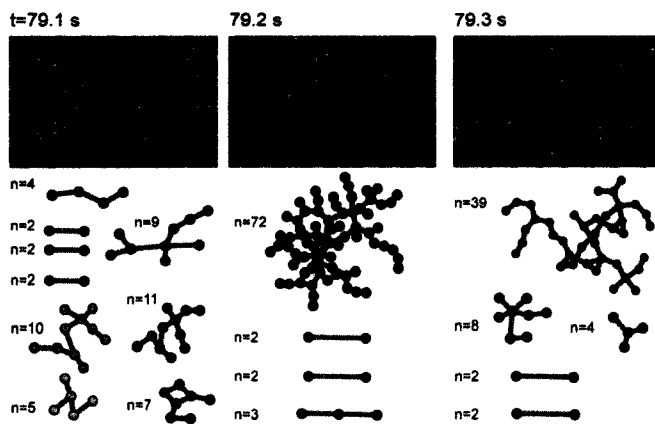
Figure 3.6 illustrates self-organization in the network using two illustrative sets of snapshots of the early inspiratory population from the same data plotted in Fig. 3.4B, 3.5. Each early inspiratory neuron is denoted by a square where black squares are refractory or susceptible neurons, white are active neurons with no synaptic connections to any other active neurons (i.e., these are active components of size 1), and the other colors represent active neurons within connected active components. Active

components exceeding size 1 have been laid out below the grid to illustrate just the active components and their size and shape.

Fig. 3.6A shows the assembly and disassembly of components of neurons during the ectopic burst. The neurons assemble several small components, but none of the other early inspiratory neurons are active. On the left ($t=79.1$), there are nine active components ($n=2,2,2,4,5,7,9,10,11$) and fifteen active components of size 1. At the next time increment ($t=79.2$), many neurons have joined the blue component to become a larger active component ($n=72$). In the next time step ($t=79.3$), the large component breaks apart and becomes a smaller component ($n=39$) with additional new active neurons but a net decrease. The active component disintegrates as intrinsic cellular properties bring on refractoriness (e.g., I_{NaP} inactivation, or I_{SK-Ca} and $I_{Na/K-ATPase}$ activation), which is not counter balanced by positive feedback to maintain activity in the active neurons. This illustrates that active components are fluid and evolve dynamically. This also shows that positive feedback can be prevented by intrinsic currents.

Figure 3.6B shows the rapid assembly of a giant component during the onset of the full burst. Here we can see that many small active components have been subsumed into the giant component, which includes all early inspiratory neurons since by this time the vast majority have relaxed back to their intrinsic susceptible states. The giant component grows as more neurons evolve toward the susceptible state and get recruited by active cells already contained in the giant component. This is because more refractors have become susceptible to activation.

A. An active component assembles and breaks down



B. Giant active component required for a burst (t=80.3)

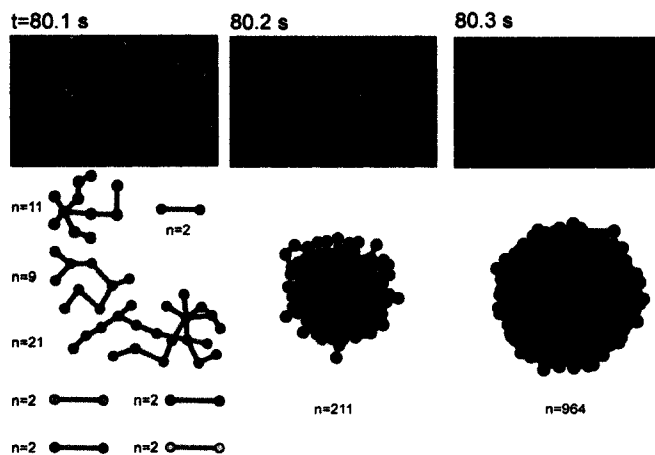


Figure 3.6. Dynamics of active component assembly. Each early inspiratory neuron is indicated by a square in the grid with black squares indicating inactive neurons, and the colors indicate active neurons in contact with other active neurons (part of an active component). Compare each snapshot's time to Figure 3.4. **A**, Three snapshots illustrating the evolution of active components during the assembly and disassembly during an ectopic burst. **B**, Three other snapshots showing the assembly of a giant component.

The role of persistent sodium current

The role of I_{NaP} and pacemaker neurons has been experimentally tested using riluzole, which blocks I_{NaP} with half-maximal doses (EC_{50}) of 3 μ M (Del Negro et al. 2002a; Doble 1996; Paton et al. 2006; Ptak et al. 2005; Urbani and Belluzzi 2000). This is a critical test of any viable model simulating how the respiratory rhythm is generated. We simulated the experiment and found that fully blocking I_{NaP} did not prevent network-wide rhythmicity (Fig. 3.7), in agreement with experiments (Del Negro et al. 2002b; Del Negro et al. 2005; Pace et al. 2007b; Paton et al. 2006; Pena et al. 2004). Removal of I_{NaP} reduced the

number of spikes per burst, consistent with its important role in promoting high spike frequency (Lee and Heckman 2001; Pace et al. 2007b).

After the elimination of I_{NaP} , the fundamental assembly of the giant component is the same (Fig. 3.7B) as when I_{NaP} was present (Fig. 3.5B). Therefore, I_{NaP} and voltage-dependent pacemaker neurons are not necessary for rhythmic network activity. However, I_{NaP} is not irrelevant because it promotes the high frequency spiking that drives robust output and the temporal summation of EPSPs among interconnected early inspiratory neurons during positive feedback. Also due to its subthreshold voltage dependence, I_{NaP} promotes spontaneous spiking in neurons, which means that neurons that contain high amounts of this current can serve a similar purpose as broadcaster neurons by spontaneously exciting neighboring neurons that can serve to initiate a network-wide inspiratory burst if the susceptibility conditions are satisfied.

Lesions of rhythm-generating neurons in the preBötC

In the first chapter, we discussed how the ribosomal toxin, saporin, has been used to lesion NKR^+ neurons *in vivo* as an SP-saporin conjugate. The SP-saporin lesioning of NKR^+ cells in the preBötC first disrupts breathing during sleep (McKay et al. 2005) and then progresses to respiratory ataxia and severe pathophysiology (Gray et al. 2001).

We were interested in determining if simulations of this experiment would offer insights into how robust the inspiratory network is to destruction of its members since little is known about the degree of interconnections between preBötC neurons. We simulated these experiments by progressively removing portions of the NKR^+ early inspiratory population and assuming that we have a successful inspiratory effort when the spike density across the whole late inspiratory population crosses a motor threshold of 50 spikes/bin. This motor threshold has arbitrary magnitude that represents the ability of premotoneurons to sufficiently excite motoneurons.

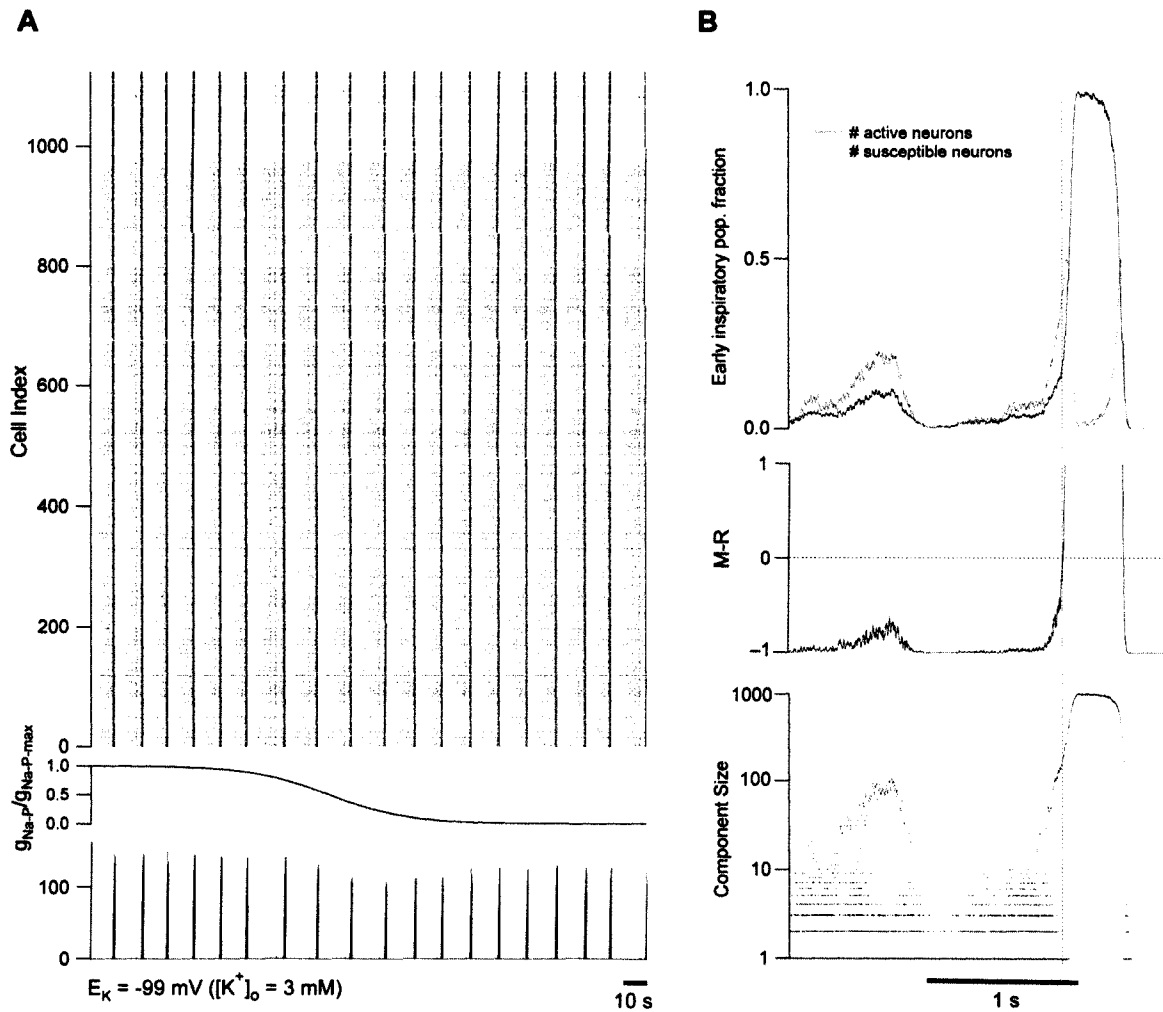


Figure 3.7. Blockade of persistent Na^+ current does not prevent rhythmogenesis. The simulated extracellular K^+ concentration ($[\text{K}^+]_o$) was decreased and the $g_{\text{tonic-e}}$ conductance was increased to simulate *in vivo* conditions. **A**, A raster plot showing the population activity as the persistent Na^+ current is attenuated over time to simulate an application of riluzole. Compare to Fig. 3.3. **B**, Blockade of persistent Na^+ current does not affect the ability to generate ectopic or inspiratory bursts. Compare to Fig. 3.4.

We randomly selected 580 of 975 (60%) early inspiratory neurons and classified them as NKR^+ . Figure 3.8A shows how the respiratory period changes as the number of early inspiratory neurons destroyed increases, which depends on sufficient spiking in the late inspiratory population to cross motor threshold. Lesioning of just the NKR^+ subpopulation results in a minimal decrease in period until lesioned cells reach 80%, at

which time we observe some longer-lasting silent intervals because rhythmic activity in the early inspiratory neurons fails to generate enough activity to cause late inspiratory neurons to cross the motor threshold. At 90% lesioned, the synaptic drive from the rhythm generator is rarely sufficient to cause motor output, which we interpret as the model exhibiting central apneas (a failure to inspire).

The inspiratory rhythm is robust to the 80% lesion because of the abundance of synaptic connections. Even as neurons are removed from the early inspiratory population, giant components can be formed. As we illustrated in Fig. 3.7 the giant component can grow or contract in size as active cells come and go, but the presence of the giant component ensures that all the active early inspiratory neurons are synchronized, and so the total number of cells driving the late inspiratory neurons is still quite high, even when 80% of the NKR⁺ early inspiratory neurons are gone that may also participate in the drive to the late inspiratory neurons.

However, these data raise the interesting possibility of recovering *in vivo* breathing even in the case of severe loss of NKR⁺ neurons (Gray et al. 2001; McKay et al. 2005). In simulations it is possible to cross the motor threshold even up to nearly 90% lesioning by enhancing the maximum synaptic conductance by 15% and the time constant of AMPAR de-sensitization by 50% which is analogous to an application of cyclothiazide (Funk et al. 1995). These modifications cannot increase the number of connections, but do effectively increase the time window for active neurons to recruit susceptible and refractory cells, thereby boosting the burst-sustaining effects of feedback loops. This makes the existing synaptic connections more effective at exerting a postsynaptic response. The net result is an enhancement of the ability of active neurons to collectively organize into active components, and then agglomerate into a

giant component. As long as a giant component can form (and the network is not fractured) then inspiratory motor output can occur and breathing is not lost.

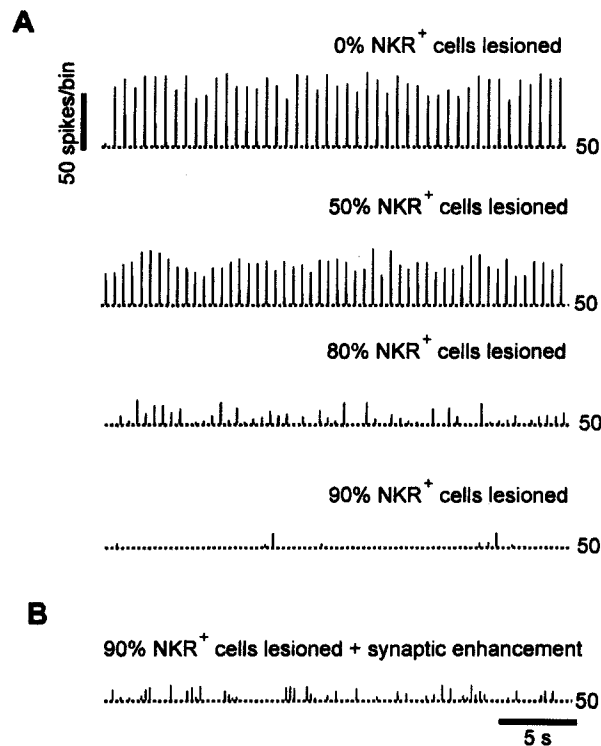


Figure 3.8. Simulated SP-saporin lesioning of NKR⁺ neurons. **A**, Progressive lesioning reduces the drive to premotoneurons which eventually results in periods of simulated apnea (>90% lesioned). **B**, Simulated cyclothiazide, which enhances AMPAR-mediated phasic excitation, recovers much of the drive back to the premotoneurons.

Both the simulated fraction of NKR⁺ inspiratory neurons and total number of neurons in the network are much higher than what we recently estimated the actual values to be (see Fig. 1.10 and Chapter 1's Discussion). For this modeling study, these values were roughly estimated based on the limited information available at the time. The motor threshold was imposed because even at 100% NKR⁺ lesioning with this topology and network size, there were synchronous rhythmic bursts in the network (not shown). Since the actual percentage of NKR⁺ neurons is apparently less than what we simulate here, the analysis may still be valid depending on the degree of connectivity between inspiratory neurons.

The *in vivo* system contains many additional layers of complexity, including the embedding of the preBötC in an extensive respiratory pattern formation network and

sensory feedback. Nevertheless, insights from our analyses make several testable predictions about the breathing system in whole animals. First, in order for functional breathing rhythms, a finite fraction of NKR⁺ neurons (on the order of 15-20%) must exist and must be highly synaptically interconnected and thus able to form feedback loops, (2) sporadic periods of apnea due to NKR⁺ neuron destruction can result from a failure to drive motoneurons, not necessarily the loss of central rhythmogenesis, (3) that the enhancement of synaptic strength within the preBötC may be able to recover breathing over some finite range of lesioning that was previously causing periods of apnea.

3.4. Appendix 1: Group-Pacemaker Model Equations and Configuration

Units

$$I = pA$$

$$g = nS$$

$$V = mV$$

$$C = pF$$

Initial Values

$$V_0 = -55 \text{ mV}$$

$$[Ca^{2+}]_0 = 0.3 \text{ } \mu\text{M}$$

$$[Na^{+}]_0 = 4.5 \text{ mM}$$

$$(m_A)_0 = 0.12$$

$$(h_A)_0 = 0.24$$

$$(s_{\text{AMPA}})_0 = 0.002$$

$$(m_{\text{Ca}})_0 = 0.017$$

$$(h_{\text{Ca}})_0 = 0.43$$

$$(m_H)_0 = 0.8$$

$$(m_{\text{SK-Ca}})_0 = 0.01$$

$$(n_{\text{K-DR}})_0 = 0.002$$

$$(h_{\text{NaP}})_0 = 0.61$$

$$(s_{\text{NMDA}})_0 = 0.002$$

$$(m_{\text{Na}})_0 = 0.01$$

$$(h_{\text{Na}})_0 = 0.981$$

Network Topology

A neuron may never connect to itself and may not have duplicate synapses to another neuron. Target neurons for synaptic connections are picked from a uniform distribution of the target population.

Chemical Connections:

Every early inspiratory neuron, with membrane capacitance C_m , is connected to $\varphi_{\text{chem}} C_m$ other neurons, where $\varphi_{\text{chem}} = \langle N_{\text{in}} \rangle / \langle C_m \rangle$ and the number of inbound synapses of the target neuron cannot exceed $\varphi_{\text{chem}} C_m$. Late inspiratory neurons do not have any outbound synapses because they represent the output of the preBötC.

Electrical Connections:

Every early inspiratory neuron is electrically connected to $\varphi_{elec} C_m$ other early inspiratory neurons, where $\varphi_{elec} = \langle N_{elec} \rangle / \langle C_m \rangle$ and the neuron may not connect both chemically and electrically to the same target neuron.

975 Early Inspiratory (where 580 random neurons are NK1R⁺)
150 Late Inspiratory

Parameters

$$C_{m\text{-early}} = 45 \pm 8.5 \text{ pF}$$

$$C_{m\text{-late}} = 86 \pm 13 \text{ pF}$$

$$\langle N_{out} \rangle = \langle N_{in} \rangle = 10$$

$$\langle N_{elec} \rangle = 13$$

$$A_{(cm^2)} = 1 \times 10^{-6} \frac{cm^2}{pF} \cdot C_m$$

$$r_{(m)} = 1 \times 10^{-2} \sqrt{\frac{A_{(cm^2)}}{4\pi}}$$

$$Vol_{(m^3)} = \frac{4\pi r_{(m)}^3}{3}$$

$$Vol_{(L)} = 1 \times 10^3 Vol_{(m^3)}$$

$$Vol_{(nL)} = 1 \times 10^9 Vol_{(L)}$$

$$Vol_{(pL)} = 1 \times 10^{12} Vol_{(L)}$$

$$F = 96500 \text{ C/mol}$$

$$\frac{RT}{F} = 25.9 \text{ mV}$$

$$[K^+]_i = 140 \text{ mM}$$

$$[Na^+]_i = 5 \text{ mM}$$

$$[Na^+]_o = 150 \text{ mM}$$

$$[Ca^{2+}]_o = 1.5 \text{ mM}$$

$$[Mg^{2+}]_o = 1 \text{ mM}$$

$$E_{Ca} = 40 \text{ mV}$$

$$E_{CAN} = 0 \text{ mV}$$

$$E_h = -40 \text{ mV}$$

$$E_{Na} = 80 \text{ mV}$$

$$E_{syn-e} = 0 \text{ mV}$$

$$k_{CAN} = 0.5 \mu\text{M}$$

$$k_{Na/K-ATPase} = 10 \text{ mM}$$

$$k_{SK-Ca} = 0.3 \mu\text{M}$$

$$\begin{aligned}
\theta_{h-A} &= -60 \text{ mV} \\
\theta_{h-Ca} &= -52.4 \text{ mV} \\
\theta_{h-Na-F} &= -44.1 \text{ mV} \\
\theta_{h-Na-P} &= -48 \text{ mV} \\
\theta_{m-A} &= -37 \text{ mV} \\
\theta_{m-Ca} &= -27.82 \text{ mV} \\
\theta_{m-h} &= -78 \text{ mV} \\
\theta_{m-Na-F} &= -36 \text{ mV} \\
\theta_{m-Na-P} &= -40 \text{ mV} \\
\theta_{n-K-DR} &= -30 \text{ mV} \\
\theta_{s-AMPA} &= -10 \text{ mV} \\
\theta_{s-NMDA} &= -10 \text{ mV}
\end{aligned}$$

$$\begin{aligned}
\sigma_{h-A} &= 8 \text{ mV} \\
\sigma_{h-Ca} &= 5.23 \text{ mV} \\
\sigma_{h-Na-F} &= 7 \text{ mV} \\
\sigma_{h-Na-P} &= 6 \text{ mV} \\
\sigma_{m-A} &= -7 \text{ mV} \\
\sigma_{m-Ca} &= -5.69 \text{ mV} \\
\sigma_{m-h} &= 7 \text{ mV} \\
\sigma_{m-Na-F} &= -8.5 \text{ mV} \\
\sigma_{m-Na-P} &= -6 \text{ mV} \\
\sigma_{n-K-DR} &= -5 \text{ mV} \\
\sigma_{s-AMPA} &= -5 \text{ mV} \\
\sigma_{s-NMDA} &= -5 \text{ mV}
\end{aligned}$$

$$\begin{aligned}
\tau_{AMPA} &= 5 \text{ ms} \\
\tau_{Ca} &= 1600 \text{ ms} \\
\tau_{h-A} &= 500 \text{ ms} \\
\tau_{h-Ca} &= 15 \text{ ms} \\
\tau_{h-Na} &= 8 \text{ ms} \\
\bar{\tau}_{h-Na-P} &= 10000 \text{ ms} \\
\tau_{m-A} &= 1 \text{ ms} \\
\tau_{m-Ca} &= 5 \text{ ms} \\
\bar{\tau}_{n-K-DR} &= 15 \text{ ms} \\
\tau_{NMDA} &= 30 \text{ ms} \\
\tau_{SK-Ca} &= 10 \text{ ms} \\
\gamma &= 100 \text{ pA}
\end{aligned}$$

If any conductance/current is less than zero the value is recalculated from the given distributions (mean \pm standard deviation):

$$\begin{aligned}
\bar{g}_A &= 500000 \pm 500000 \cdot A_m \text{ nS} \\
\bar{g}_{AMPA} &= 1125 \pm 1875 \cdot A_m \text{ nS} \\
\bar{g}_{Ca} &= 1125 \pm 1875 \cdot A_m \text{ nS} \\
\bar{g}_{CAN} &= 300000 \pm 30000 \cdot A_m \text{ nS} \\
\bar{g}_{elec} &= 300 \pm 30 \cdot A_m \text{ nS} \\
\bar{g}_h &= 25000 \pm 50000 \cdot A_m \text{ nS} \\
\bar{g}_{Na-F} &= 7500000 \cdot A_m \text{ nS} \\
\bar{g}_{Na-P} &= 25000 \pm 25000 \cdot A_m \text{ nS} \\
\bar{g}_{K-DR} &= 0.4 \cdot \bar{g}_{Na-F} \text{ nS} \\
\bar{g}_{SK-Ca} &= 50000 \pm 45000 \cdot A_m \text{ nS} \\
\bar{g}_{L-K} &= 87500 \pm 35000 \cdot A_m \text{ nS} \\
\bar{g}_{NMDA} &= 3000 \pm 250 \cdot A_m \text{ nS} \\
\bar{i}_{Na/K-ATPase} &= 0.9e7 \pm 1.8e3 \cdot A_m \text{ nS}
\end{aligned}$$

For *in vitro* slice simulations

$$E_K = -71 \text{ mV}$$

$$\bar{g}_{tonic-e} = 1.5 \text{ nS}$$

For *in vivo* simulations

$$E_K = -99 \text{ mV}$$

$$\bar{g}_{tonic-e} = 7.5 \text{ nS}$$

$$C_m \frac{dV}{dt} = -I_A - I_h - I_{Ca} - I_{CAN} - I_{Na/K-ATPase} - I_{SK-Ca} - I_{Na-F} - I_{Na-P} - I_{K-DR} - I_{L-K} - I_{tonic-e} - I_{AMPA} - I_{NMDA} - I_{elec} + \xi(t) + I_{app}$$

$$\frac{d[Ca^{2+}]_i}{dt} = \frac{-(I_{Ca} + \theta I_{NMDA})}{2Vol_{(nL)}F} - \frac{[Ca^{2+}]_i}{\tau_{Ca}}$$

$$\theta([Ca^{2+}]_o) = \frac{1}{1 + \left(\frac{65.6}{0.5[Ca^{2+}]_o(11.3)} \right)}$$

$$\theta(1.5) = 0.114$$

$$\frac{d[Na^+]_i}{dt} = \frac{I_{Na-F} + I_{Na-P} + \alpha_{Na/K}(E_{CAN}, 5)I_{CAN} + \alpha_{Na/K}(E_{syn-e}, 5)(I_{AMPA} + I_{NMDA}) + \alpha_{Na/K}(E_h, 5)I_h + 3I_{Na/K-ATPase}}{-Vol_{(pL)}F}$$

$$\alpha_{Na/K}(E_{rev}, [Na^+]_i) = \frac{[K^+]_o - [K^+]_i e^{\left(\frac{E_{rev}F}{RT}\right)}}{[Na^+]_i e^{\left(\frac{E_{rev}F}{RT}\right)} - [Na^+]_o}$$

$$\alpha_{Na/K}(E_{CAN}, 5) = 0.938$$

$$\alpha_{Na/K}(E_{syn-e}, 5) = 0.938$$

$$\alpha_{Na/K}(E_h, 5) = 0.167$$

$$I_{CAN} = \bar{g}_{CAN} \langle s_{AMPA} \rangle_{in} (V - E_{CAN}) \left(\frac{[Ca^{2+}]}{[Ca^{2+}] + k_{CAN}} \right)$$

$$\langle s_{AMPA} \rangle_{in} = \frac{\sum_i^{N_{in}} (s_{AMPA})_i}{N_{in}}$$

$$I_{Na-F} = \bar{g}_{Na-F} (m_{Na-F}(V))^3 h_{Na-F}(V - E_{Na})$$

$$\frac{dm_{Na}}{dt} = m_{Na-\infty}(V) - m_{Na}$$

$$m_{Na-\infty}(V) = \frac{1}{1 + e^{(V - \theta_{m-Na}) / \sigma_{m-Na}}}$$

$$\frac{dh_{Na}}{dt} = \frac{h_{Na-\infty}(V) - h_{Na}}{\tau_{h-Na}}$$

$$h_{Na-\infty}(V) = \frac{1}{1 + e^{(V - \theta_{h-Na}) / \sigma_{h-Na}}}$$

$$I_{Na-P} = \bar{g}_{Na-P} (m_{Na-P-\infty}(V)) h_{Na-P}(V - E_{Na})$$

$$m_{Na-\infty}(V) = \frac{1}{1 + e^{(V - \theta_{m-Na-P}) / \sigma_{m-Na-P}}}$$

$$\frac{dh_{Na-P}}{dt} = \frac{h_{Na-P-\infty}(V) - h_{Na-P}}{\bar{\tau}_{h-Na-P}}$$

$$h_{Na-\infty}(V) = \frac{1}{1 + e^{(V - \theta_{h-Na-P}) / \sigma_{h-Na-P}}}$$

$$I_{K-DR} = \bar{g}_{K-DR} n_{K-DR}^4 (V - E_K)$$

$$\frac{dn_{K-DR}}{dt} = \frac{n_{K-DR-\infty}(V) - n_{K-DR}}{\tau_{n-K-DR}(V)}$$

$$n_{K-DR-\infty}(V) = \frac{1}{1 + e^{(V - \theta_{n-K-DR}) / \sigma_{n-K-DR}}}$$

$$\tau_{n-K-DR}(V) = \frac{\bar{\tau}_{n-K-DR}}{\cosh\left(\frac{V - \theta_{n-K-DR}}{2\sigma_{n-K-DR}}\right)}$$

$$I_{Ca} = g_{Ca} m_{Ca} h_{Ca} (V - E_{Ca})$$

$$m_{Ca-\infty}(V) = \frac{1}{1 + e^{(V - \theta_{m-Ca}) / \sigma_{m-Ca}}}$$

$$\frac{dm_{Ca}}{dt} = \frac{m_{Ca-\infty}(V) - m_{Ca}}{\tau_{m-Ca}}$$

$$h_{Ca-\infty}(V) = \frac{1}{1 + e^{(V - \theta_{h-Ca}) / \sigma_{h-Ca}}}$$

$$\frac{dh_{Ca}}{dt} = \frac{h_{Ca-\infty}(V) - h_{Ca}}{\tau_{h-Ca}}$$

$$I_A = \bar{g}_A m_A h_A (V - E_K)$$

$$m_{A-\infty}(V) = \frac{1}{1 + e^{(V-\theta_{m-A})/\sigma_{m-A}}}$$

$$\frac{dm_A}{dt} = \frac{m_{A-\infty} - m_A}{\tau_{m-A}}$$

$$h_{A-\infty}(V) = \frac{1}{1 + e^{(V-\theta_{h-A})/\sigma_{h-A}}}$$

$$\frac{dh_A}{dt} = \frac{h_{A-\infty} - h_A}{\tau_{h-A}}$$

$$I_h = \bar{g}_h m_h (V - E_h)$$

$$m_{h-\infty}(V) = \frac{1}{1 + e^{(V-\theta_{m-h})/\sigma_{m-h}}}$$

$$\tau_{m-h}(V) = 1255.8e^{0.0262V}$$

$$\frac{dm_h}{dt} = \frac{m_{h-\infty} - m_h}{\tau_{m-h}(V)}$$

$$I_{SK-Ca} = \bar{g}_{SK-Ca} m_{SK-Ca}^2 (V - E_K)$$

$$m_{SK-Ca-\infty}([Ca^{2+}]_i) = \frac{1}{1 + \left(\frac{k_{SK-Ca}}{[Ca^{2+}]_i}\right)^4}$$

$$\frac{dm_{SK-Ca}}{dt} = \frac{m_{SK-Ca-\infty} - m_{SK-Ca}}{\tau_{SK-Ca}}$$

$$I_{Na/K-ATPase} = \bar{i}_{Na/K-ATPase} \frac{[Na^+]_i^3}{[Na^+]_i^3 + (k_{Na/K-ATPase})^3}$$

$$I_{AMPA} = \bar{g}_{AMPA} \sum_i^{N_{in}} (s_{AMPA})_i (V - E_{syn-e})$$

$$\frac{ds_{AMPA}}{dt} = \frac{(1 - s_{AMPA})s_{AMPA-\infty}(V) - s_{AMPA}}{\tau_{AMPA}}$$

$$s_{AMPA-\infty}(V) = \frac{1}{1 + e^{(V-\theta_{s-AMPA})/\sigma_{s-AMPA}}}$$

$$I_{NMDA} = \frac{\bar{g}_{NMDA} \sum_i^{N_{in}} (s_{NMDA})_i (V - E_{syn-e})}{1 + \frac{[Mg^{2+}]_o}{3.57} e^{-0.062V}}$$

$$\frac{ds_{NMDA}}{dt} = \frac{(1 - s_{NMDA})s_{NMDA-\infty}(V) - s_{NMDA}}{\tau_{NMDA}}$$

$$s_{NMDA-\infty}(V) = \frac{1}{1 + e^{(V - \theta_{s-NMDA})/\sigma_{s-NMDA}}}$$

$$I_{elec} = \bar{g}_{elec} \sum_i^{N_{elec}} (V - V_i)$$

$$I_{ionic-e} = \bar{g}_{ionic-e} (V - E_{syn})$$

$$I_{L-K} = \bar{g}_{L-K} (V - E_K)$$

$$\langle \xi(t) \rangle = 0$$

$$\langle \xi(t) \xi(t') \rangle = \gamma \delta(t - t')$$

$$\xi(t) = \text{gauss}(0, \sqrt{\gamma/\Delta t})$$

3.5. Appendix 2: Implementation and Operation of *neuronetsim*

This appendix describes how the software program, *neuronetsim*, may be used to simulate large networks of a variety of neurons. These neurons are described in the Hodgkin-Huxley style and use ordinary differential equations (ODEs) coded in a style similar to XPPaut. The main advantage of *neuronetsim* over similar programs such as XPPaut is that separate .ode files that describe different neuron types may be easily compiled together into a binary file that is optimized for speed. Emphasis was placed on modularity of both the source code, to make core modifications easier, as well as the modularity of use, to make development of large networks of diverse neuron types easier.

Model definitions of Neuron Types

The set of ODEs that describe neuron types may be different for each neuron type. The model author has extensive control over how the equations are calculated by potentially defining snippets of C code that can optimize the execution of specific operations.

Once the definitions of each neuron have been constructed, a script can be executed that compiles binaries, associating neuron types into “experiments”, that may be used to simulate the neurons. As long as the model equations for the experiment do not change, a new binary does not need to be created.

Listing 3.1. illustrates the model definition of an early inspiratory neuron as described in the preceding text and defined in the previous appendix. Comments appear with ‘#’ preceding each line which describe what the subsection of the model defines. Initial conditions and neuron parameters for the ODEs will be defined in the network files (described in the next subsection of this appendix).

Listing 3.1. Earlyl_Neuron.ode

```
# Model of Group-Pacemaker neurons within the preBotC

# Current Equations
INaF(m_NaF, h_NaF, V) = g_Na_F*m_NaF*m_NaF*m_NaF*h_NaF*(V-E_Na)
Iampa(V) = g_ampa*sum_s_ampa()**(V-E_syn_e)
Inmda(V) = g_nmda*sum_s_nmda()**(V-E_syn_e)/(1+MgConc*(exp(-
    0.062*V))/3.57)
I_NaK(Nai, V) = calcINaK(Nai, V)
INaP(h_NaP, V) = g_Na_P*x_inf(theta_m_Na_P, sigma_m_Na_P, V)*h_NaP*(V-E_Na)
IK(n_KDR, V) = g_K*n_KDR*n_KDR*n_KDR*n_KDR*(V-E_K)
ICa(m_Ca, h_Ca, V) = g_Ca*m_Ca*(h_Ca+h_inf)*(V-E_Ca)
IKCa(m_KCa, V) = g_KCa*(m_KCa*m_KCa)*(V-E_K)
IL(V) = g_L_K*(V-E_K)+g_L_Na*(V-E_Na)
I_A(m_A, h_A, V) = g_A*m_A*h_A*(V-E_K)
IH(m_H, V) = g_H*m_H*(V-E_H)
ICAN(Cai, V) = g_CAN*avg_s_ampa()**(V-E_CAN)*(Cai/(Cai+kCAN))
I_nz() = gauss(0.0f, sqrt(gamma/dt))
I(m_NaF, h_NaF, h_NaP, m_H, m_A, h_A, m_Ca, h_Ca, n_KDR, m_KCa, Nai,
    Cai, V, nzVar) = ((INaF(m_NaF, h_NaF, V) + INaP(h_NaP, V) + IH(m_H, V)
    + I_A(m_A, h_A, V) + IK(n_KDR, V) + IL(V) + Itonic(V) + ICa(m_Ca, h_Ca,
    V) + I_NaK(Nai, V) + ICAN(Cai, V) + Ielec(V) + IKCa(m_KCa, V) + Iapp
    + nzVar)) + (Iampa(V) + Inmda(V))

Ielec(V) = g_e*Velec()
```

```

Itonic(V)=g_tonic_e*(V-E_syn_e)

# Differential Equations
dV/dt = -I(m_NaF, h_NaF, h_NaP, m_H, m_A, h_A, m_Ca, h_Ca, n_KDR,
  m_KCa, Nai, Cai, V, nzVar)/C

dCai/dt=- (ICa(m_Ca, h_Ca, V)+0.114f*Inmda(V))/(2.0f*Vol_nL*F)-
  (Cai/1600.0f)
dm_A/dt=dxdt(x_inf(-37.0f,-7.0f,V),m_A,tau_m_A)
dh_A/dt=dxdt(x_inf(-60.0f,8.0f,V),h_A,tau_h_A)
ds_AMPA/dt=dxdt((1-s_AMPA)*x_inf(theta_s_ampa, sigma_s_ampa, V),k_r *
  s_AMPA,tau_s_ampa)
dm_Ca/dt=dxdt(x_inf(theta_Cam,-5.69,V),m_Ca,tau_Cam)
dh_Ca/dt=dxdt(x_inf(theta_Cah,5.23,V)*(1.0f-h_inf),h_Ca,tau_Cah)
dm_H/dt=dxdt(x_inf(-78.0,7.0,
  V),m_H,gaussian(1735.0,41.56f,5500.0f,V,18.54f))
dm_KCa/dt=dxdt(hilleqngl(kKCa,Cai,4.0),m_KCa,tau_KCa)
dn_KDR/dt=dxdt(tau_n, theta_n,sigma_n,n_KDR,V)
dh_NaP/dt=dxdt(tau_h_Na_P, theta_h_Na_P,sigma_h_Na_P,h_NaP,V)
ds_NMDA/dt=((1-s_NMDA)*x_inf(theta_s_nmda, sigma_s_nmda, V) - k_r *
  s_NMDA)/tau_s_nmda
dNai/dt=- (INaF(m_NaF, h_NaF, V) + INaP(h_NaP, V) + 0.938f*(ICAN(Cai,
  V)+Inmda(V)+Iampa(V)) + 0.167f*IH(m_H, V)+g_L_Na*(V-E_Na) + 3.0f*
  I_NaK(Nai, V))/(Vol_pL*F)
dm_NaF/dt=dxdt(x_inf(theta_m_Na_F, sigma_m_Na_F, V),m_NaF,1.0f)
dh_NaF/dt=dxdt(x_inf(theta_h_Na_F, sigma_h_Na_F, V),h_NaF,8.0f)

# Auxiliary Functions

inline float EarlyI_Neuron::calcINaK(float Nai, float V) const
{
  return i_NaK*hilleqngl(kNaK,Nai,3.0);
}

inline void EarlyI_Neuron::initializeUnconnectedDelay()
{
  dVariables[EarlyI_Neuron_s_AMPA_INDEX] = 0.0f;
  dVariables[EarlyI_Neuron_s_NMDA_INDEX] = 0.0f;
}

inline float EarlyI_Neuron::sum_s_ampa() const
{
  float s_ampa = 0.0f;
  for (int j = 0; j < excitedFromLength; j++) {
    Neuron* fromNeuron = (excitatoryConnectionFrom[j]);
    s_ampa += fromNeuron->get_s_AMPA();
  }
  return s_ampa;
}

inline float EarlyI_Neuron::avg_s_ampa() const
{
  float s_ampa = sum_s_ampa();
  if (excitedFromLength > 0) {
    s_ampa /= (float)excitedFromLength;
  }
}

```



```

    else {
        s_ampa = 0.0f;
    }
    return s_ampa;
}

inline float EarlyI_Neuron::sum_s_nmda() const
{
    float s_nmda = 0.0f;
    for (int j = 0; j < excitedFromLength; j++) {
        Neuron* fromNeuron = (excitatoryConnectionFrom[j]);
        s_nmda += fromNeuron->get_s_NMDA();
    }
    return s_nmda;
}

inline float EarlyI_Neuron::Velec() const
{
    float V_elec = 0.0f;
    for (int j = 0; j < electricalLength; j++) {
        Neuron* fromNeuron = (electricalConnection[j]);
        V_elec += (getV() - fromNeuron->getV());
    }
    return V_elec;
}

```

Network and neuron parameter definitions

We have separated the definition of neuronal models from the particular parameters of each neuron within the network. Along with network structure, this data is contained in network definition files (.net files). Network files keep track of this information by listing a definition of each neuron in series within a text file. Each neuron definition maintains parameter values, such as maximum conductance values of whole-cell currents, as well as which other neurons it is connected to by excitatory connections (AMPA-, NMDA-mediated), inhibitory connections (glycinergic-mediated), or electrical coupling through gap junctions. Listing 3.2 illustrates a simple example of a two-neuron network of early inspiratory neurons arranged in a feedback cycle. These files may be modified in standard text editors, although due to the large size and complexity of these files, non-trivial changes are best accomplished with simple scripts as described in the next subsection.

Listing 3.2. default.net

network: default.net

Network Name: SimpleNetwork
Neurons: 2
Network Type: None

Neuron(s) Info:

Neuron ID: 1
Neuron Name: EarlyI_Neuron
of inbound excitatory connections: 1
of outbound excitatory connections: 1
of inbound inhibitory connections: 0
of outbound inhibitory connections: 0
of electrical connections: 8
Excitatory Connections To:
2
Inhibitory Connections To:
Electrical Connections:

Initial Conditions:

0	-55
1	0.3
2	0.12
3	0.24
4	0.002
5	0.017
6	0.43
7	0.8
8	0.01
9	0.002
10	0.61
11	0.002
12	4.5
13	0.01
14	0.981

Associated Variable Values:

C	39.7457743716
E_CAN	0.0
E_Ca	40.0
E_H	-40.0
E_K	-71.0
E_Na	80.0
E_syn_e	0.0
F	96500.0
Iapp	0.0
MgConc	1.0
Vol_L	2.35618972351e-11
Vol_nL	0.0235618972351
Vol_pL	23.5618972351
area	3.97457743716e-05
g_A	25.0201050273

g_CAN	12.4157990903
g_Ca	1.10413365284
g_H	0.440410463875
g_K	32.7902638565
g_KCa	1.91808335607
g_L_K	4.393743858
g_L_Na	0.0
g_Na_F	81.9756596414
g_Na_P	1.37523460191
g_ampa	0.46756593312
g_e	0.0112708454119
g_nmda	0.111974304452
g_tonic_e	1.5
gamma	100.0
h_inf	0.0
i_NaK	357.635074337
id	1
kCAN	0.5
kKCa	0.3
kNaK	10.0
k_r	1.0
name	EarlyI_Neuron
radius	0.00177844545295
sigma_h_Na_F	7.0
sigma_h_Na_P	6.0
sigma_m_Na_F	-8.5
sigma_m_Na_P	-6.0
sigma_n	-5.0
sigma_s_ampa	-5.0
sigma_s_nmda	-5.0
tau_Cah	15.0
tau_Cam	5.0
tau_KCa	10.0
tau_h_A	500.0
tau_h_Na_P	10000.0
tau_m_A	1.0
tau_n	15.0
tau_s_ampa	5.0
tau_s_nmda	30.0
theta_Cah	-52.4
theta_Cam	-27.82
theta_h_Na_F	-44.1
theta_h_Na_P	-48.0
theta_m_Na_F	-36.0
theta_m_Na_P	-40.0
theta_n	-30.0
theta_s_ampa	-10.0
theta_s_nmda	-10.0

Neuron ID: 2
 Neuron Name: EarlyI_Neuron
 # of inbound excitatory connections: 1
 # of outbound excitatory connections: 1
 # of inbound inhibitory connections: 0
 # of outbound inhibitory connections: 0
 # of electrical connections: 0

Excitatory Connections To:
1
Inhibitory Connections To:
Electrical Connections:

Initial Conditions:
0 -55
1 0.3
2 0.12
3 0.24
4 0.002
5 0.017
6 0.43
7 0.8
8 0.01
9 0.002
10 0.61
11 0.002
12 4.5
13 0.01
14 0.981

Associated Variable Values:
C 38.0098781943
E_CAN 0.0
E_Ca 40.0
E_H -40.0
E_K -71.0
E_Na 80.0
E_syn_e 0.0
F 96500.0
Iapp 0.0
MgConc 1.0
Vol_L 2.20352778012e-11
Vol_nL 0.0220352778012
Vol_pL 22.0352778012
area 3.80098781943e-05
g_A 9.00131009937
g_CAN 11.2976380619
g_Ca 1.10912734388
g_H 0.495979939012
g_K 31.3581495103
g_KCa 0.877335100107
g_L_K 4.5930265925
g_L_Na 0.0
g_Na_F 78.3953737757
g_Na_P 1.51199993795
g_ampa 0.419593761236
g_e 0.0108231241714
g_nmda 0.12333005872
g_tonic_e 1.5
gamma 100.0
h_inf 0.0
i_NaK 342.189979423
id 2
kCAN 0.5

kKCa	0.3
kNaK	10.0
k_r	1.0
name	EarlyI_Neuron
radius	0.00173917509195
sigma_h_Na_F	7.0
sigma_h_Na_P	6.0
sigma_m_Na_F	-8.5
sigma_m_Na_P	-6.0
sigma_n	-5.0
sigma_s_ampa	-5.0
sigma_s_nmda	-5.0
tau_Cah	15.0
tau_Cam	5.0
tau_KCa	10.0
tau_h_A	500.0
tau_h_Na_P	10000.0
tau_m_A	1.0
tau_n	15.0
tau_s_ampa	5.0
tau_s_nmda	30.0
theta_Cah	-52.4
theta_Cam	-27.82
theta_h_Na_F	-44.1
theta_h_Na_P	-48.0
theta_m_Na_F	-36.0
theta_m_Na_P	-40.0
theta_n	-30.0
theta_s_ampa	-10.0
theta_s_nmda	-10.0

Manipulation of network structure and neuron parameters

When large networks of neurons are simulated it is essential to make the data easily accessible and usable for manipulation. This is primarily accomplished by the development and execution of Python scripts.

When the experiment is compiled into a binary, as described earlier, Python code similar to Listing 3.3 is automatically generated. The model author has to fill in the details of how neuronal parameters are defined. This can entail simply setting constant parameter values, or more complex operations that the Python programming language makes available. In this example, a random cellular capacitance is generated (“self.C”) from a normal distribution and the volume and surface area of the neuron is calculated

as if it were a sphere. Then, using the surface area, the script sets each cellular conductance by a random conductance density multiplied by the surface area. In this manner, as shown in Listing 3.4, we can easily create a network of early inspiratory neurons with heterogeneous parameters.

Listing 3.3. EarlyI_Neuron.py

```
#!/usr/bin/env python

from Connection import *
from math import *
from random import *
from Neuron import *
import sys

class EarlyI_Neuron(Neuron):
    '''Represents a glutamatergic and rhythmogenic inspiratory neuron'''

    def __init__(self):
        '''Initializes the neuron with default parameters.'''
        Neuron.__init__(self)

        self.id = 1
        self.name = "EarlyI_Neuron"

        # cellular parameters
        self.C = gauss(45.0, 8.5)

        # reversal potentials
        self.E_CAN = 0.0
        self.E_Ca = 40.0
        self.E_H = -40.0
        self.E_K = -71.0
        self.E_Na = 80.0
        self.E_syn_e = 0.0

        # bias current (units in pA)
        self.Iapp = 0.0

        # This calculates the area(cm^2), radius (cm), and volume of
        # the cell based on capacitance
        self.calculateGeometry()

        self.F = 96500.0 # C/mol
        self.MgConc = 1.0 # mM

        # cellular conductances (units in nS)
        self.g_A = -1.0
        while self.g_A < 0.0:
            self.g_A = gauss(500000.0, 500000.0)*self.area
```

```

self.g_Ca = gauss(30000.0, 2500.0)*self.area
self.g_CAN = gauss(300000.0, 30000.0)*self.area
self.g_H = -1.0
while self.g_H < 0.0:
    self.g_H = gauss(25000.0, 50000.0)*self.area

self.g_KCa = -1.0
while self.g_KCa < 0.0:
    self.g_KCa = gauss(50000.0, 45000.0)*self.area

self.g_L_K = -1.0
while self.g_L_K < 0.0:
    self.g_L_K = gauss(87500.0, 35000.0)*self.area

self.g_Na_P = -1.0
while self.g_Na_P < 0.0:
    self.g_Na_P = gauss(25000.0, 25000.0)*self.area
self.i_NaK = gauss(0.9e7, 1.8e3)*self.area
self.g_L_Na = 0.0
self.g_Na_F = 7500000.0*self.area
self.g_K = 0.4*self.g_Na_F

self.g_ampa = gauss(11250.0, 250.0)*self.area
self.g_e = gauss(300.0, 30.0)*self.area
self.g_nmda = gauss(3000.0, 250.0)*self.area
self.g_tonic_e = 1.5

# noise
self.gamma = 100.0

# activation/inactivation parameters
self.h_inf = 0.0
self.kCAN = 0.5
self.kKCa = 0.3
self.kNaK = 10.0
self.k_r = 1.0
self.sigma_h_Na_F = 7.0
self.sigma_h_Na_P = 6.0
self.sigma_m_Na_F = -8.5
self.sigma_m_Na_P = -6.0
self.sigma_n = -5.0
self.sigma_s_ampa = -5.0
self.sigma_s_nmda = -5.0
self.tau_Cah = 15.0
self.tau_Cam = 5.0
self.tau_KCa = 10.0
self.tau_h_A = 500.0
self.tau_m_A = 1.0
self.tau_h_Na_P = 10000.0
self.tau_n = 15.0
self.tau_s_ampa = 5.0
self.tau_s_nmda = 30.0
self.theta_Cah = -52.4
self.theta_Cam = -27.82
self.theta_h_Na_F = -44.1
self.theta_h_Na_P = -48.0

```

```

self.theta_m_Na_F = -36.0
self.theta_m_Na_P = -40.0
self.theta_n = -30.0
self.theta_s_ampa = -10.0
self.theta_s_nmda = -10.0

# simulation initial conditions
dVariables = []
dVariables.append(-55)      # EarlyI_Neuron_V_INDEX 0
dVariables.append(0.3)     # EarlyI_Neuron_Cai_INDEX 1
dVariables.append(0.12)    # EarlyI_Neuron_m_A_INDEX 2
dVariables.append(0.24)    # EarlyI_Neuron_h_A_INDEX 3
dVariables.append(0.002)   # EarlyI_Neuron_s_AMPA_INDEX 4
dVariables.append(0.017)   # EarlyI_Neuron_m_Ca_INDEX 5
dVariables.append(0.43)    # EarlyI_Neuron_h_Ca_INDEX 6
dVariables.append(0.8)     # EarlyI_Neuron_m_H_INDEX 7
dVariables.append(0.01)    # EarlyI_Neuron_m_KCa_INDEX 8
dVariables.append(0.002)   # EarlyI_Neuron_n_KDR_INDEX 9
dVariables.append(0.61)    # EarlyI_Neuron_h_NaP_INDEX 10
dVariables.append(0.002)   # EarlyI_Neuron_s_NMDA_INDEX 11
dVariables.append(4.5)     # EarlyI_Neuron_Nai_INDEX 12
dVariables.append(0.01)    # EarlyI_Neuron_m_NaF_INDEX 13
dVariables.append(0.981)   # EarlyI_Neuron_h_NaF_INDEX 14
self.setStateVariables(dVariables)

```

Listing 3.4. buildSimpleAllToAllNetwork.py

```

#!/usr/bin/env python
from Network import *

numberOfNeurons = 50
neuronType = "EarlyI_Neuron"

# Create an empty network
network = Network()

# Generate 50 early inspiratory neurons with default parameters
network.addNewNeurons(neuronType, numberOfNeurons)

# get a reference to the list of neurons
neurons = network.getNeuronsByType(neuronType)

# iterate over the neurons and assign random excitatory connections to
# the other neurons within the list of neurons
for neuron in neurons:
    neuron.assignRandomConnections(neurons, 49, Connection.EXCITATORY)

# save the network to a file
network.save("default.net")

```


Model execution

The network model may be executed from the command-line or shell scripts, such as Listing 3.5. The available arguments to the program are given in Listing 3.6. Data for individual neurons are output into files named “neuron_[ID].dat” in the current directory with a separate row for every timestamp. Columns indicate different data that the user can specify from the command-line with the default being the membrane potential. The “ID” is the unique “Neuron ID” number indicated in the “networkFilename.” The corresponding timestamp for each row of neuronal data is output in the “time.dat” file with a matching row number.

These data can be manipulated in any program that can read in row and tab-delimited text or by other scripts.

Listing 3.5. execute.sh

```
#!/bin/sh
../../bin/control -l default.net -d 0.1 -M 20000 -m rk4wc -p 5 -c 10000
```

Listing 3.6. neuronetsim/bin/control help output

Executed Command: ./control

usage: executeNetwork
version: 3.0

-l [networkFilename]	-- Executes the given network
-d [step-size]	-- The step-size for the integration (required)
-M [maximum time]	-- The maximum time for the integration (required)
-m [euler, rk4, rk4wc, rk4adap]	-- The integration method to use (default = rk4)
-p [number]	-- The number of data points to skip when printing out data (default = 10)
-c [cache_frequency]	-- The number of points to store before flushing to the file system
-u [unconnected delay]	-- The time in ms to wait before connecting the network (default = 0)

```

-i [neuron ID]           -- The neuron ID to voltage
                        clamp
-v [command voltage]    -- The command voltage
-s [start ID printout]  -- Start with this ID to print
                        out data
-q [junk]               -- Quiet Mode, neuron and time
                        traces are not output
-o [output variable]    -- A parameter or state variable
                        or function to be stored at each
                        timestep
-t [neuron type to apply -o to] -- -o options are paired up, in
                        the order they are received,
                        with -t opts
-w [input filepath]     -- A filename whose 1st entry is
                        the #of input vars in that file,
                        second row is a space or tab
                        delimited list of the names of
                        each variable to be input All
                        subsequent lines should be the
                        values of each of the variables
                        for that timestep in order
-x [input type]         -- Type of neuron to apply -w to
                        (note, max of one file per
                        neuron)

```

note: to have a -o applied to all neurons, use -t all

With these tools and the other associated scripts, a model developer can explore the behavior of complex neuronal models with arbitrary network arrangements and relative ease.

3.5. References

Ballanyi K, Onimaru H, and Homma I. Respiratory network function in the isolated brainstem-spinal cord of newborn rats. *Prog Neurobiol* 59: 583-634, 1999.

Ballerini L, Bracci E, and Nistri A. Pharmacological block of the electrogenic sodium pump disrupts rhythmic bursting induced by strychnine and bicuculline in the neonatal rat spinal cord. *J Neurophysiol* 77: 17-23, 1997.

Bianchi AL, Denavit-Saubie M, and Champagnat J. Central control of breathing in mammals: neuronal circuitry, membrane properties, and neurotransmitters. *Physiol Rev* 75: 1-45, 1995.

Bieger D, and Hopkins DA. Viscerotopic representation of the upper alimentary tract in the medulla oblongata in the rat: the nucleus ambiguus. *J Comp Neurol* 262: 546-562, 1987.

Brockhaus J, and Ballanyi K. Synaptic inhibition in the isolated respiratory network of neonatal rats. *Eur J Neurosci* 10: 3823-3839, 1998.

Butera RJ, Jr., Rinzel J, and Smith JC. Models of respiratory rhythm generation in the pre-Botzinger complex. I. Bursting pacemaker neurons. *J Neurophysiol* 82: 382-397, 1999a.

Butera RJ, Jr., Rinzel J, and Smith JC. Models of respiratory rhythm generation in the pre-Botzinger complex. II. Populations Of coupled pacemaker neurons. *J Neurophysiol* 82: 398-415, 1999b.

Crowder EA, Saha MS, Pace RW, Zhang H, Prestwich GD, and Del Negro CA. Phosphatidylinositol 4,5-Biphosphate Regulates Inspiratory Burst Activity in the Neonatal Mouse PreBötzinger Complex. *Journal of Physiology* submitted: 2007.

Darbon P, Tscherter A, Yvon C, and Streit J. The role of the electrogenic Na/K pump in disinhibition-induced bursting in cultured spinal networks. *J Neurophysiol* 2003.

Del Negro CA, Hsiao CF, and Chandler SH. Outward currents influencing bursting dynamics in guinea pig trigeminal motoneurons. *J Neurophysiol* 81: 1478-1485, 1999.

Del Negro CA, Johnson SM, Butera RJ, and Smith JC. Models of respiratory rhythm generation in the pre-Bötzinger complex. III. Experimental tests of model predictions. *J Neurophysiol* 86: 59-74, 2001.

Del Negro CA, Koshiya N, Butera RJ, Jr., and Smith JC. Persistent sodium current, membrane properties and bursting behavior of pre-botzinger complex inspiratory neurons in vitro. *J Neurophysiol* 88: 2242-2250, 2002a.

Del Negro CA, Morgado-Valle C, and Feldman JL. Respiratory rhythm: an emergent network property? *Neuron* 34: 821-830, 2002b.

Del Negro CA, Morgado-Valle C, Hayes JA, Mackay DD, Pace RW, Crowder EA, and Feldman JL. Sodium and calcium dependent pacemaker neurons and respiratory rhythm generation. *J Neurosci* 25: 446-453, 2005.

Doble A. The pharmacology and mechanism of action of riluzole. *Neurology* 47: S233-241, 1996.

Elsen FP, and Ramirez JM. Calcium currents of rhythmic neurons recorded in the isolated respiratory network of neonatal mice. *J Neurosci* 18: 10652-10662, 1998.

Fall CP. *Computational cell biology.* New York: Springer, 2002, p. 302-304.

Feldman JL. Neurophysiology of breathing in mammals. In: *Handbook of Physiology; Section I: The Nervous System; Volume IV: Intrinsic Regulatory Systems of the Brain*, edited by Bloom FE. Bethesda, MD: Am. Physiol. Soc., 1986, p. 463-524.

Feldman JL, and Cleland C. Possible roles of pacemaker neurons in mammalian respiratory rhythmogenesis. In: *Cellular Pacemakers*, edited by Carpenter D. New York: Wiley, 1982, p. 104-128.

Feldman JL, and Del Negro CA. Looking for inspiration: new perspectives on respiratory rhythm. *Nat Rev Neurosci* 7: 232, 2006.

Feldman JL, and Smith JC. Cellular mechanisms underlying modulation of breathing pattern in mammals. *Ann N Y Acad Sci* 563: 114-130, 1989.

Funk GD, Smith JC, and Feldman JL. Modulation of neural network activity in vitro by cyclothiazide, a drug that blocks desensitization of AMPA receptors. *J Neurosci* 15: 4046-4056, 1995.

Gray PA, Janczewski WA, Mellen N, McCrimmon DR, and Feldman JL. Normal breathing requires preBotzinger complex neurokinin-1 receptor-expressing neurons. *Nat Neurosci* 4: 927-930, 2001.

Gray PA, Rekling JC, Bocchiario CM, and Feldman JL. Modulation of respiratory frequency by peptidergic input to rhythmogenic neurons in the preBotzinger complex. *Science* 286: 1566-1568, 1999.

Grillner S. The motor infrastructure: from ion channels to neuronal networks. *Nat Rev Neurosci* 4: 573-586, 2003.

Guyenet PG, Sevigny CP, Weston MC, and Stornetta RL. Neurokinin-1 receptor-expressing cells of the ventral respiratory group are functionally heterogeneous and predominantly glutamatergic. *J Neurosci* 22: 3806-3816, 2002.

Guyenet PG, and Wang H. Pre-Bötzinger neurons with preinspiratory discharges "in vivo" express NK1 receptors in the rat. *J Neurophysiol* 86: 438-446, 2001.

Hille B. *Ion Channels of Excitable Membranes, Third Edition.* Sunderland, MA: Sinauer Associates, 2001, p. 722.

Jahr CE, and Stevens CF. A quantitative description of NMDA receptor-channel kinetic behavior. *J Neurosci* 10: 1830-1837, 1990a.

Jahr CE, and Stevens CF. Voltage dependence of NMDA-activated macroscopic conductances predicted by single-channel kinetics. *J Neurosci* 10: 3178-3182, 1990b.

Johnson SW, Seutin V, and North RA. Burst firing in dopamine neurons induced by N-methyl-D-aspartate: role of electrogenic sodium pump. *Science* 258: 665-667, 1992.

Koch C, and Segev I. *Methods in neuronal modeling : from ions to networks.* Cambridge, Mass.: MIT Press, 1998, p. xiii, 671 p.

Lee RH, and Heckman CJ. Essential role of a fast persistent inward current in action potential initiation and control of rhythmic firing. *J Neurophysiol* 85: 472-475, 2001.

Li YX, Bertram R, and Rinzel J. Modeling N-methyl-D-aspartate-induced bursting in dopamine neurons. *Neuroscience* 71: 397-410, 1996.

Marder E. Moving rhythms. *Nature* 410: 755, 2001.

Marder E, and Calabrese RL. Principles of rhythmic motor pattern generation. *Physiol Rev* 76: 687-717, 1996.

McKay LC, Janczewski WA, and Feldman JL. Sleep-disordered breathing after targeted ablation of preBotzinger complex neurons. *Nat Neurosci* 8: 1142-1144, 2005.

Mendenhall JM, Hayes JA, and Del Negro CA. A Two-Compartment Model of PreBötC Neurons Incorporating ICAN. *The Xth Oxford Conference on Modeling and Control of Breathing* A34: 2006.

Mironov SL, Langohr K, and Richter DW. Hyperpolarization-activated current, I_h, in inspiratory brainstem neurons and its inhibition by hypoxia. *Eur J Neurosci* 12: 520-526, 2000.

Molloy M, and Reed B. A Critical-Point for Random Graphs with a Given Degree Sequence. *Random Structures & Algorithms* 6: 161-179, 1995.

Orlovsky GN, Deliagina TG, and Grillner S. *Neuronal control of locomotion: from mollusc to man.* New York: Oxford University Press, 1999, p. 322.

Pace RW, Mackay DD, Feldman JL, and Del Negro CA. Inspiratory bursts in the preBotzinger Complex depend on a calcium-activated nonspecific cationic current linked to glutamate receptors. *J Physiol* jphysiol.2007.133660, 2007a.

Pace RW, Mackay DD, Feldman JL, and Del Negro CA. Role of Persistent Sodium Current in Mouse PreBotzinger Neurons and Respiratory Rhythm Generation. *J Physiol (Lond)* jphysiol.2006.124602, 2007b.

Paton JF, Abdala AP, Koizumi H, Smith JC, and St-John WM. Respiratory rhythm generation during gasping depends on persistent sodium current. *Nat Neurosci* 9: 311-313, 2006.

Pena F, Parkis MA, Tryba AK, and Ramirez JM. Differential Contribution of Pacemaker Properties to the Generation of Respiratory Rhythms during Normoxia and Hypoxia. *Neuron* 43: 105-117, 2004.

Ptak K, Zummo GG, Alheid GF, Tkatch T, Surmeier DJ, and McCrimmon DR. Sodium currents in medullary neurons isolated from the pre-Botzinger complex region. *J Neurosci* 25: 5159-5170, 2005.

Rekling JC, Champagnat J, and Denavit-Saubie M. Electroresponsive properties and membrane potential trajectories of three types of inspiratory neurons in the newborn mouse brain stem in vitro. *J Neurophysiol* 75: 795-810, 1996a.

Rekling JC, Champagnat J, and Denavit-Saubie M. Thyrotropin-releasing hormone (TRH) depolarizes a subset of inspiratory neurons in the newborn mouse brain stem in vitro. *J Neurophysiol* 75: 811-819, 1996b.

Rekling JC, and Feldman JL. PreBötzinger complex and pacemaker neurons: hypothesized site and kernel for respiratory rhythm generation. *Annu Rev Physiol* 60: 385-405, 1998.

Rekling JC, Shao XM, and Feldman JL. Electrical coupling and excitatory synaptic transmission between rhythmogenic respiratory neurons in the preBotzinger complex. *J Neurosci* 20: RC113, 2000.

Seutin V, Shen KZ, North RA, and Johnson SW. Sulfonylurea-sensitive potassium current evoked by sodium-loading in rat midbrain dopamine neurons. *Neuroscience* 71: 709-719, 1996.

Smith JC, Butera RJ, Koshiya N, Del Negro C, Wilson CG, and Johnson SM. Respiratory rhythm generation in neonatal and adult mammals: the hybrid pacemaker-network model. *Respir Physiol* 122: 131-147, 2000.

Stein PSG. *Neurons, networks, and motor behavior.* Cambridge: MIT Press, 1997, p. 305.

Stocker M. Ca(2+)-activated K⁺ channels: molecular determinants and function of the SK family. *Nat Rev Neurosci* 5: 758-770, 2004.

Stornetta RL, Rosin DL, Wang H, Sevigny CP, Weston MC, and Guyenet PG. A group of glutamatergic interneurons expressing high levels of both neurokinin-1 receptors and somatostatin identifies the region of the pre-Bötzinger complex. *J Comp Neurol* 455: 499-512, 2003.

Thoby-Brisson M, and Ramirez JM. Identification of two types of inspiratory pacemaker neurons in the isolated respiratory neural network of mice. *J Neurophysiol* 86: 104-112, 2001.

Thoby-Brisson M, Telgkamp P, and Ramirez JM. The role of the hyperpolarization-activated current in modulating rhythmic activity in the isolated respiratory network of mice. *J Neurosci* 20: 2994-3005, 2000.

Ullrich ND, Voets T, Prenen J, Vennekens R, Talavera K, Droogmans G, and Nilius B. Comparison of functional properties of the Ca²⁺-activated cation channels TRPM4 and TRPM5 from mice. *Cell Calcium* 37: 267-278, 2005.

Urbani A, and Belluzzi O. Riluzole inhibits the persistent sodium current in mammalian CNS neurons. *Eur J Neurosci* 12: 3567-3574, 2000.

Wang H, Stornetta RL, Rosin DL, and Guyenet PG. Neurokinin-1 receptor-immunoreactive neurons of the ventral respiratory group in the rat. *J Comp Neurol* 434: 128-146, 2001.

CHAPTER 4. Modulation of a voltage-insensitive, mixed cation current by cyclic AMP

4.1. Introduction

We characterized a SP-evoked current (I_{SP}) in an attempt to determine whether or not inspiratory neurons expressed neurokinin receptors (NKRs) in Chapter 1. SP excites preBötC neurons and thus can reverse the effects of μ -opioid agonists, somatostatin, and other drugs that depress the respiratory rhythm (Ballanyi et al. 1999; Chen et al. 1990a; 1996; Chen et al. 1991; Johnson et al. 1996; Murakoshi et al. 1985). NK1R expression begins at the same embryonic stage as the respiratory rhythm (Pagliardini et al. 2003; Thoby-Brisson et al. 2005). Moreover, NK1Rs provide a convenient (albeit imperfect) marker for the preBötC, and are essential for maintaining breathing during short bouts of hypoxia in adult mice (Ptak et al. 2002). Therefore, the biophysical basis for this receptor's action may yield important clues about respiratory rhythm generation, development, and regulation. This chapter begins to examine the intracellular signaling mechanism that activates I_{SP} in preBötC neurons.

In Chapter 1, we highlighted the shared properties of a current activated by cholinergic agonists (i.e. acetylcholine, carbachol, muscarine, I_{CCh}) (Shao and Feldman 2000) and I_{SP} . Both whole-cell currents are TTX-insensitive, voltage-independent, mixed

cation currents. Furthermore, Shao and Feldman found I_{CCh} in 88% of sampled neurons and we found I_{SP} in 87% of inspiratory neurons (in the absence of carbenoxolone). Muscarine and SP have been shown to act via convergent ionic mechanisms in other systems. For example, pontine locus coeruleus neurons express a cation current that responds to both muscarine and SP (Shen and North 1992a; b). I_{SP} and I_{CCh} are widely expressed in inspiratory neurons and they may reflect the same underlying class of cation channels, which suggests that their activation mechanism may be the same too.

Molecular (Lai et al. 2001) and electrophysiological (Shao and Feldman 2000) evidence suggests that the muscarinic response in preBötC neurons is mediated by M3 muscarine receptors (M3Rs). M3Rs and NK1Rs usually interact with the membrane-bound α subunits of the $G_{q/11}$ family (Caulfield and Birdsall 1998; Kwatra et al. 1993; Macdonald et al. 1996; McConalogue et al. 1998), which is coupled to intracellular signaling cascades via phospholipase C.

However, the excitatory effects of muscarine and SP in respiratory neurons are thought to involve cyclic adenosine monophosphate (cAMP) because muscarine and SP reverse the effects of drugs like DAMGO that down-regulate adenylyl cyclase activity via a $G_{i/o}$ -mediated mechanism (Ballanyi 2004; Ballanyi et al. 1999; Yamamoto et al. 1992).

Previous studies have examined the effects of cAMP on preBötC neurons and respiratory activity *in vitro*. In general, increasing cytosolic cAMP within inspiratory neurons by forskolin (Arata et al. 1993; Ballanyi et al. 1997; Mironov et al. 1999; Mironov and Richter 1998; Shao et al. 2003) or serotonin (Manzke et al. 2003) tend to increase network activity. Conversely, lowering cAMP via μ - or δ -opioid agonists (Ballanyi et al. 1997; Ballanyi et al. 1999; Johnson et al. 1996; Manzke et al. 2003; Suzue 1984), norepinephrine (Errchidi et al. 1991; Johnson et al. 1996), adenosine (Mironov et al.

1999) and somatostatin (Chen et al. 1991; Chen et al. 1990b; Kalia et al. 1984) decreases the frequency of respiratory rhythm.

Since cAMP signaling has profound effects on respiratory frequency *in vitro* through a wide array of metabotropic receptor-coupled systems, the mechanism by which cAMP influences rhythmogenic neurons is a critical issue. We hypothesized that cAMP directly evokes inward currents that can depolarize preBötC neurons and affect rhythm generation.

4.2. Methods

The *in vitro* slice preparation used in this chapter is the same as Chapter 1 and Chapter 2. Voltage-clamp recordings that isolated the forskolin-evoked current ($I_{\text{forskolin}}$) replicated conditions of Fig. 1.7. Inside-out patches were formed after achieving high-impedance seals ($\sim >5 \text{ G}\Omega$), which also allowed us to identify neurons as inspiratory based on extracellular unit spiking detectable in on-cell mode. Then, the patch pipette was slowly withdrawn until the tip was well above the slice surface to establish the inside-out configuration. Adenosine 3',5'-monophosphate (cAMP) and forskolin were obtained from Sigma-Aldrich (St. Louis, MO) while 1,9-dideoxyforskolin was obtained from BIOMOL International, LP (Plymouth Meeting, PA).

4.3. Results and Discussion

Increasing cytosolic cAMP evokes a whole-cell current that resembles I_{SP}

We examined the effects of cAMP on membrane properties in inspiratory neurons.

We first tested whether forskolin could evoke a membrane current similar to I_{SP} . Forskolin stimulates cAMP production via adenylyl cyclase, which increases the frequency of the respiratory rhythm (Mironov et al. 1999; Mironov and Richter 1998;

Muller et al. 2005; Shao et al. 2003). However, forskolin can also directly modulate voltage-gated K^+ channels (Heuschneider and Schwartz 1989; Hoshi et al. 1988). Therefore, we applied an analog of forskolin, 1,9-dideoxyforskolin, that cannot activate adenylyl cyclase but retains the ability to modulate channels, before applying forskolin. This analog is a good negative control to confirm that forskolin is activating channels by increasing cAMP (Shao et al. 2003).

Using a holding potential of -80 mV, we stepped from -100 to $+5$ mV in 1-s pulses and measured the steady-state current response at each potential (Fig. 4.1). We blocked Na^+ , Ca^{2+} , K^+ , and hyperpolarization-activated currents using a cocktail of antagonists including extracellular TTX, Cd^{2+} , TEA, Cs^+ , and a Cs^+ -based patch solution containing and TEA (see Chapter 1 methods). This is similar to the experimental conditions in Fig. 1.7 where we first isolated I_{SP} . While 1,9-dideoxyforskolin did not affect the steady-state current-voltage (IV) relationship, we did observe a response to forskolin that was consistent with the opening of a mixed cation current like I_{SP} (see Chapter 1).

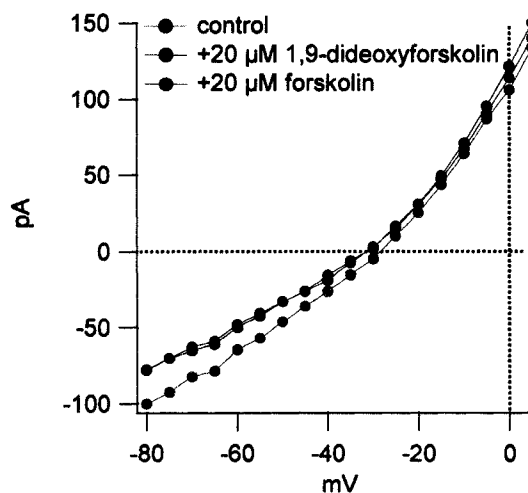


Figure 4.1. Forskolin activates a mixed cation current ($I_{\text{forskolin}}$) in preBötC neurons by up-regulating adenylyl cyclase.

In inspiratory neurons, forskolin is known to increase the open probability of L-type Ca^{2+} channels (Mironov and Richter 1998) as well as to enhance the magnitude of AMPA-mediated EPSPs (Shao et al. 2003). Since our ACSF contained $200 \mu\text{M } Cd^{2+}$, L-

type Ca^{2+} channels should have been blocked. Also, since these experiments were in 1 μM TTX, most AMPA-mediated EPSPs should have been suppressed. Since the data in both Fig. 4.1 and 1.7 indicate the opening of a mixed cation current ($I_{\text{forskolin}}$), our data are consistent with cAMP modulating a current with properties similar to I_{SP} and I_{CCn} .

Since we hypothesized that forskolin and SP were both activating the same mixed cation current, we tested whether forskolin could occlude the effects of SP. Using the same conditions and voltage-clamp protocol as Fig. 4.1, we applied forskolin and then SP (Fig. 4.2). $I_{\text{forskolin}}$ was enhanced only slightly by SP while the reversal potential (where the traces converge) was very nearly the same. This suggests that forskolin and SP were both acting on the same channels, although it is unclear from this experiment whether activation of the channels occurred through the same pathway (i.e., a cAMP-mediated pathway).

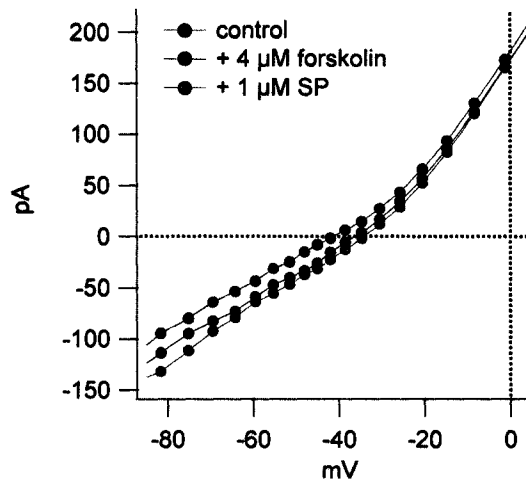


Figure 4.2. Forskolin occludes the effect of SP in preBötC neurons.

Potential candidates for channels that mediate the effects of I_{SP}

Transient receptor potential (TRP) channels are implicated in a wide range of cellular behaviors and are considered good candidates for metabotropic receptor-mediated currents, specifically the 'canonical TRP' (TRPC) subtype (Clapham 2003; Moran et al. 2004). However, TRPCs are voltage-dependent and are generally associated with

activation via the PLC pathway (Montell 2005; Ramsey et al. 2006). Therefore, they are almost certainly not candidates for mediating $I_{\text{forskolin}}$, and we infer from the occlusion experiment that they are not likely contenders for I_{SP} .

Two alternative candidates for the I_{SP} channels are a recently discovered Na^+ leak channel (NaLCN) characterized in hippocampal neurons or a cyclic nucleotide-gated channel (CNGC) similar to channels found in olfactory neurons (Kaupp and Seifert 2002; Kleene 2000). Both NaLCNs and CNGCs appear to be widely expressed in the central nervous system (Bradley et al. 1997; Kingston et al. 1999; Lu et al. 2007).

Both NaLCN and CNGCs are also blocked by the L-type Ca^{2+} channel blocker verapamil (Lang et al. 2000; Lu et al. 2007). To test whether I_{SP} was attributable to either channel type we attempted to block $I_{\text{forskolin}}$ with this drug.

In the same neuron illustrated in Fig. 4.1, we added 500 μM verapamil after forskolin, which reversed $I_{\text{forskolin}}$ and is apparent in both the raw traces (Fig. 4.3A) and IV curve (Fig. 4.3B). This experiment confirmed that we have a means to block the neuronal response to forskolin and perhaps SP.

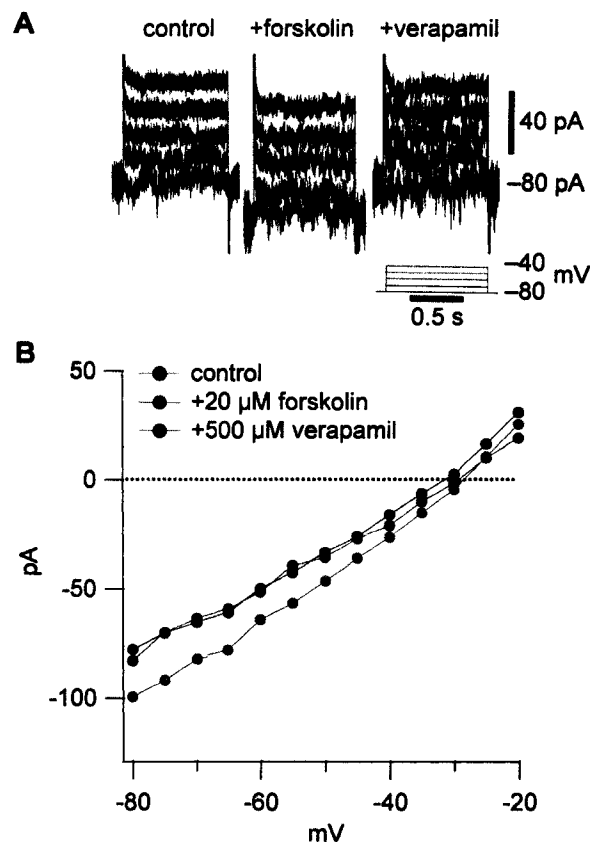


Figure 4.3. Verapamil blocks $I_{\text{forskolin}}$. **A**, Representative current traces showing current responses to voltage steps in control, forskolin, and verapamil. **B**, The corresponding steady-state IV relation under the same conditions.

Therefore, we predicted that verapamil would also block the respiratory response to SP in the context of network rhythm. Under control conditions, SP increases respiratory activity (Fig. 4.4A). In contrast, applying a high concentration of verapamil causes the amplitude of the network activity to decrease and SP cannot reverse the effects. This is particularly interesting because SP is frequently used to recover respiratory activity due to a loss in excitability of preBötC neurons (Del Negro et al. 2005; Pace et al. 2007; Pena and Aguilera 2007; Tryba et al. 2006) as well as reversing the effects of other neuromodulators that depress respiratory activity (Ballanyi et al. 1999; Chen et al. 1990a; 1996; Chen et al. 1991; Johnson et al. 1996; Murakoshi et al. 1985). Therefore, this response is consistent with verapamil blocking the channels that give rise to SP.

NaLCN and CNGC channels share strong structural similarities to Nav and Cav channels, which influences their sensitivity to pharmacological tools. One potential way to further

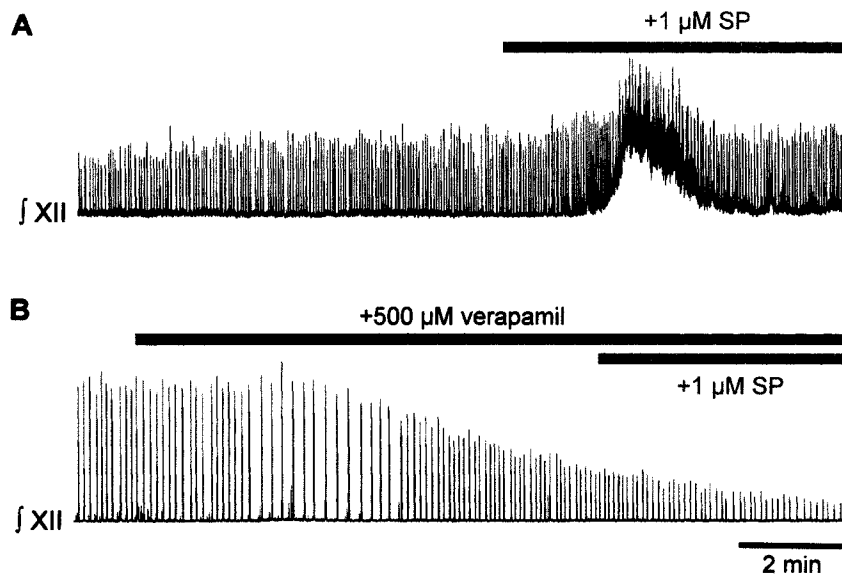


Figure 4.4. Verapamil prevents the network-level response to SP. **A**, SP causes an increase in network activity. **B**, Verapamil attenuates the amplitude of network activity and SP does not have any apparent effects.

distinguish between NaLCN and CNGCs is that CNGCs are expected to exhibit discrete open and close gating transitions in the presence of cAMP, while cAMP would simply increase the unitary conductance of NaLCN channels.

Therefore, we tested the hypothesis that cAMP-gated channels are present in inspiratory preBötC neurons. We first identified inspiratory neurons in the on-cell configuration (Fig. 4.5A). In one of 3 inside-out patches with symmetric intra- and extracellular solutions, we observed discrete channel openings with ~30 pS unitary conductance in the presence of bath-applied 200 μ M cAMP and the effect was reversible (Fig. 4.5B). This is comparable to the unitary conductance of CNGCs (Hatt and Ache 1994; Zufall et al. 1991) but since the solutions were symmetric we cannot compare the reversal potential of this channel to I_{SP} or $I_{forskolin}$ measured under our previous conditions. Hyperpolarization-activated mixed cation channels that give rise to I_h currents are phylogenetically related to CNGCs and can be directly activated by cAMP (Hille 2001) and are present in some inspiratory neurons (Mironov et al. 2000; Thoby-Brisson et al. 2000). However, the unitary conductance of these currents are less than 10 pS (Kole et al. 2006; Simeone et al. 2005) suggesting that the channels we were recording were indeed CNGCs.

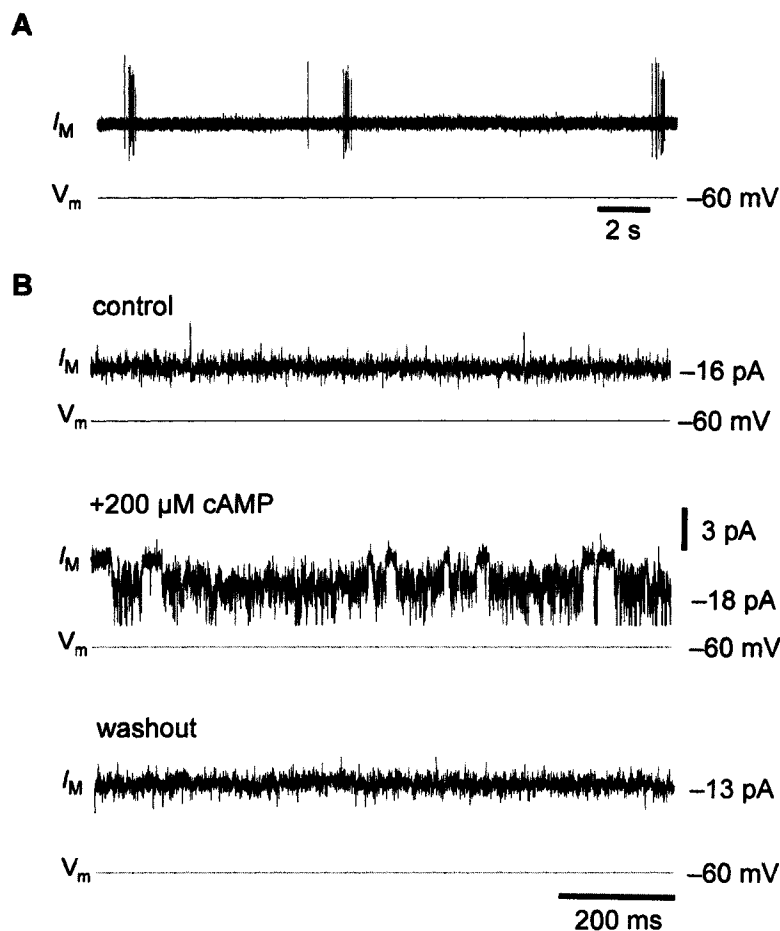


Figure 4.5. cAMP-gated channels are present in preBötC neurons. **A**, Inspiratory neurons were identified from their on-cell activity. **B**, In inside-patches, bath-applied cAMP caused discrete open and close events of a channel and the response was reversible.

Possible roles for a cAMP-modulated mixed cation current

In respiratory neurons, an inward-rectifying potassium current (I_{K-IR}) has been implicated in mediating the effects of μ -opioid agonists (Gray et al. 1999; Johnson et al. 1996) and GABA_B agonists through a convergent signaling pathway utilizing $G_{i/o}$ activation (Johnson et al. 1996). However, I_{K-IR} may not completely account for the results from experiments using these agonists. This is because Ba^+ only partly reverses the effects of these agonists on the frequency of respiratory rhythm and pertussis toxin, a blocker of $G_{i/o}$ proteins, would nearly completely reverse the effects of these agonists. Since Ba^+ only partly reversed the effects on frequency of the μ -opioid agonist, those authors

suggested that a Ba^{+} -insensitive current may also be involved in depressing respiratory activity. A constitutively activated mixed cation channel, that is depressed by a decline in cAMP, could be this hypothesized Ba^{+} -insensitive current. This hypothesis is supported by our data that shows verapamil depressed respiratory activity in the network.

Extending this further, Manzke et al. (2003) postulated that μ -opioid receptors and 5-HT₄ receptors were also convergently acting to modulate respiratory frequency by decreasing and increasing production of cAMP through adenylyl cyclase. However, the specific mechanism by which cAMP modulates neuronal excitability has remained unclear.

A voltage-insensitive inward current, modulated or gated by cAMP, could be very significant in maintaining and modulating neuronal excitability, and their presence in rhythmogenic neurons could have profound effects on the respiratory activity if conflicting drugs compete to up- or downregulate cytosolic cAMP.

4.4. References

Arata A, Onimaru H, and Homma I. Effects of cAMP on respiratory rhythm generation in brainstem-spinal cord preparation from newborn rat. *Brain Res* 605: 193-199, 1993.

Ballanyi K. Neuromodulation of the Perinatal Respiratory Network. *Current Neuropharmacology* 2: 221-243, 2004.

Ballanyi K, Lalley PM, Hoch B, and Richter DW. cAMP-dependent reversal of opioid- and prostaglandin-mediated depression of the isolated respiratory network in newborn rats. *J Physiol* 504 (Pt 1): 127-134, 1997.

Ballanyi K, Onimaru H, and Homma I. Respiratory network function in the isolated brainstem-spinal cord of newborn rats. *Prog Neurobiol* 59: 583-634, 1999.

Bradley J, Zhang Y, Bakin R, Lester HA, Ronnett GV, and Zinn K. Functional expression of the heteromeric "olfactory" cyclic nucleotide-gated channel in the hippocampus: a potential effector of synaptic plasticity in brain neurons. *J Neurosci* 17: 1993-2005, 1997.

Caulfield MP, and Birdsall NJ. International Union of Pharmacology. XVII. Classification of muscarinic acetylcholine receptors. *Pharmacol Rev* 50: 279-290, 1998.

Chen Z, Hedner J, and Hedner T. Substance P in the ventrolateral medulla oblongata regulates ventilatory responses. *J Appl Physiol* 68: 2631-2639, 1990a.

Chen Z, Hedner J, and Hedner T. Substance P-induced respiratory excitation is blunted by delta-receptor specific opioids in the rat medulla oblongata. *Acta Physiol Scand* 157: 165-173, 1996.

Chen ZB, Engberg G, Hedner T, and Hedner J. Antagonistic effects of somatostatin and substance P on respiratory regulation in the rat ventrolateral medulla oblongata.

Brain Res 556: 13-21, 1991.

Chen ZB, Hedner T, and Hedner J. Local application of somatostatin in the rat ventrolateral brain medulla induces apnea. *J Appl Physiol* 69: 2233-2238, 1990b.

Clapham DE. TRP channels as cellular sensors. *Nature* 426: 517-524, 2003.

Del Negro CA, Morgado-Valle C, Hayes JA, Mackay DD, Pace RW, Crowder EA, and Feldman JL. Sodium and Calcium Current-Mediated Pacemaker Neurons and Respiratory Rhythm Generation. *J Neurosci* 25: 446-453, 2005.

Errchidi S, Monteau R, and Hilaire G. Noradrenergic modulation of the medullary respiratory rhythm generator in the newborn rat: an in vitro study. *J Physiol* 443: 477-498, 1991.

Gray PA, Rekling JC, Bocchiario CM, and Feldman JL. Modulation of respiratory frequency by peptidergic input to rhythmogenic neurons in the preBötzinger complex. *Science* 286: 1566-1568, 1999.

Hatt H, and Ache BW. Cyclic nucleotide- and inositol phosphate-gated ion channels in lobster olfactory receptor neurons. *Proc Natl Acad Sci U S A* 91: 6264-6268, 1994.

Heuschneider G, and Schwartz RD. cAMP and forskolin decrease gamma-aminobutyric acid-gated chloride flux in rat brain synaptoneurosomes. *Proc Natl Acad Sci U S A* 86: 2938-2942, 1989.

Hille B. *Ion Channels of Excitable Membranes, Third Edition.* Sunderland, MA: Sinauer Associates, 2001, p. 722.

Hoshi T, Garber SS, and Aldrich RW. Effect of forskolin on voltage-gated K⁺ channels is independent of adenylate cyclase activation. *Science* 240: 1652-1655, 1988.

Johnson SM, Smith JC, and Feldman JL. Modulation of respiratory rhythm in vitro: role of G_{i/o} protein-mediated mechanisms. *J Appl Physiol* 80: 2120-2133, 1996.

Kalia M, Fuxe K, Agnati LF, Hokfelt T, and Harfstrand A. Somatostatin produces apnea and is localized in medullary respiratory nuclei: a possible role in apneic syndromes. *Brain Res* 296: 339-344, 1984.

Kaupp UB, and Seifert R. Cyclic nucleotide-gated ion channels. *Physiol Rev* 82: 769-824, 2002.

Kingston PA, Zufall F, and Barnstable CJ. Widespread expression of olfactory cyclic nucleotide-gated channel genes in rat brain: implications for neuronal signalling. *Synapse* 32: 1-12, 1999.

Kleene SJ. Spontaneous gating of olfactory cyclic-nucleotide-gated channels. *J Membr Biol* 178: 49-54, 2000.

Kole MH, Hallermann S, and Stuart GJ. Single I_h channels in pyramidal neuron dendrites: properties, distribution, and impact on action potential output. *J Neurosci* 26: 1677-1687, 2006.

Kwatra MM, Schwinn DA, Schreurs J, Blank JL, Kim CM, Benovic JL, Krause JE, Caron MG, and Lefkowitz RJ. The substance P receptor, which couples to G_{q/11}, is a

substrate of beta-adrenergic receptor kinase 1 and 2. *J Biol Chem* 268: 9161-9164, 1993.

Lai J, Shao XM, Pan RW, Dy E, Huang CH, and Feldman JL. RT-PCR reveals muscarinic acetylcholine receptor mRNA in the pre-Bötzinger complex. *Am J Physiol Lung Cell Mol Physiol* 281: L1420-1424, 2001.

Lang R, Lee G, Liu W, Tian S, Rafi H, Orias M, Segal AS, and Desir GV. KCNA10: a novel ion channel functionally related to both voltage-gated potassium and CNG cation channels. *Am J Physiol Renal Physiol* 278: F1013-1021, 2000.

Lu B, Su Y, Das S, Liu J, Xia J, and Ren D. The neuronal channel NALCN contributes resting sodium permeability and is required for normal respiratory rhythm. *Cell* 129: 371-383, 2007.

Macdonald SG, Dumas JJ, and Boyd ND. Chemical cross-linking of the substance P (NK-1) receptor to the alpha subunits of the G proteins Gq and G11. *Biochemistry* 35: 2909-2916, 1996.

Manzke T, Guenther U, Ponimaskin EG, Haller M, Dutschmann M, Schwarzacher S, and Richter DW. 5-HT4(a) receptors avert opioid-induced breathing depression without loss of analgesia. *Science* 301: 226-229, 2003.

McConalogue K, Corvera CU, Gamp PD, Grady EF, and Bunnett NW. Desensitization of the neurokinin-1 receptor (NK1-R) in neurons: effects of substance P on the distribution of NK1-R, Galphaq/11, G-protein receptor kinase-2/3, and beta-arrestin-1/2. *Mol Biol Cell* 9: 2305-2324, 1998.

Mironov SL, Langohr K, and Richter DW. A1 adenosine receptors modulate respiratory activity of the neonatal mouse via the cAMP-mediated signaling pathway. *J Neurophysiol* 81: 247-255, 1999.

Mironov SL, Langohr K, and Richter DW. Hyperpolarization-activated current, I_h, in inspiratory brainstem neurons and its inhibition by hypoxia. *Eur J Neurosci* 12: 520-526, 2000.

Mironov SL, and Richter DW. L-type Ca²⁺ channels in inspiratory neurones of mice and their modulation by hypoxia. *J Physiol* 512 (Pt 1): 75-87, 1998.

Montell C. The TRP superfamily of cation channels. *Sci STKE* 2005: re3, 2005.

Moran MM, Xu H, and Clapham DE. TRP ion channels in the nervous system. *Curr Opin Neurobiol* 14: 362-369, 2004.

Muller M, Mironov SL, Ivannikov MV, Schmidt J, and Richter DW. Mitochondrial organization and motility probed by two-photon microscopy in cultured mouse brainstem neurons. *Exp Cell Res* 303: 114-127, 2005.

Murakoshi T, Suzue T, and Tamai S. A pharmacological study on respiratory rhythm in the isolated brainstem-spinal cord preparation of the newborn rat. *British journal of pharmacology* 86: 95-104, 1985.

Pace RW, Mackay DD, Feldman JL, and Del Negro CA. Role of persistent sodium current in mouse preBötzinger Complex neurons and respiratory rhythm generation. *J Physiol* 580: 485-496, 2007.

Pagliardini S, Ren J, and Greer JJ. Ontogeny of the pre-Bötzinger complex in perinatal rats. *J Neurosci* 23: 9575-9584, 2003.

Pena F, and Aguilera MA. Effects of riluzole and flufenamic acid on eupnea and gasping of neonatal mice in vivo. *Neurosci Lett* 415: 288-293, 2007.

Ptak K, Burnet H, Bianchi B, Sieweke M, De Felipe C, Hunt SP, Monteau R, and Hilaire G. The murine neurokinin NK1 receptor gene contributes to the adult hypoxic facilitation of ventilation. *Eur J Neurosci* 16: 2245-2252, 2002.

Ramsey IS, Delling M, and Clapham DE. An introduction to TRP channels. *Annu Rev Physiol* 68: 619-647, 2006.

Shao XM, and Feldman JL. Acetylcholine modulates respiratory pattern: effects mediated by M3-like receptors in preBötzinger complex inspiratory neurons. *J Neurophysiol* 83: 1243-1252, 2000.

Shao XM, Ge Q, and Feldman JL. Modulation of AMPA receptors by cAMP-dependent protein kinase in preBötzinger complex inspiratory neurons regulates respiratory rhythm in the rat. *J Physiol* 547: 543-553, 2003.

Shen KZ, and North RA. Muscarine increases cation conductance and decreases potassium conductance in rat locus coeruleus neurones. *J Physiol* 455: 471-485, 1992a.

Shen KZ, and North RA. Substance P opens cation channels and closes potassium channels in rat locus coeruleus neurons. *Neuroscience* 50: 345-353, 1992b.

Simeone TA, Rho JM, and Baram TZ. Single channel properties of hyperpolarization-activated cation currents in acutely dissociated rat hippocampal neurones. *J Physiol* 568: 371-380, 2005.

Suzue T. Respiratory rhythm generation in the in vitro brain stem-spinal cord preparation of the neonatal rat. *J Physiol* 354: 173-183, 1984.

Thoby-Brisson M, Telgkamp P, and Ramirez JM. The role of the hyperpolarization-activated current in modulating rhythmic activity in the isolated respiratory network of mice. *J Neurosci* 20: 2994-3005, 2000.

Thoby-Brisson M, Trinh JB, Champagnat J, and Fortin G. Emergence of the pre-Bötzinger respiratory rhythm generator in the mouse embryo. *J Neurosci* 25: 4307-4318, 2005.

Tryba AK, Pena F, and Ramirez JM. Gasping activity in vitro: a rhythm dependent on 5-HT_{2A} receptors. *J Neurosci* 26: 2623-2634, 2006.

Yamamoto Y, Onimaru H, and Homma I. Effect of substance P on respiratory rhythm and pre-inspiratory neurons in the ventrolateral structure of rostral medulla oblongata: an in vitro study. *Brain Res* 599: 272-276, 1992.

Zufall F, Firestein S, and Shepherd GM. Analysis of single cyclic nucleotide-gated channels in olfactory receptor cells. *J Neurosci* 11: 3573-3580, 1991.

Conclusions

The research in this dissertation has advanced our understanding of how respiratory behavior arises by examining how intrinsic currents influence phenotypic neuronal properties, such as discharge pattern, and by examining how those properties influence interactions of neurons involved in the generation of mammalian breathing.

The first chapter identifies putatively rhythmogenic preBötC neurons based on electrophysiological properties *in vitro* which may allow us to distinguish rhythmogenic neurons from premotoneurons found in the preBötC. An interesting future set of experiments could entail determining if our electrophysiological distinction is really reliable. Evidence for NKRs was present in both subpopulations, however, NKR^+ neurons did not have an apparently distinct electrophysiological phenotype from their NKR^- counterparts. This raises the question: how are NKR^+ neurons functionally different from NKR^- neurons? The most likely explanation is that they make up a population of inspiratory neurons that inhibit expiratory neurons (as opposed to NKR^+ neurons which are predominantly glutamatergic). However, if NKR^- inspiratory neurons are also glutamatergic they may directly participate in rhythm-generation and NKR^+ neurons may not be sufficient for rhythmic activity in the preBötC.

A related prediction is discussed in both Chapter 1 and Chapter 3 where we suggested that NKR^- neurons may be able to generate respiratory activity alone. This

could be tested with *in vitro* lesioning experiments, possibly by ablating individual preBötC NKR⁺ neurons using a laser, and monitoring the network activity. If our estimate for the population size of NKR⁺ rhythmogenic neurons is realistic, then we expect network activity would diminish rapidly with the eventual cessation of motor output. Then, as we showed in simulations from Chapter 3, it may be possible to recover motor output by applying drugs that increase phasic excitatory synaptic input among the remaining, and predominantly NKR⁻, preBötC neurons.

In this dissertation, we have also shown how SP can raise the excitability of the inspiratory population of neurons via the opening of a voltage-independent mixed cation current (Chapter 1). This response was similar to the response observed when we increased cAMP (Chapter 4), and we have shown that this current may arise from the activation of an intrinsic cAMP-gated mixed cation current. Full characterization of these channels remains under investigation, but the presence of cAMP-modulated mixed cation channels, that are the target of multiple neuromodulators, may provide a novel means by which different types of afferent activity could modulate the speed of respiratory rhythm.

We also developed a model that relies on recurrent excitation through positive feedback synaptic connections to generate periodic respiratory-like rhythms. This represents the first attempt at simulating a network of respiratory group-pacemaker neurons. This model motivated us to perform experiments to determine what was a realistic size of the critical rhythm-generating population (i.e., Chapter 1), what degree rhythmogenic neurons express NKR⁺ so we could investigate how neuron lesioning affects rhythmogenesis (Chapter 1), and examine the, heretofore unknown, biophysical properties of I_A (Chapter 2). This work has profoundly influenced the work of three additional separate projects that examine how recurrent excitation can generate

respiratory rhythm-like behavior. One of the projects also relies on the software developed as part of this dissertation (Chapter 3, Appendix 2) to simulate high-dimensional, realistic neuronal models of inspiratory neurons and will provide a means to easily combine these neurons into realistic networks in the future.

A major question in trying to develop realistic models of the preBötC network is: what is the connection topology of the rhythm-generating network? Initially, this will probably be inferred from experimental data that examines the pattern in network connectivity originating from an individual inspiratory neuron. We know that some glutamatergic inspiratory neurons are connected to other glutamatergic inspiratory neurons monosynaptically. However, no one has yet demonstrated how many synapses, on average, are needed to make a full positive feedback cycle. The recurrent excitation described in the modeling work emphasizes why the answer to this question is important: positive feedback loops are essential within the rhythm-generating population for a group-pacemaker to function!

This issue may also be important in fully understanding how I_A impacts respiratory rhythmogenesis. In Chapter 2, we showed that I_A plays a role in maintaining coherent rhythmic activity within the preBötC. We found that this intrinsic current makes important contributions in shaping the incremental discharge pattern (i.e., a phenotypic property) associated with early inspiratory neurons (see Chapter 1) and suggested this behavior was related to I_A 's characteristic role in synaptic integration. Our experiments and modeling insights suggest an additional novel role for the neurons that express I_A . When I_A is widely expressed in neurons arranged with positive feedback connections, these neurons may act as logical AND gates by primarily passing high-frequency output to postsynaptic neurons only in the presence of massive convergent presynaptic activity. We expect this would prevent spurious network assembly from transforming into full

inspiratory bursts (i.e., a giant component of activity, see Chapter 3) until the vast majority of rhythmogenic neurons have recovered from refractoriness. This could more completely account for how I_A plays an important role in regulating the period of synchronized respiratory activity.

Altogether, this dissertation has made important contributions in our understanding of how preBötC neurons behave individually and interact, but also raises new questions. The answers to all these questions will potentially help us understand what qualities are necessary for maintaining inspiratory activity and potentially aid researchers develop therapies for central respiratory failure.

VITA

John Ashley Hayes

April 25, 1979	Born, Lexington, Kentucky
2004-Present:	Ph.D. Graduate Student Department of Applied Science The College of William and Mary Williamsburg, Virginia
May, 2004:	Master of Science Department of Applied Science The College of William and Mary Williamsburg, Virginia
2002-2004:	M.S. Graduate Student
1999-2002:	Senior Software Engineer INCOGEN, Inc. Williamsburg, Virginia
May, 2001	Bachelor of Science Biosystems Engineering Clemson University Clemson, South Carolina

Publications and Presentations

Hayes JA, and Del Negro CA. Neurokinin Receptor-Expressing PreBötzing Complex Neurons in Neonatal Mice Studied In Vitro. *J Neurophysiol*, 97:4215-4224, 2007.

Hayes JA, and Del Negro CA. Neurokinin Receptor-Expressing Neurons in the Neonatal Mouse PreBötzing Complex: Roles in Respiratory Rhythmogenesis. *The College of William and Mary Graduate Research Symposium*. Slide presentation, March 30, 2007.

Hayes JA, and Del Negro CA. Network Structure and Composition in Respiratory Rhythmogenesis. *The College of William and Mary Neuroscience Symposium*. Slide presentation, October 31, 2006.

Hayes JA, and Del Negro CA. The role of network structure and composition in respiratory rhythmogenesis. *Soc. Neurosci. Abs.* 308.3. Slide session, Oct. 16, 2006.

Del Negro C A, Pace RW, and Hayes JA. What role do pacemaker neurons play in respiratory rhythm generation?. *The Xth Oxford Conference on Modeling and Control of Breathing*. Slide session and proceedings chapter, September 2006.

Hayes JA, and Del Negro CA. The role of cellular phenotypes and network structure in respiratory rhythmogenesis. *The Xth Oxford Conference on Modeling and Control of Breathing*. Poster session A22, September 2006.

Mendenhall JL, Hayes JA, and Del Negro CA. A Two-Compartment Model of PreBötC Neurons Incorporating I_{CAN} . *The Xth Oxford Conference on Modeling and Control of Breathing*. Poster session A34, September 2006.

Hayes JA, and Del Negro CA. Structure and Function of the Rhythm Generator for Breathing. The College of William and Mary Graduate Research Symposium. Slide presentation, March 2006.

Hayes JA, Pace RW, Del Negro CA. Inspiratory Rhythm Generation. *University of Alberta Perinatal Respiratory Research Group Seminar*. Slide presentation, February 2006.

Hayes JA, and Del Negro CA. A Modeling and Experimental Study of Rhythm Generation in the PreBötzinger Complex of mice. *Soc. Neurosci. Abs. 866.5*. Poster session, November 16, 2005.

Pace RW, MacKay DD, Hayes JA, Crowder EA, Feldman JL, Del Negro CA. Calcium-activated nonspecific cationic currents (I_{CAN}) and inspiratory burst potentials in pre-Bötzinger Complex neurons *in vitro*: the role and activation mechanism of I_{CAN} . *Soc. Neurosci. Abs. 352.15*. Slide session, November 14, 2005.

Hayes JA, and Del Negro CA. A Modeling and Experimental Study of Inspiratory Rhythmogenesis in Mammals. *The College of William and Mary REU Group Seminar*. Slide presentation, July 8, 2005.

Del Negro CA, Morgado-Valle C, Hayes JA, Mackay DD, Pace RW, Crowder EA, and Feldman JL. Sodium and calcium dependent pacemaker neurons and respiratory rhythm generation. *J Neurosci* 25: 446-453, 2005.

Hayes JA. A Framework for Implementing Bioinformatics Knowledge-Exploration Systems. *M. S. Thesis*, May 2004.